AN INVESTIGATION OF POTENTIAL INDUCED DEGRADATION OF SOLAR PHOTO-VOLTAIC MODULES UNDER MALAYSIAN CLIMATE CONDITION

MD. AMINUL ISLAM

INSTITUTE OF GRADUATE STUDIES
UNIVERSITY OF MALAYA
KUALA LUMPUR

2018

AN INVESTIGATION OF POTENTIAL INDUCED DEGRADATION OF SOLAR PHOTO-VOLTAIC MODULES UNDER MALAYSIAN CLIMATE CONDITION

MD. AMINUL ISLAM

THESIS SUBMITTED IN FULFILMENT OF THE REQUIREMENTS FOR THE DEGREE OF DOCTOR OF PHILOSOPHY

INSTITUTE OF GRADUATE STUDIES
UNIVERSITY OF MALAYA
KUALA LUMPUR

2018

UNIVERSITY OF MALAYA

ORIGINAL LITERARY WORK DECLARATION

Name of Candidate: Md. Aminul Islam [redacted]

Matric No: HHD140010

Name of Degree: Doctor of Philosophy

Title of Project Paper/Research Report/Dissertation/Thesis ("this Work"): **An Investigation of Potential Induced Degradation of Solar Photo-voltaic Modules Under Malaysian Climate Condition**

Field of Study: Power System Protection

I do solemnly and sincerely declare that:

(1) I am the sole author/writer of this Work;
(2) This Work is original;
(3) Any use of any work in which copyright exists was done by way of fair dealing and for permitted purposes and any excerpt or extract from, or reference to or reproduction of any copyright work has been disclosed expressly and sufficiently and the title of the Work and its authorship have been acknowledged in this Work;
(4) I do not have any actual knowledge nor do I ought reasonably to know that the making of this work constitutes an infringement of any copyright work;
(5) I hereby assign all and every rights in the copyright to this Work to the University of Malaya ("UM"), who henceforth shall be owner of the copyright in this Work and that any reproduction or use in any form or by any means whatsoever is prohibited without the written consent of UM having been first had and obtained;
(6) I am fully aware that if in the course of making this Work I have infringed any copyright whether intentionally or otherwise, I may be subject to legal action or any other action as may be determined by UM.

Candidate's Signature Date:

Subscribed and solemnly declared before,

Witness's Signature Date:

Name:

Designation:

AN INVESTIGATION OF POTENTIAL INDUCED DEGRADATION OF SOLAR PHOTO-VOLTAIC MODULES UNDER MALAYSIAN CLIMATE CONDITION

ABSTRACT

Photovoltaic (PV) modules experience unanticipated decline in lifespan due to high voltage stress (HVS) of large PV string recognized as potential induced degradation (PID). Real-time data on PID behaviour of PV module under the climate conditions of Malaysia is necessary to estimate the operating capacity of a PV plant which far deviates from the installed capacity after several years of aging. On-site degradation characteristics of PV module under the typical Malaysian climatic condition have been investigated. A quantitative characterization method of PV modules degradation by using electroluminescence (EL) imaging technique has been introduced in this research. About 42% degradation of PV module has been noticed due to nine years field aging under a negative voltage stress produced from 240 V string, whereas during the same period the PV module degrades about 17% over as a consequence of light induced degradation (LID). Shunt resistance of negative end PV module is found 75% lower than that of the positive end module. PV cell crack initiation is observed to be accelerated as a result of cyclic high voltage stress at on-site. The LID characteristics of different poly and monocrystalline silicon PV modules due to real field aging for various time spans have been measured by EL imaging along with the measurement of maximum power and analysis of dark I-V curve. Degradation values of PV modules obtained are 1.78, 7.06, 13.92, 17.04 and 17.42% due to aging for a period of 8 months, 16 months, 4 years, 9 years and 11 years respectively. This degradation is due to the reduction in shunt resistance which declines gradually as a result of aging.

PID of PV module depends on the leakage current characteristics. Effect of various operating parameters for example PV module temperature, wet surface condition, dust

and salt deposition on module surface and aging on leakage current behaviour are investigated by applying high DC voltage stresses in laboratory condition. Dust particles collected from the PV plant site are characterized by means of field emission scanning electron microscopy (FESEM), energy dispersive X-ray (EDX) spectroscopy and X-ray diffraction (XRD) techniques. It has been observed that, the leakage current increases with the increase of voltage stress at room temperature. An increase of module surface temperature causes a moderate increase of leakage current, but the rising trend is drastic in the presence of water film on module surface. Leakage current values under 1500 V stress are found 7.8, 8.9 and 29.8 μA at 25°C (dry), 60°C (dry) and 45°C (wet) conditions, respectively. The leakage current increases linearly as a consequence of increase in salt existence. Slight amount ($2gm/m^2$) of dust along with water film is found sufficient to trigger leakage current generation in PV module. Tiny dust particles as observed from FESEM are found to attain charged state and can easily attach with ionic compounds that exist in coastal areas, which further instigate the leakage current flow in PV module. Aging of the PV module causes dwindle in leakage current as well as PID resistance property of PV modules resulting from the decline of encapsulant electrical resistance.

Keywords: potential induced degradation; PV module; leakage current; aging effect; EL imaging.

PENYIASATAN KE ATAS DEGRADASI TERARUH POTENSI BAGI MODUL SOLAR FOTO-VOLTIK DI BAWAH KEADAAN IKLIM MALAYSIA

ABSTRAK

Jangka hayat modul fhotovoltaik (PV) berkurangan akibat daripada tekanan voltan tinggi dari saiz tali PV yang besar; yang dikenali juga sebagai 'potential induced degradation (PID)'. Data sebenar PID pada modul PV di bawah keadaan iklim Malaysia adalah perlu untuk menganggarkan kapasiti operasi sebuah jana kuasa PV yang jauh menyimpang dari jumlah kapasiti asal selepas beberapa tahun beroperasi. Siasatan mengenai kelakuan PID pada modul PV telah dijalankan di bawah iklim Malaysia yang tipikal. Proses pengukuran degradasi kuantitatif modul PV melalui pengimejan EL telah diperkenalkan didalam penyelidikan ini. Pemerhatian mendapati bahawa modul PV merosot sebanyak 42% akibat dari penuaan medan selama 9 tahun di bawah tekanan voltan negatif yang dijana daripada saiz tali 240V, manakala modul PV menurun hampir 17% dalam tempoh yang sama disebabkan oleh cahaya degradasi teraruh (LID). Rintangan selari modul negatif adalah 75% lebih rendah daripada modul positif. Retakan modul dipercepatkan akibat daripada tekanan voltan tinggi siklik di tapak jana kuasa PV. Kadar cahaya degradasi teraruh pelbagai modul PV seperti silikon poli dan mono kristal akibat penuaan pada jangka masa yang pelbagai telah dikesan oleh pengimejan EL, pengukuran kuasa maksimum dan analisis I-V gelap. Nilai degradasi yang diperolehi daripada modul PV masing-masing adalah 1.78, 7.06, 13.92, 17.04 dan 17.42% yang disebabkan oleh penuaan pada tempoh 8 bulan, 16 bulan, 4 tahun, 9 tahun dan 11 tahun. Faktor disebalik degradasi ini adalah disumbangkan oleh pengurangan rintangan selari yang menurun secara beransur-ansur akibat penuaan modul PV.

Arus kebocoran adalah salah satu penyebab kepada PID. Kesan parameter seperti suhu permukaan modul, filem air pada permukaan modul, pengumpulan garam dan

habuk pada permukaan modul dan keadaan penuaan disiasat dengan menggunakan jumlah tekanan voltan tinggi yang berbeza-beza di dalam kondisi makmal. Pengumpulan debu debu di janakusa PV telah dikategorikan melalui mikroskop elektron pengimbasan pelepasan bidang (FESEM), teknik spektroskopi dispersi sinar-X (EDX) dan teknik difraksi sinar-X (XRD). Dari pemerhatian, arus kebocoran meningkat selari dengan tekanan voltan pada suhu bilik. Arus kebocoran meningkat pada kadar sederhana dengan peningkatan suhu pada dasar modul dan ianya meningkat secara drastik dengan kehadiran filem air pada permukaan modul. Arus kebocoran pada tekanan 1500 V ialah 7.8, 8.9 dan 29.8 μA pada bacaan suhu 25 ° C (kering), 60 ° C (kering) dan 45 ° C (basah). Kandungan garam juga telah meningkatkan arus kebocoran secara selari. Sejumlah kecil (2gm / m2) habuk di dalam filem air sudah mencukupi untuk mencetuskan kebocoran arus pada modul PV. Zarah-zarah debu kecil yang dijumpai melalui FESEM dilinat mengandungi cag dan mempunyai keupayaan untuk melekat dengan beberapa sebatian ionik dari kawasan pantai yang mendorong kepada kebocoran arus modul PV. Penuaan modul PV menyebabkan penurunan arus kebocoran serta sifat rintangan PIDnya yang mungkin disebabkan oleh penurunan rangkuman rintangan electrik.

Kata kunci: degradasi teraruh potensi; modul PV; current kebocoran; kesan penuaan; EL pengimejan.

ACKNOWLEDGEMENTS

My utmost gratitude and earnest obligations to the almighty Allah Subh'anahu Wa Ta'ala for the guidance that He bestowed upon me through all these years of my research work.

I express my sincere appreciation and thanks to my supervisors **Professor Dr. Nasrudin Abd Rahim** and **Dr. Md. Hasanuzzaman** for their brilliant supervision, cordial help, enthusiastic encouragement and kind support. I am deeply indebted to all the lab and office personnel of UMPEDAC for their help and technical support. In this connection, I would like to acknowledge the financial support of University of Malaya (UM) to carry out this research work.

My deepest gratitude goes to my parents and my sister for their blessings and love they hold for me all the way. Finally, I must recognize the unwavering support from my beloved wife that kept me steadfast to the goal through all the pains and sufferings throughout this journey. I could not have achieved this much without her assiduous clinch and unremitting love and care.

TABLE OF CONTENTS

LIST OF FIGURES

LIST OF TABLES

LIST OF SYMBOLS AND ABBREVIATIONS

Symbols:

A_{cell}	:	Solar cell area (m^2)
E_a	:	Activation energy (J/mol)
E_{ab}	:	PV module to surface total energy absorption (W)
E_b	:	Total transferred energy from top surface to bottom surface by convection and conduction processes (W)
E_{ctop}	:	Overall energy loses from top surface to ambient by convection (W)
E_e	:	PV module electrical energy output (W)
E_{mean}	:	Mean EL intensity
eV	:	Electron volt
$E_{mean(STC)}$	:	Nondegraded PV module mean EL intensity
FF	:	Fill factor
G	:	Irradiation (W/m^2)
I_{max}	:	Maximum current (A)
I_{sc}	:	Short circuit current (A)
J_{sc}	:	Short circuit current density (A/m^2)
K	:	Kelvin
K_b	:	Boltzmann constant
LC	:	Leakage current (A)
$LC0$	:	Leakage current at 0°K (A)
P_{max}	:	Maximum power (W)
$P_{max/Pmax\ nom}$	:	Normalized maximum power (W)
p_{sc}	:	Packing factor
R_p	:	Parallel resistance (Ω)

R_s	:	Series resistance (Ω)
R_{sh}	:	Shunt Resistance (Ω)
T_a	:	Ambient Temperature (°C)
T_b	:	Temperature of the back surface of PV module (°C)
T_{sc}	:	Solar cell temperature (°C)
U_{sca}	:	Total heat transfer coefficient from module top surface to ambient (W/m^2K)
U_t	:	Total heat transfer coefficient from module top surface to the back (W/m^2K)
V_{bias}	:	Biased voltage (V)
$V_{bias}/V_{oc\ nom}$	:	Normalized biased voltage
V_{oc}	:	Open circuit voltage (V)
$V_{oc}/V_{oc\ nom}$	:	Normalized open circuit voltage
V_{op}	:	Operating voltage (V)
$V_{op}/V_{max\ nom}$	:	Normalized operating voltage
γ	:	Temperature coefficient of maximum power (%/^oC)

Abbreviations and Acronyms:

AC	:	Alternating current
ARC	:	Anti-reflection coating
BOS	:	Balance of system
CCD	:	Charge coupling device
CSG	:	Chemically strengthen glass
DC	:	Direct current
DH	:	Damp heat
DIV	:	Dark current voltage
DLIT	:	Dark lock-in thermography

DSIMS	:	Dynamic secondary ion mass spectrometry
EBIC	:	Electron beam induced current
EDX	:	Energy dispersive X-ray
EL	:	Electroluminescence
EVA	:	Ethylene vinyl acetate
FESEM	:	Field emission scanning electron microscope
FIB	:	Focused-ion beam
Fraunhofer ISE	:	Fraunhofer Institute for Solar Energy Systems
GHG	:	Greenhouse gas
GW_p	:	Gigawatt peak
HRTEM	:	High-resolution transmission electron microscopy
HVS	:	High voltage stress
IEC	:	International Electrotechnical Commission
I-V	:	Current-voltage
LAICP-MS	:	Laser ablation inductively coupled plasma mass spectrometry
LC	:	Leakage current
LED	:	Light emitting diode
LID	:	Light-induced degradation
LIT	:	Lock in thermography
MPPT	:	Maximum power point tracker
NREL	:	National Renewable Energy Laboratory (USA)
PDMS	:	Polydimethylsiloxane
PE	:	Polyethylene
PECVD	:	Plasma enhanced chemical vapour deposition
PI Berlin	:	Photovoltaic Institute of Berlin
PID	:	Potential induced degradation
POE	:	Polyolefin elastomer
PSG	:	Phosphorous silicate glass

PV	:	Photovoltaic
PVB	:	Polyvinyl butyral
PVT	:	Photovoltaic thermal
QE	:	Quantum efficiency
RH	:	Relative humidity
SEM	:	Scanning electron microscopy
SF	:	Stacking fault
SIMS	:	Secondary ion mass spectroscopy
STC	:	Standard test condition
STEM	:	Scanning transmission electron microscopy
TEM	:	Transmission electron microscopy
ToF-SIMS	:	Time-of- flight secondary ion mass spectroscopy
TPSE	:	Thermoplastic silicone elastomer
XRD	:	X- ray diffraction

CHAPTER 1: INTRODUCTION

1.1 Potential Induced Degradation

Potential induced degradation (PID) is the dilapidation in the performance of photovoltaic (PV) modules incurred by high voltage. Although factors (voltage, temperature, and humidity) that provoke PID to exist in isolated PV systems, PID mostly occurs in large PV power plants wherein transformerless inverters and/or PV modules with low resistance ethylene vinyl acetate (EVA) are employed. There is a clear trend in the PV industry to use transformerless inverter topologies because it is more compact and lightweight and provides higher conversion efficiency compared to the transformer based topologies (Kerekes et al., 2011). Moreover, PID is likely in modules with PID prone cell. In recent years, concern about PID is intensifying as the string voltage of PV modules is increasing rapidly due to fast growth in PV power plant. From both technical and financial viewpoint, PID has got an immense adversative effect on installation and operation of big scale PV power plants. Accordingly, much attention and effort to remove or reduce PID and its effect of PV module has been commenced by the researchers as well as the manufacturers and investors.

This chapter relates the background and importance of PID study, an overview of the worldwide status of PV power generation, a brief description of PV module degradation, specific problem statement, and the objectives of the present research and realistic scope along with brief research method.

1.2 Status of Photovoltaic Power Generation System

Global energy demand is increasing enormously day by day due to population growth as well as rapid socio-economic development, advancement in human lifestyle, and industrialization of the developing countries (Saha & Rowley, 2015). The current

energy sector is mainly dependent on fossil fuels with their availability being site-specific and reserve limited (Hossain et al., 2015). On the other hand, greenhouse gas (GHG) emission from the burning of fossil fuels is responsible for global warming and climate change, causing serious human health issues and dislodgement of inhabitation (Wu et al., 2016). Hence, safe and sustainable energy sources are essential to ensure an incessant supply of energy and to preserve the nature and environment as well (Kim et al., 2000). Solar energy is one of the most promising and prospective renewable energy resources that has the potential to be a sustainable candidate to solve the above problems. The PV system becomes promising due to its flexibility in design and size, moderate installation cost, long lifespan with low operating cost and environmental friendly service (Almasoud & Gandayh, 2015; Serrano-Luján et al., 2015; Solangi et al., 2015; Yu et al., 2016). Since the last 10 years, PV industry has become one of the fastest growing industries in the world with an annual growth rate of 50% and its size is increasing day by day. (Jäger-Waldau, 2013). The global cumulative PV installation capacity from 2005 to 2015 is shown in Figure 1.1. In 2005, the global PV installation capacity was only 5.1 GW and reached to a significant level of 277 GW in 2015 (REN21, 2016). Crystalline silicon (c-Si) PV technology captures the largest share of the worldwide PV installation. Some technologies such as thin film, dye-sensitization and perovskite etc. are very already proved to be potential to compete with the c-Si technology. Development of new materials and improvement in manufacturing expertise is making PV technology more and more cost-effective with other renewable energy technologies. However, low conversion efficiency, especially at high module temperature, is still a concern in PV power generation. Figure 1.2 shows the market share of three different PV technologies where the crystalline silicon (c-Si) modules are dominated. The mono and multi-crystalline Si solar cell were responsible for more than 90% of the global energy generated by solar cells in 2015, with roughly 23% on mono-

Si and 70% for multi-Si. The thin film technologies which include amorphous Si (a-Si), CdTe and $CuIn_xGa_{(1-x)}Se_2$ (CIGS) have market penetration around 7%.

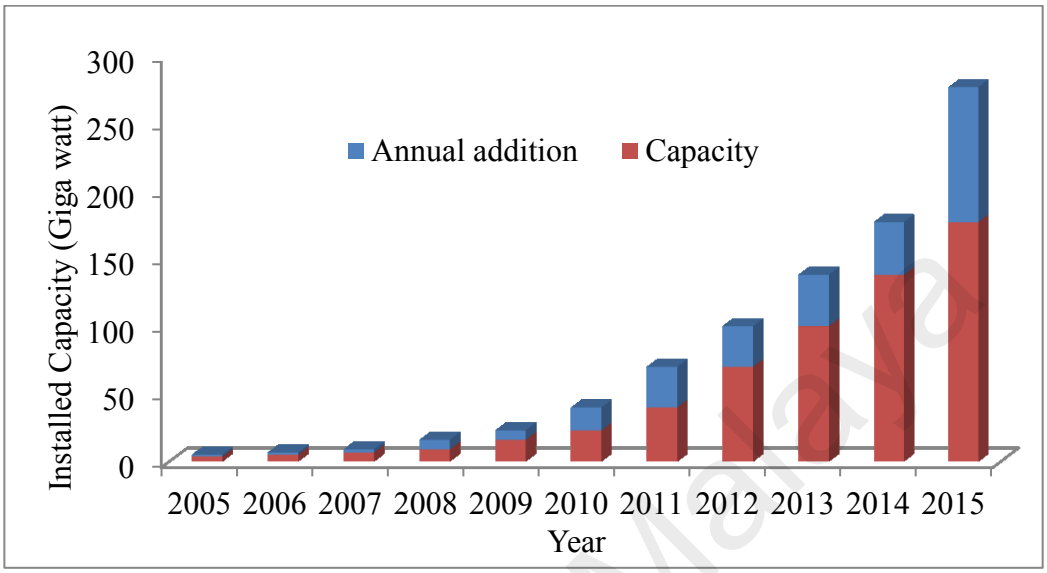

Figure 1.1: Growth of worldwide PV installed capacity from 2005 to 2015 (REN21, 2016)

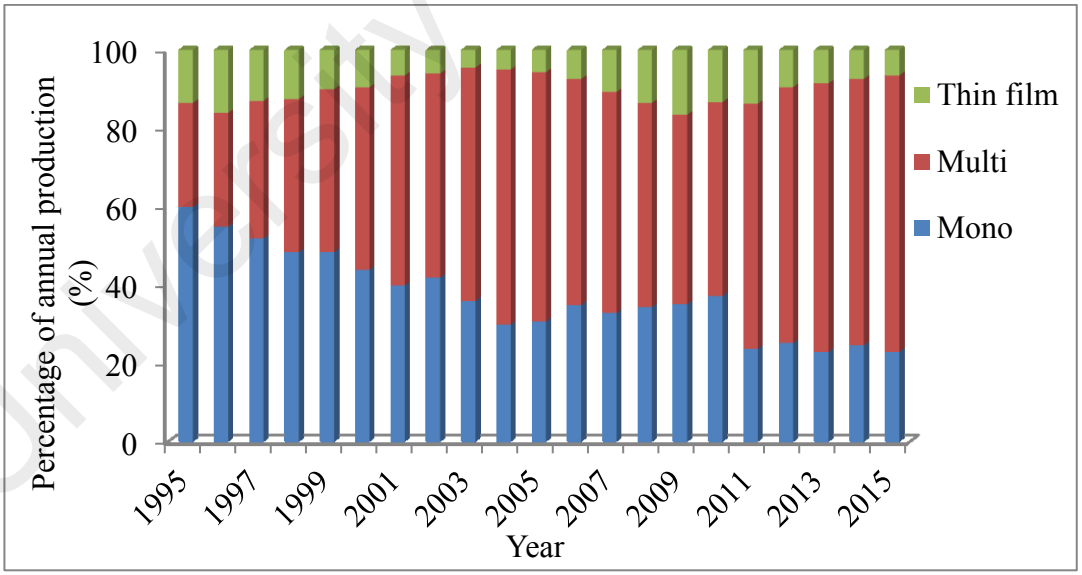

Figure 1.2: Percentage shares of three PV technologies in global annual PV production
(Fraunhofer, 2016)

1.3 Degradation Behaviour of PV Modules

The two key factors that determine cost-effective energy harvesting from the solar radiation are: (i) efficiency at which sunlight is converted into power and (ii) how this conversion relationship changes over time due to aging. Along with system price and capital interest rate, PV module lifetime is the vital factor that determines the cost of solar electricity. The lifespan of PV modules are shortened by two phenomena, viz., light induced degradation (LID) and potential induced degradation (PID).

Generally, PV solar modules are degraded due to longtime field aging of either the glass or encapsulant or cell materials. Several types of digression or degeneration can be observed at the module level, such as discoloration of encapsulant in some degrees and extend from yellow to dark brown, moisture intrusion, delamination of encapsulant and corrosion (Quintana et al., 2002), tears and bubbles in the back sheet etc. In cell level, performance of silicon-based PV (both crystalline and amorphous) decreases due to light socking which is known as light-induced degradation (LID). While LID is the most common phenomenon responsible for PV performance deterioration, several other processes such as reduction of anti-reflective (AR) coating performance, the formation of hotspots (Simon & Meyer, 2010), and cracks in PV cell caused by mechanical stress etc. are also liable for degradation. In addition, optical/physical, electrical and thermal degradation effects may be linked with PV power and performance degradation (Parretta et al., 2005). It is to be noted that several causes of degradation effects may co-exist in the same module, even in the same cell (Kaplani, 2012). Normally, the estimated lifetime of the PV modules is about 20–25 years. PV modules power should not drop more than 20% of their nominal power over this period (Thevenard & Pelland, 2013; Bandou et al., 2015).

The number and the size of PV plant has increased quite rapidly in last decade (Mints, 2012). Figure 1.3 shows the capacity of several large-scale PV power plant, e.g., 300 MW in France (2015), 345 MW in India (2012), 480 MW in China (2013) and the largest power plant installed in 2015 at California, USA has a capacity of 579 MW (Wesoff, 2015). In the PV systems, the modules are usually linked in series into the strings in order to increase the system voltage. The number of solar panels connected in series increases as a result of increase of PV plant capacity, and the system voltage is reached as highs of 1500 V (Moskowitz, 2015).

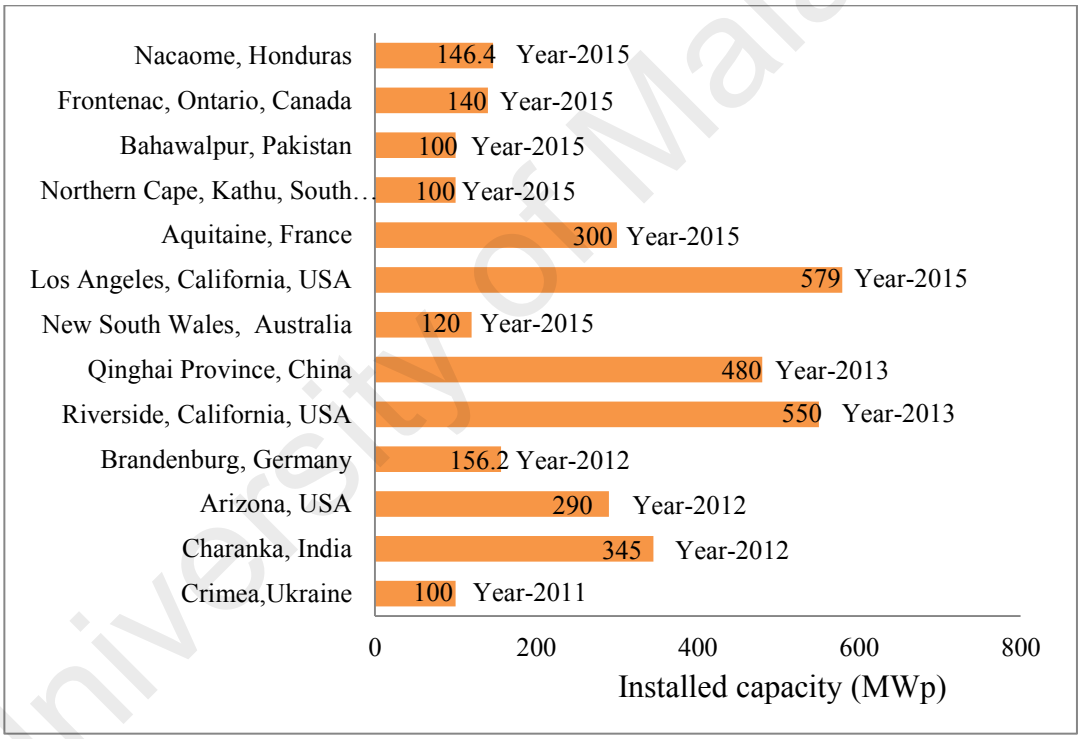

Figure 1.3: Several large-scale PV power plant installations in the world (Andrew, 2011; Wesoff, 2015; PVresources, 2016)

The metallic casings of the modules are typically grounded. This prompts a voltage predisposition of the individual modules with respect to their frame resulting in a delineation of high potential difference to the panel in respect to ground which causes a high voltage stress (HVS). This phenomenon was pointed out and investigated by

Hoffman and Ross (1978). The sign and magnitude of HVS depend on the string length, type of inverter used for coupling the DC yield to the AC system and the position of the module in the string. HVS causes a gradual power reduction of PV system as a consequence of leakage current flow from module frame to the solar cell (del Cueto & McMahon, 2002; Shiradkar et al., 2013; Dhere et al., 2014b). As a result of leakage current flow, ions are deposited on solar cell surface. Migrated ions alter the emitter performance of the solar cell. The ions also go into the emitter layer and produce one-dimensional metallic lines by accepting an electron from the emitter, as a result, ohmic shunt is produced (Lausch et al., 2014b) and produces potential induced degradation (PID).

In 2005, potential induced degradation (PID) was first detected in PV power plant by Sun-power in the n-type crystalline silicon solar cells when subjected to high positive potential (Swanson et al., 2005). A significant reduction of fill factor (FF), short-circuit current density (J_{sc}) and open-circuit voltage (V_{oc}) were also reported. At high negative potential, p-type crystalline silicon solar cells are also affected by PID as confirmed by NREL and Solon at 2010 (Koch et al., 2011) and the effect of PID can be accelerated in presence of high temperature and humidity (Hacke et al., 2010). Nowadays PID has become a vital issue because of the increment in the utility-scale arrangement of high system voltage installation in the large solar power plants which are near 1000-1500V (Ali-Oettinger, 2015; Ding et al., 2016).

1.4 Demand of PID Research

Potential induced degradation is becoming a matter of growing concern to the PV manufacturer because it can reduce the system power output as high as 70%, incurring a huge operation and maintenance cost of the PV system (Rutschmann, 2012). PID cause enormous power loss by shunting of cells in a PV module. A study on PID, directed by

PI Berlin, reported that PID in 20 power plants in Germany each with 12 strings of PV modules, demonstrated 10-15% power degradation in 39% of the strings. In another study in a 10.7-MW solar power plant in Spain, it was found that PID affected 41% of the modules (Singh, 2015). As reliability and durability are the key factors to make the PV system cost effective compared to other traditional energy sources, PID of PV modules has now become a great challenge for the module manufacturers. Therefore, researchers, industries, and policymakers are giving more attention to increase the PV module lifetime with a desirable performance. Figure 1.4 shows the different countries involved in PID research where United States dominates the share and Figure 1.5 shows the involvement of different famous research institutes involve in the PID research.

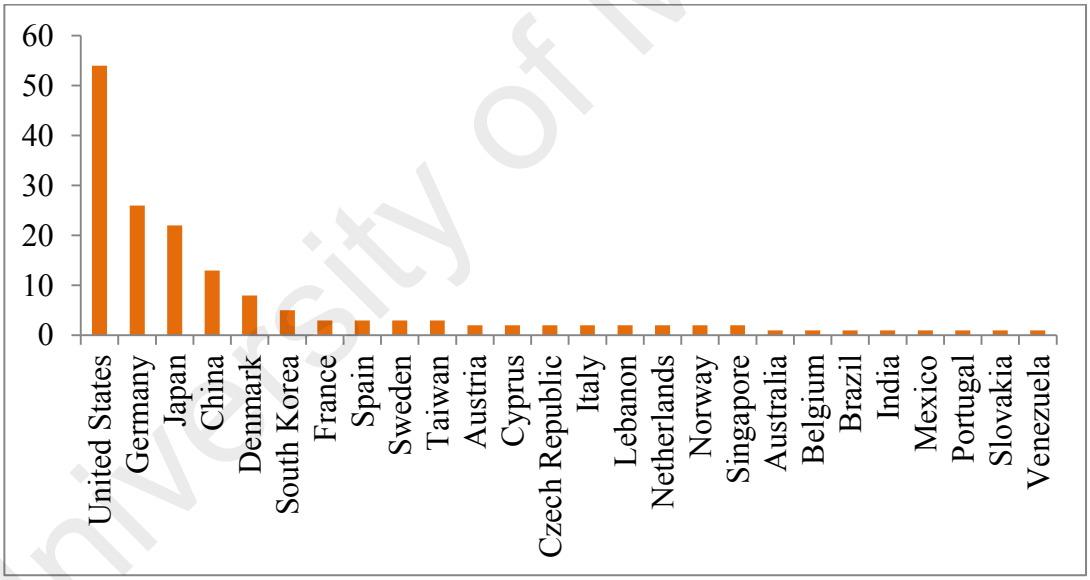

Figure 1.4: Number of PID research conducted by different countries over the world taken from Scopus database
(Scopus, 2018)

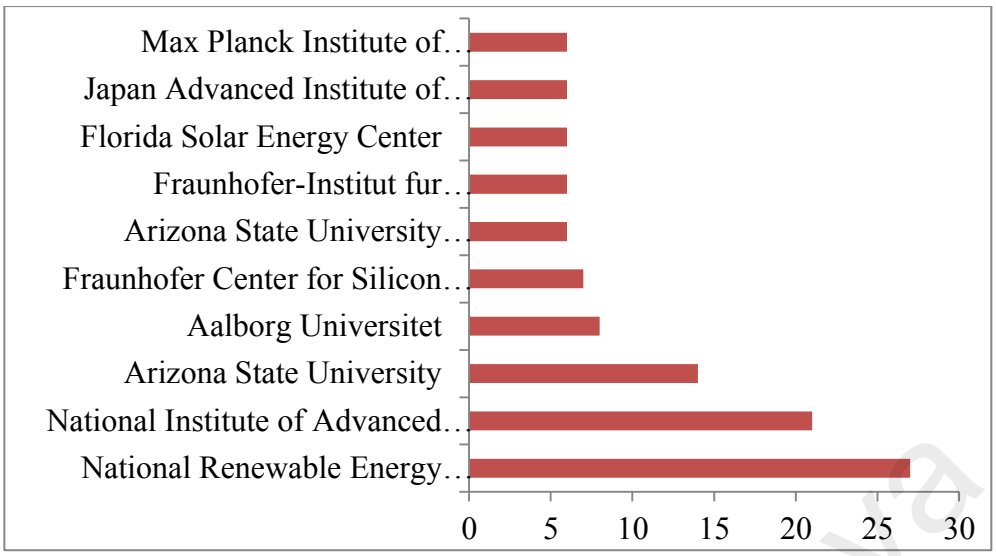

Figure 1.5: Different famous renewable energy research institutes involving in PID research data taken from Scopus database
(Scopus, 2018)

1.5 Problem Statement

In the presence of HVS on the solar PV module, the flow of leakage current can be from cell to the frame of PV module or from frame to cell depending on the high voltage polarity. The HVS leakage current of PV module is an important factor that indicates the PID performance of that PV module. Recently, Kang et al. (2015) have mentioned that PID of a PV module at certain voltage stress is proportional to the total leakage current. The PV modules' leakage current varies according to the different PV system design, operating and environmental conditions such as string voltage size, temperature of PV module, humidity, wet surface condition, deposition of salt or dust on the surface etc. The knowledge concerning the effect of different operating conditions on the leakage current behaviour of PV module is encouraging because this assists to estimate the possibility of degradation of PV module due to PID under a definite environmental condition. In addition, the leakage current behaviour of PV module can be degraded due to field aging. Furthermore, the leakage current enhances with the high module surface temperature and moisture. Therefore, an investigation on

the degradation due to leakage current behaviour as a result of aging of the PV module at real field condition is important.

In order to investigate actual PID characteristic of PV module, an on-site testing method is used. However, this process is very much lengthy and may take several years (del Cueto & Rummel, 2010). The extent of degradation of PV modules at a certain high string voltage (600V or 1000V or 1500V) after the lifetime is imperative for PV power plant. Before installation, the PV module should be tested according to the standard PID test procedure. International Electrotechnical Commission (IEC) has published standards for PID testing in laboratory condition titled as IEC TS 62804-1:2015 (IEC 62804, 2015). A relationship in-between the on-site PV module and IEC standard for laboratory PID testing is very much essential from which a prediction of power loss PV module due to PID in the real field can be obtained. At on-site, silicon PV module naturally degraded due to long-time light socking which is termed as light-induced degradation (LID). Both PID and LID take place together in most PV power plants.

The major problems has identified as research gaps regarding the PID behaviour of PV module are summarized as follows:

- Investigation of the effect of operating parameters (such as temperature of PV module surface, wet surface condition, dust or salt deposition on the module surface etc.) on the high voltage leakage current.
- Most of the investigations on PID behaviour of PV module have been done by using laboratory testing method. However, the investigation on on-site real field PID is rare in literature. So to explore the actual PID characteristic of PV

module, it is crucial to investigate the on-site degradation characteristic of PV module.

- A comparative investigation in-between the laboratory PID test standard and on-site PID of similar modules.
- Investigation on the effect of long-time real field aging on performance degradation of PV module.

1.6 Objectives of the Research

The aim of the research is to investigate the PV module's degradation behaviour both on-site and laboratory condition to establish a functional relationship between them as well as to study the impact of different environmental and operating parameters on the HVS leakage current which accelerates the PID phenomenon. The specific objectives of the present research can be enumerated as follows:

1. To investigate the effect of different operating factors on the high voltage stress leakage current of PV modules;
2. To investigate the on-site potential induced degradation behaviour of PV modules under Malaysian climate;
3. To analyse the light-induced degradation of PV module due to real field aging in Malaysia climate under certain condition;
4. To examine the effect of field aging on the leakage current of PV module.

1.7 Scope and Limitation of the Research

The current research covers the following specific works:

1. To investigate the amount and rate of degradation of PV modules under a certain string voltage for a certain period of time. Degradation is related to the measurement of maximum power and shunt resistance of PV module.
2. To analyse PV module degradation in terms of power output and shunt resistance due to different periods of field aging under a certain climate condition. In this case, PV modules are free of string stress and degradation occurs only due to the impact of different environmental impacts such as long-time sunlight exposure, ingress of moisture and dust deposition etc.
3. To investigate the different environmental factors such as high surface module temperature due to exposure to sunlight, surface wetting due to rain or dew etc., deposition of dust and salt on the module surface.
4. To evaluate the effect of different field aging periods on the high voltage stress leakage current as well as PID of PV module.

There are some limitations in this research work as follows:

1. The on-site PID degradation has been investigated only for 240V string size. Investigation of the effect of different higher string sizes like 300, 400, 500V etc. on the on-site PID is not possible due to existing of only one type string voltage size in the on-site PV plant.
2. Laboratory PID test has been carried out only by aluminium foil method; chamber method has not been followed. So a comparative investigation in-between on-site PID and laboratory PID by chamber method is a limitation in this work.

3. Light-induced degradation due to real field aging has been compared in between different PV modules made by different manufacturers.

1.8 Organization of the Thesis

In the present research work, investigation on the effect of high voltage stress (HVS) on PV module performances has been carried out through focusing the real field PV module degradation both in presence and absence of high string voltage stress conditions and then investigating the effect of different operating parameters on the HVS leakage current characteristics of different PV modules. The background, methodology and outcomes of the research have been detailed in six (6) chapters, the first chapter being a general introduction along with specific objectives and scope. The rest of the chapters are organized as follows:

Chapter 2: This chapter is the summary of the previous literature about the high voltage stress leakage current, PID, and other possible degradation of PV module due long time field aging. This chapter is ended up by re-counting with a summary of the research gap.

Chapter 3: This chapter presents some theoretical background related to the fundamentals of PID and recovery process of PV module, PID detection techniques, IEC standard test condition of PID and a theoretical concept of the relationship between EL intensity with the PV module performance.

Chapter 4: The detail research methodology along with the meteorological condition of the PV plant site, specifications of different PV modules used to conduct the experiment, experimental setup, instrumentations and lastly the experimental testing conditions are described in this chapter.

Chapter 5: The experimental results along with corresponding explanation behind have been discussed in this chapter. The outcome of the experiments such as effect of different factors on the leakage current, on-site PID and performance degradation of PV module due to different field aging are detailed in this chapter.

Chapter 6: The thesis wraps up with some concluding remarks and recommendations of future work in chapter 6.

CHAPTER 2: LITERATURE REVIEW

2.1 Introduction

Potential integrated degradation (PID) was first detected in 2005 (Swanson et al., 2005). An extensive overview of such research works has been compiled in this chapter wherein integrative method has been followed to make critical scrutiny of the available hypotheses regarding PID that will be helpful to find the research gaps in this field. Relevant literature has been gathered basically from peer-reviewed journal articles, specialized conference articles, thesis reports, internet sources, and personal communications with the specialist in PID. This chapter starts with a description of the impact of high voltage stress leakage current on PV modules, followed by possible pathways of leakage current and different environmental factors that affect the PV module leakage current behavior. Then it contains the overview of different PV module PID mechanisms, testing, and prevention process. Finally, a brief description of possible research gap has been stated to set up the objective of the research.

2.2 Leakage Current

Generally, PV modules in PV power plants experience a high voltage stress (HVS) from the string voltage owing to the difference in potential between the frame of PV module and active circuit, HVS being dependent on the string size and module position within string. The HVS generates leakage current through the PV array, which has been identified as one of the primary cause behind PID (del Cueto & McMahon, 2002; Shiradkar et al., 2013; Dhere et al., 2014b).

2.2.1 Impact of Leakage Current on PV Module

The flow of leakage current through glass and EVA prompts the collection of charges on the surface of solar cells. As a consequence, the surface recombination of the

light generated minority carrier increases and finally drops the output performance of PV module. The higher the leakage current, the higher the amount of ions will deposit on the cell surface. Hence, HVS leakage current is an important parameter and a determinant of PID characteristics of PV modules. There are several pathways of a PV module's leakage current (described in details in the following section) where some are not detrimental in initiating PID. Generation of leakage current is influenced by humidity and module temperature. There have been many attempts to correlate PID and leakage current. Kang et al. (2015) reported a mathematical relationship between the leakage current and PID is followed as:

$$PID_{T_1H_1V_1t_1} = PID_{T_2H_2V_2t_2} \times \frac{t_1}{t_2} \times \frac{I_{T_1H_1V_1}}{I_{T_2H_2V_2}} \quad (2.1)$$

where $PID_{T_1H_1V_1t_1}$ and $I_{T_1H_1V_1}$ are the PID and respective leakage current of PV module at stress condition voltage V_1, humidity H_1 and module temperature T_1 with a time period of t_1. $PID_{T_2H_2V_2t_2}$ and $I_{T_2H_2V_2}$ are the PID and respective leakage current for the stress condition of voltage stress V_2, humidity H_2 and module temperature T_2 with a time period of t_2.

2.2.2 Leakage Current Pathways

Leakage currents can flow along several different pathways for a typical c-Si PV module; these are described by the followings paths 1 to 6 and also shown in Figure 2.1 (a) (Pingel et al., 2010; Luo et al., 2017).

1. $Cell_{Surface} \Leftrightarrow Bulk_{Encapsulant} \Leftrightarrow Bulk_{Frontglass} \Leftrightarrow Surface_{Frontglass} \Leftrightarrow Frame_{Module}$

2. $Cell_{Surface} \Leftrightarrow Bulk_{Encapsulant} \Leftrightarrow Bulk_{Frontglass} \Leftrightarrow Bulk_{Sealant} \Leftrightarrow Frame_{Module}$

3. $Cell_{Surface} \Leftrightarrow Bulk_{Encapsulant} \Leftrightarrow Interface_{(glass-encapsulant)} \Leftrightarrow Bulk_{Sealant} \Leftrightarrow Frame_{Module}$

4. $Cell_{Surface} \Leftrightarrow Bulk_{Encapsulant} \Leftrightarrow Bulk_{Sealant} \Leftrightarrow Frame_{Module}$

5. $Cell_{Surface} \Leftrightarrow Bulk_{Encapsulant} \Leftrightarrow Interface_{(Backsheet-encapsulant)} \Leftrightarrow Bulk_{Sealant} \Leftrightarrow Frame_{Module}$

6. $Cell_{Surface} \Leftrightarrow Bulk_{Encapsulant} \Leftrightarrow Bulk_{Backsheet} \Leftrightarrow Surface_{Backsheet} \Leftrightarrow Frame_{Module}$

Leakage current pathways of a typical thin film PV module are shown in Figure 2.1(b). Normally, in a thin PV module, a transparent conducting oxide (TCO) layer exists in between the glass and cell. Moreover, a glass cover is also often used as the back sheet in thin film PV module. Despite the variances in the module assembly, thin-film PV modules usually have the analogous leakage current pathways to those of c-Si PV modules, excluding that an extra pathway through the bulk of glass back sheet of the module. Among the leakage current pathways, the 1st pathway is often exaggerated in outside operating conditions because the glass surface conductivity influences significantly due to change of different environmental factors such as dust deposition, rain, module temperature and high relative humidity (Hoffmann & Koehl, 2012; Dhere et al., 2014c).

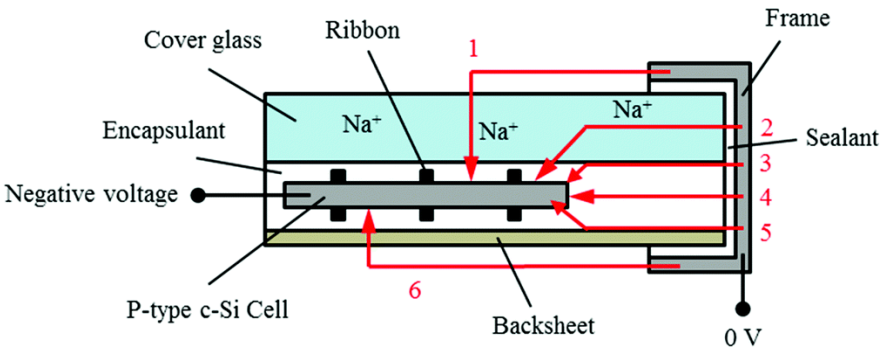

(a)

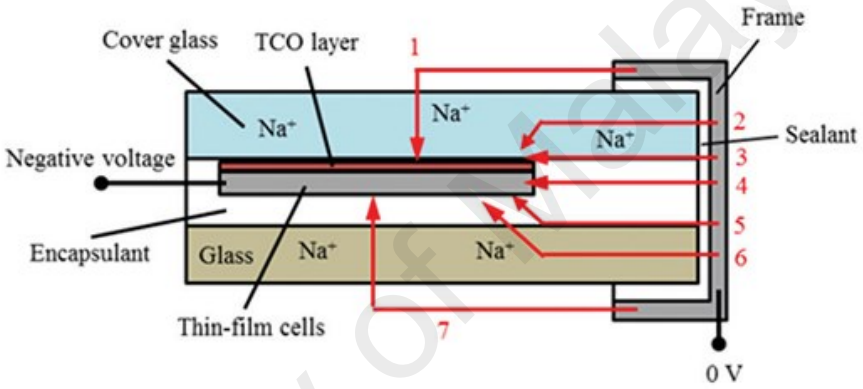

(b)

Figure 2.1: High voltage stress leakage current pathway of (a) p-type c-Si (b) thin film PV module
(Luo et al., 2017)

2.2.3 Controlling Factors of Leakage Current

Leakage current of PV module relies upon a few factors, for example, (1) PV module factors (glass surface electrical resistance, composition of glass, encapsulant electrical resistance) (2) system or environmental factors (string voltage, module surface temperature, humidity, rain, dew or fog, dust and so on. The effect of module temperature and humidity on the PV module leakage current has been reported to observe under a HVS of 600 V (Hoffmann & Koehl, 2012; Dhere et al., 2014c) Figure 2.2 shows the leakage current characteristics at several voltage stresses and different

module temperatures and humidity; on the other hand, consequence of humidity on the HVS leakage current is presented in Figure 2.3. It can be observed that for very low and high humidity levels the leakage current tends to saturate; however, in the middle range 25-70%, the leakage current linearly increases with relative humidity. At high humidity level, leakage current becomes saturated due to the fact that glass surface conductivity increases enough after certain threshold humidity.

At high cell temperature, the diffusion of metal ions towards the cell surface is seen to increase. The volume resistivity of encapsulant materials decreases with the increase of temperature. For EVA the volume resistivity can be dropped 2 fold orders due to an increase in temperature from 23 to 75°C (Kapur et al., 2015).

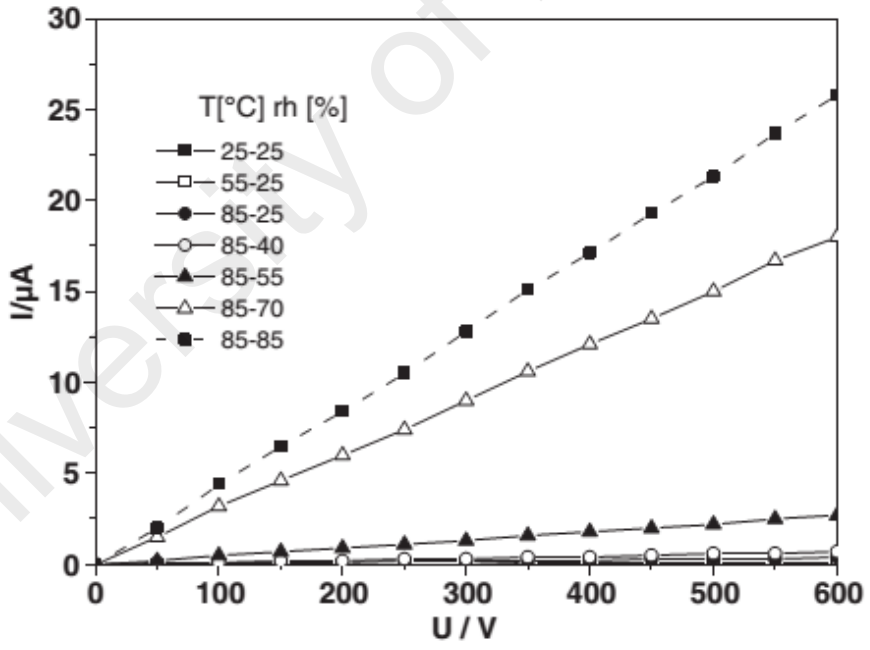

Figure 2.2: Leakage current as a function of the high voltage bias for different temperature/humidity conditions in the climatic cabinet (Hoffmann & Koehl, 2012)

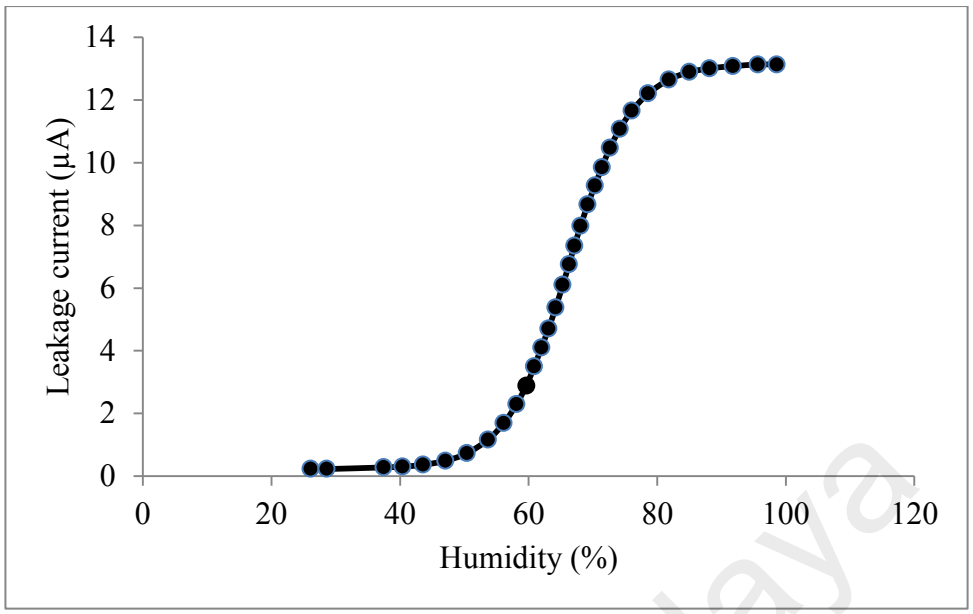

Figure 2.3: Effect of humidity on the leakage current of PV module at the stress of 300V and 85°C
(Hoffmann & Koehl, 2013)

Figure 2.4 shows an Arrhenius plot of the leakage current at 1000 V negative bias for three identical modules with different methods of contact: frame only (air), aluminium foil on the glazing (Al) and damp-heat exposure at 85% relative humidity (Hoffmann & Koehl, 2012). Koehl and Hoffmann (2016) reported that at outdoor under similar condition, the increase of PV outdoor exposure time causes to increase the leakage current of that PV module. The authors assumed a soiling effect which grew due to the deposition of salty aerosols and dust on the module surface which provides an excellent matrix for humidity, keep it stored, and in addition ions from the soil increases the surface conductivity of module surface. The mathematical relationship of relative humidity (*RH*), voltage (*V*) stress and module temperature (*T*) in the Arrhenius equation is given as (Kindyni & Georghiou, 2013):

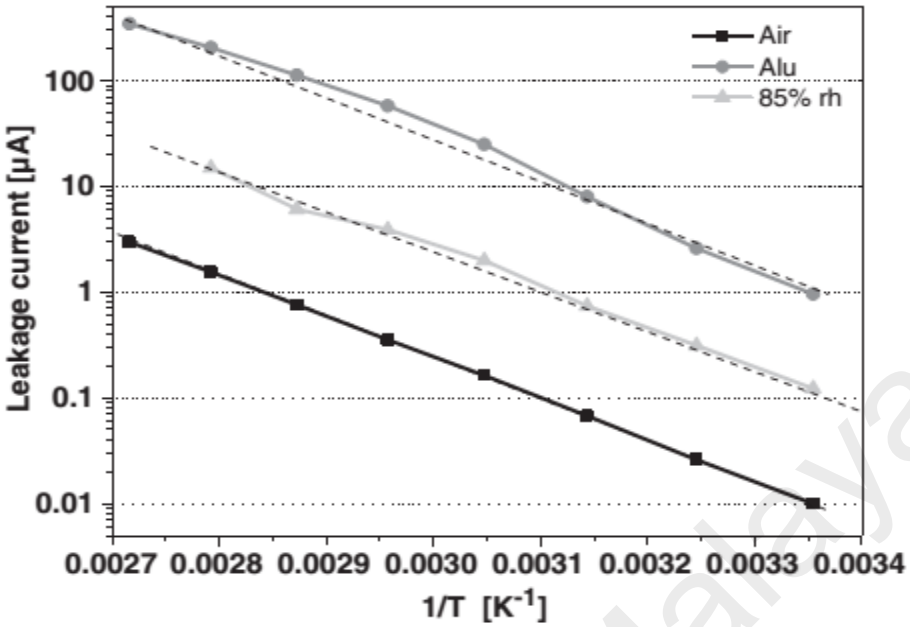

Figure 2.4: Effect of module temperature on high voltage PV module leakage current
(Hoffmann & Koehl, 2012)

$$I_{LC} = I_{LC\,0} \exp^{-[E_a / k_b T]} \tag{2.2}$$

$$\ln I_{LC} = \ln I_{LC\,0} - (E_a / k_b) \times \frac{1}{T} \tag{2.3}$$

where I_{LC} is leakage current, I_{LC0} is leakage current at 0K, E_a is the activation energy, k_b is Boltzmann's constant ($k_b = 8.617 \times 10^{-5}$ eV/K), T is the module's absolute temperature in Kelvin.

Deposition and accumulation of dust, and salt on the PV module surface is very much likely, especially in coastal areas. Rate of dust accumulation may vary place to place. Adinoyi and Said (2013) found 6.184 g/m^2 of dust on PV module for an exposure period of ten months (February to December) at Saudi Arabia (Dhahran). Cabanillas and Munguía (2011) reported 2.326 mg/cm^2 of dust within 20 days at México. The surface of glass become wetted as a consequence of rain, dew, fog or mist and the

presence of dust and salt in wet surface condition, the properties of glass become changed (Hacke et al., 2015a; Yilbas et al., 2015). Suzuki et al. (2015) observed that, as a consequence of salt mist preconditioning, the PID of PV module becomes accelerated.

Performance of PV module is degraded because of field aging, too. Pozza and Sample (2016) reports age degradation behaviour of PV module due to 20 years field exposure, wherein the authors found an average power degradation rate of 0.22% per year. The authors concluded that the principal cause of PV module performance failure is yellowing of encapsulant material which might occur due to moisture ingresses, chemical leached out of the encapsulant materials. Moreover, Sinha et al. (2016) mentioned that the electrical property of PV module deteriorates as a consequence of EVA discoloration. So that long-time field aging has a significant to alter the high voltage degradation of PV modules.

Table 2.1: Leakage current at different conditions

Author	Experiment Site	Experimental Condition	Leakage Current
Schutze et al. (2011a)	Freiburg, Germany	600V, Module temperature 25°C, Wet surface condition	0.95µA
Hoffmann and Koehl (2012)	Freiburg, Germany	P-type c-Si PV module, 600V, Module temperature 10°C, Module surface humidity above 90%	95nA
Dhere et al. (2014a)	Florida, USA	60 cell multi crystalline Si PV module, 600 V, outdoor	Maximum ~ 400nA
Dhere et al. (2014c)	Florida, USA	60 cell multi crystalline Si PV module, 600 V, outdoor	~ 4 µA in rainy condition
Koehl and Hoffmann (2016)	Canary Island, Spain	60 cell Crystalline Si PV module, 100 and 150V stress outdoor condition	Maximum 2µA and 3µA respectively

2.3 Explanation of PID Mechanism

In order to mitigate PID, it is important to understand the degradation mechanism i.e. the root cause of PID, how it develops and from where it starts in solar modules. Some common phenomena such as polarization, electrochemical corrosion, ionic diffusion, and sometimes structural degradation occur in PV modules as a result of high system voltage exposure its material (Joh et al., 2011). In a PV system, during electrolytic corrosion electrolysis might occur due to high voltage, where water vapour acts as an electrolyte solution, the PV cell acts as an anode, and the frame acts as a cathode; consequently, material such as silicon nitride (used as anti-reflection coating or simply ARC), ethyl vinyl acetate (or simply EVA used as an encapsulant) and the active cells are degraded. Electrochemical corrosion causes the transport of ionic elements which results in leakage current flowing from the cell to the module exterior (Ross et al., 1989). In the last couple of years, operative advancement has been accomplished in realizing the mechanism of PID. There are a few speculations concerning the main driver of this PID process. The overall PID process can be split into three different phenomena, such as (i) polarization of the PV module, (ii) ionic migration, and (iii) shunting of the PV cell p-n junction. The phenomena are explained in the following sections.

2.3.1 Polarization Process

Polarization is the development of dipole moment within the module component, such as glass, encapsulant or antireflection coating (ARC). This is a reversible and non-destructive process. At high voltage, the surface of a PV module can be polarized because of the dielectric behaviour of module components and as a result, static charges accumulate on PV cell surface. Due to the exposure of the positive voltage on the module to the ground, leakage current will flow from the cell to the ground as a result

which a negative charge is left on the front surface of the cell (Swanson et al., 2005). This negative charge attracts positive charge carriers of n-type emitters on the front surface of p-type solar cells, where they recombine with electrons and are lost. In this way, the bands in the emitter are locally destroyed. However, when a module is exposed to a negative voltage the surface polarization reverses which has no adverse effects on the module, rather its performances may be slightly enhanced because the light-created holes are now repulsed by the front surface and gathered back into the junction (Koch et al., 2011). In case of n-type solar cells, the reverse phenomenon as described above will occur.

2.3.2 Ion Migration Process

In wet condition, the PV glass surface becomes conductive and PID susceptibility of a module exposed to high voltage is increased (Hoffmann & Koehl, 2012). In the presence of high voltage, the ionic species contained in the glass can migrate towards the cell through the encapsulant and accumulate on the cell surface (Naumann et al., 2014). This creates an electric field and consequently ARC passivation or other passivation layer can be deserted; as a result, the surface recombination increases and the output power drops (Ogita & Tachihara, 2015).

2.3.3 Shunting Process

When ionic species accumulate on the ARC layer, there is a possibility that ions can diffuse into the emitter layer and act as donor atoms which neutralize the negative doping of the emitter. In this case, the junction is gradually diminished, and the PV effect of the cell decreased (Bauer et al., 2012; Naumann et al., 2012). The ionic diffusion occurring through the stacking faults, which normally generate within the solar cell during solidification, leads to a shunting of the p-n junction. As a result, a decrease in shunt resistance and power output is observed. The exact driving

mechanisms for the Na^+ migration within the solar cell are still not fully understood. However, it is elucidated in some studies that a potential of a few volts across the silicon nitride (SiN_x) layer is enough to trigger PID (Naumann et al., 2013). Sometimes lattice damage can occur by the accelerated positive charge due to high voltage over silicon nitride, which strongly reduces the parallel resistance (R_p) of the modules (Naumann et al., 2014).

2.3.4 Clarification of PID Mechanisms by Na^+ Ion Diffusion

Recently, it has been reported that Na^+ ions contained within the glass of PV modules have a crucial role in PID (Hacke et al., 2010; Stika et al., 2014). Soda lime glass, ethylene vinyl acetate (EVA) and the solar cell's anti-reflective coating (ARC) are the main components of a typical commercial PV module. Sodium is normally used as part of the glass' composition to reduce the manufacturing cost by reducing the melting point of glass (Min'ko & Binaliev, 2013). In the presence of water, liquid or vapour, Na^+ can leach out by the following ion exchange reaction (Sinton & LaCourse, 2001).

$$(Si-O-Na)glass + H_2O \rightarrow (Si-O-H)glass + Na^+ + OH^-(solution)$$

At high voltage stress, these sodium ions can diffuse from the front glass to the cell surface and precipitate at the ARC layer. They sometimes diffuse through the defect of the ARC layer and cell into the junction (Hacke et al., 2011). However, it is reported that the occurrence of PID is not only correlated with a specific ion, rather it can occur with any ionic species (Nagel et al., 2011; Schutze et al., 2011a). The rate of positive ion migration is mainly dependent on the applied system voltage electrical resistance of the encapsulant material, the humidity, and the temperature.

2.3.5 Microstructural Investigations of PID Mechanism

For further clarification of the PID mechanism, microstructural features of PV modules before and after PID have been investigated by different researchers. Using secondary ion mass spectroscopy (SIMS), it was reported that during the PID process, Na^+ ions migrate towards the solar cell through the encapsulant (Hacke et al., 2010; Nagel et al., 2011; Stika et al., 2014). It was assumed that these Na^+ ions gather on the interface between the ARC and silicon layers. By the time of flight secondary-ion-mass spectroscopy Figure 2.5, it was shown that during PID the concentration of Na^+ ions is increased both at the ARC layer and the ARC-Si interface (Naumann et al., 2012).

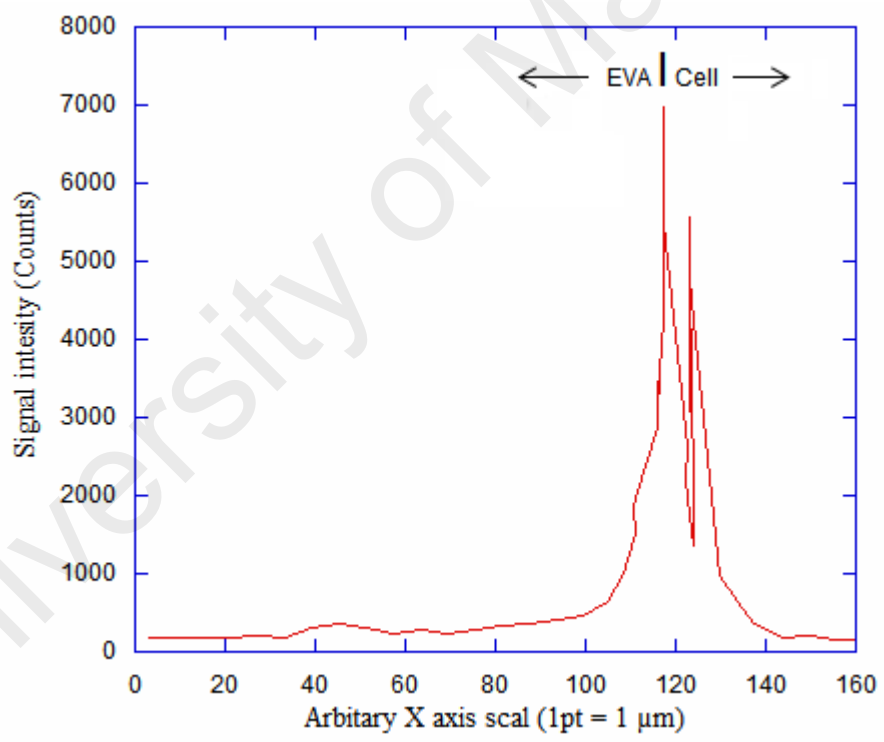

Figure 2.5: Na^+ ion profile at EVA and cell layer of a solar module after PID (Kapur et al., 2015)

Na^+ ions can diffuse into the SiN_x layer, this diffusion process depending on the characteristics of the SiN_x layer (i.e. density and refraction index). It is assumed that a distribution of positive charges within the SiN_x layer (thickness ca. 70 nm) is formed

which induces negative charges at the ARC layer. These negative charges repel the charges in the n-doped emitter resulting in band bending in the emitter section as portrayed in Figure 2.6. The solid line represents the normal band structure before ionic deposition and the dotted line represents the bent band structure after ionic deposition. The built-in potential of the p-n junction vanishes due to band bending.

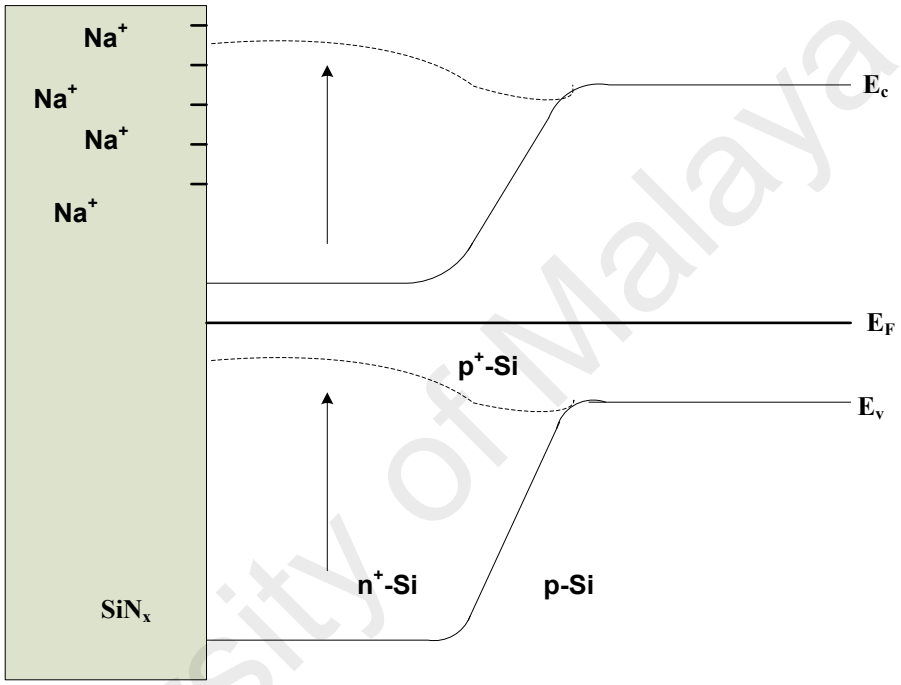

Figure 2.6: Surface charge induced band bend of a-Si solar cell before PID (solid) and after PID (dashed)
(Naumann et al., 2012)

Recently, through the lock-in electron beam induced current (EBIC) technique, Bauer et al. demonstrated the presence of a huge number of local spot shunts having diameters between 10 µm and 30 µmin on a PID affected cell (Bauer et al., 2012). This caused a sharp decrease in the parallel resistance, $R_{p,}$ of the modules. To explain the mechanism of these micro-shunts, a model has been proposed (Raykov et al., 2014). It was assumed that a large accumulation of Na^+ ions at the ARC layer created a charge double layer in the way that positive charges (Na^+ ions) entice or form a negative charge

layer between the n+ emitter and positive charges layer. So, in the vicinity of the Si negative charge layer, an electrical field is created which repels the emitter electrons, as shown in Figure 2.7. The emitter might even be inverted to a p+ conducting region due to electrical field induction.

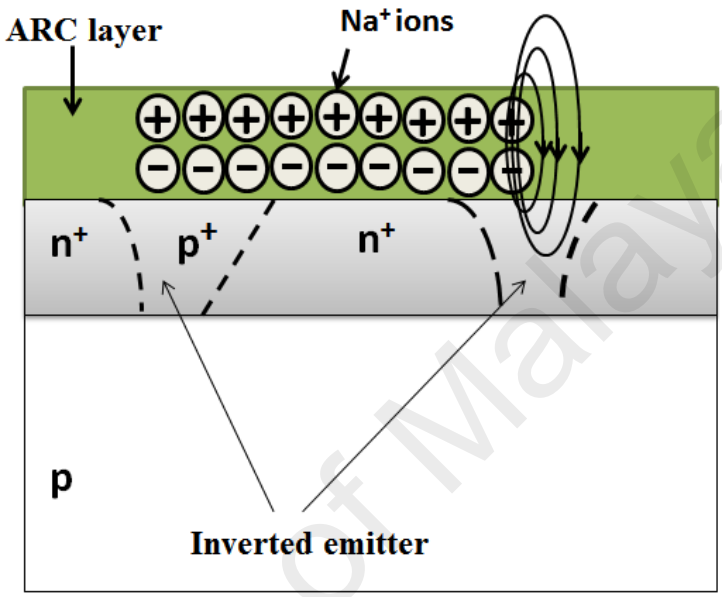

Figure 2.7: Shunting of a p-n junction due to double layer charges at the ARC (Bauer et al., 2012)

Moreover, the crystallographic stacking fault (SF) of Si can play an important role in the shunting mechanism of a p-n junction (Janghyosig et al., 2013), with sodium atoms precipitating inside the SF (Naumann et al., 2012). It is possible that stacking faults could be formed owing to oxidation during the manufacture of a p-n junction (Kumar & Park, 2014). Due to the low formation energy of SF in the (111) direction, it can extend throughout the p-n junction that provides a two-dimensional diffusion path. Naumann et al. (2014) experimentally revealed the Na^+ ion diffusion through the SF using high-resolution transmission electron microscopy (HRTEM). During the entrance to the SF, Na^+ ions are supposed to be neutralized through acceptance of the emitter's electron. A two-dimensional metallic layer is formed at the SF, in which an ohmic characteristic in

the p-n junction is observed. The presence of Na decorated SFs was further confirmed by Lausch et al. (2014b) by STEM analysis on the nanometer scale. They also reported that Na atoms diffused out during the recovery process (Lausch et al., 2014b). Figure 2.8 shows the Na^+ decoration (green line) at the stacking fault of a PID affected solar cell material.

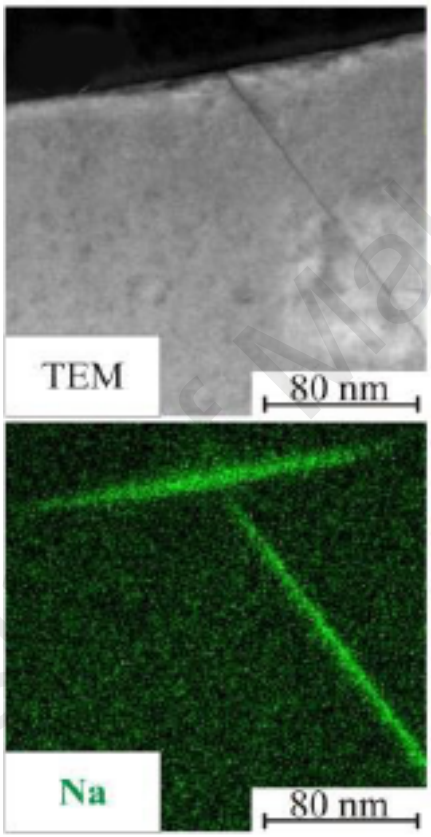

Figure 2.8: Na accumulation at the SF of a PID affected PV solar cell (Lausch et al., 2014b)

The possibility to diffuse these Na^+ ions or other metal ions into the other defects such as the grain boundary, the twin boundary or other boundaries is possible but has not observed thus far. The reason might be that the diffusion is easy in the (111) plane and the plane cannot possibly exist at the grain boundary and the twin boundary. Figure 2.9 illustrates the Na^+ ions migration process: in the presence of high voltage stress, Na^+ ions accumulated on the ARC SiN_2 and SiO_2 layers through migration from glass to the

cell surface. In the end, Na^+ ions enter the emitter layer and are neutralized by accepting electrons. SFs' presence in the solar cell is therefore decorated with Na atoms, which results in a metallic, conducting, two-dimensional layer in which shunting ensues.

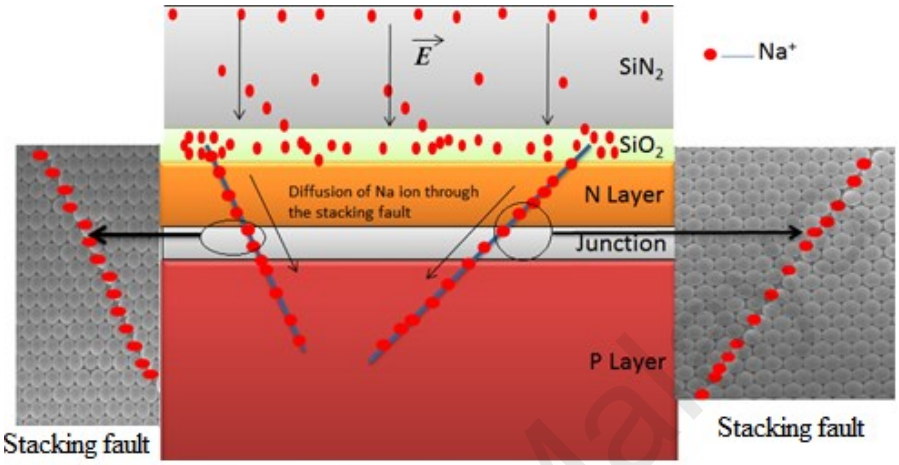

Figure 2.9: Schematic model of PID of a solar cell where Na^+ (red dots) decorates the SF
(Lausch et al., 2014b)

The source of alkali ions (Na^+ ions) is generally assumed to be from the glass front cover of solar cells. Furthermore, it has been theoretically (Ziebarth et al., 2014) and experimentally verified (by using a polymer instead of glass on the front side) that the commonly used glass is the main source of Na^+ ions (Liu et al., 2013; Schwark et al., 2013). The source of metal ions can also be from the environment such as coastal areas, and it has been reported that these environmental ions increase the PID (Liu et al., 2012).

Contrary to the ideas purported thus far, Masuda et al. (2016) claimed that Na^+ ion diffusion is not sufficient to cause PID because they have found no power loss of a p-type crystalline Si PV module after a PID test with the following conditions: Al plate, 60°C, 85% RH, -1000V and 72 hours. Despite this claim, there was an increase of Na^+ ion concentration on the cell surface of the module. On the other hand, Hara et al.

(2015b) mentioned that Na^+ ions are not a prime factor causing PID in n-type font junctions in PV modules. The authors have shown by SIMS that the Na^+ concentration does not increase at the surface of PV cells, although power dropped at PID stress conditions of Al-plated, negative (-) 50V, 85°C and 2 hours. Thus, there is still ambiguity and further research is needed to ascertain the actual mechanism of PID.

2.4 PID Testing Process

According to system and measurement techniques, PID testing can be carried out in three ways: (1) on-site testing, where modules are tested at the PV power plant (Moreno et al., 2013); (2) testing outdoors but not on-site - single module or very small scale modules are tested outdoors by simulating the PV power plant situations by applying voltage stress from a DC power source (Schneller et al., 2014); (3) indoor testing where modules are tested in a laboratory within an environmental chamber by altering a range of environmental conditions to evaluate the effect of various parameters such as temperature, humidity, and voltage (Janghyosig et al., 2013). The detail of each testing procedure is presented in the following segments.

2.4.1 On-site PID Testing

On-site testing is the only way to evaluate the real degradation features of a PV module. However, very scarce information is available in the literature on this type of testing; only a few works have been reported to perform on-site PID test (Oh et al., 2017; Yang et al., 2017; Bouraiou et al., 2018; Hylsky et al., 2018; Martínez-Moreno et al., 2018). In case of on-site PID testing generally the leakage current, EL image, IR image, I-V characteristics, and operating voltage of each module are measured and compared with their nominal values. All the experiments except EL imaging have to be taken during sunny weather, and EL images are taken during the night. Dark I-V measurements can be done by covering the module area with a blanket or other non-

transparent cover to produce a dark environment for the specific module. The major problem of on-site testing is that it is a very lengthy process and may take several years (del Cueto & Rummel, 2010). That is why simulation of the power plant in laboratories and studying PID effect in environmental chambers is a better alternative (Hara et al., 2015b).

2.4.2 Outdoor PID Testing

Outdoor tests normally carried out with a 60-cell standard module installed at the site where the PID test will be carried out. The extent of PID may vary according to climate of the test site, and environmental conditions such as solar irradiance, ambient temperature, relative humidity (RH) and rain (Hoffmann & Koehl, 2012). Generally, outdoor testing is performed by applying a DC high negative voltage (normally 1000 V) in the test module from sunrise to sunset. The leakage current between the cells and the frame/ground is measured before and after voltage application by using an ampere meter along with a data logger (Hoffmann & Koehl, 2013). The relative humidity is measured using a humidity sensor and the module temperature is measured by attaching a thermocouple to the PV back sheet and all parameters are monitored simultaneously (Schutze et al., 2011a). Rain can be identified through a rain sensor which monitors the duration and intensity of rainfall and also the surface wetness due to dew (Dhere et al., 2014c). It was observed that leakage current without rain depends highly on the humidity. A high magnitude of humidity only appears at the module's surface at temperatures below 30°C (Hoffmann & Koehl, 2013). Other module parameters such as I-V characteristics, dark I-V, operating voltage, EL and/or IR imaging are also measured before and after voltage application and are compared to assess the extent of PID (Schwark et al., 2013). Outdoor characterization of PID provides results closest to

those obtained at on-site characterization, but this process is lengthy, too (Schneller et al., 2014).

2.4.3 Laboratory PID Testing

The PID of a PV module has been tested in laboratories by simulating the real field features of PV power plants but under accelerated environmental conditions (Schutze et al., 2011b; Hacke et al., 2015b). In the case of laboratory testing, there is more control over the temperature, humidity, and light than in other forms of PID testing. Furthermore, individual effects of voltage, temperature or humidity on the PID can be easily investigated in an environmental chamber. The reliability of a PV module in harsh climate conditions can also be tested indoors through the application of high voltage under elevated temperature and humidity (Dhere et al., 2009; Pingel et al., 2010). Nevertheless, there is considerable difficulty in precisely reproducing the spectral distribution found in the natural sunlight. Filters can be used to obtain the spectral distribution as close as possible to the sunlight spectrum (Munoz et al., 2011). Usually, a single cell mini module or a 60-cell standard module is placed in the environmental chamber and a high negative voltage is applied at a controlled humidity and temperature (Pingel et al., 2010; Schwark et al., 2013). The front glass surface is normally wetted or covered with a wet blanket or aluminium foil to make it conductive. The leakage current from cells to the frame/ground is measured prior to and after the voltage stress being applied. The I-V performances of the module before and after the stress are measured at standard test conditions (STC). In most cases, both EL imaging and IR imaging are carried out, the most meaningful results of which are then presented (Pingel et al., 2010). The duration of applied voltage, stress, temperature and humidity depend on the laboratory PID test standards.

2.4.4 Different Laboratory PID Testing Procedures

PID testing is significantly dependent on the tested operating conditions such as temperature, humidity, voltage, duration of testing period and grounding system. It was reported that the speed of PID increases tenfold if a metal contact is provided over the whole front glass surface (Koch et al., 2012b). On the other hand, if a PID test is performed on a single cell mini module at 1000V/85% RH and 60°C, the degradation level is very high. Yet, if temperature and voltage are taken as 25°C and 100V, respectively, then no degradation occurs at all (Koch et al., 2012b). Hence, selection of PID testing conditions is an important issue. Different organizations have investigated the PID of PV solar modules at different testing conditions and they proposed different test methods. Some common proposals are shown in Table 2.2.

Table 2.2: Comparative testing conditions for different lab test methods to measure the PID resistance of PV modules
(FCSP, 2012; Singh, 2015)

	TÜV Rheinland	**PI Berlin**	**Fraunhofer CSE**	**Panasonic (Chemitox)**
Test Environment	Temperature controlled laboratory room	Environmental chamber	Environmental chamber	Environmental chamber
Test Conditions	Temperature: 25°C	Temperature: 85°C, RH: 85%	Temperature: 50°C, RH: 50%	Temperature: 60°C, RH: 85%
Contacting Method	Aluminium foil	Frame grounding	Aluminium foil	Frame grounding
Test Duration	168 h (7 days)	48 h	48 h	96 h
Test voltage	−1000V	−1000V	−1000V	−1000V
Pass-fail Criterion	< 5% power degradation	< 5% power degradation	< 5% power degradation	< 5% power degradation

A comparison of the environmental chambers' climate conditions is as follows: at 85°C and 85%RH, the PID speed is four times higher than at 60°C and 85% RH, and 170 times than conditions of 25°C and 35% RH. Several reports on PID testing both outdoors and indoors by use of different methods with varying temperatures, humidity,

and testing durations with water film or Al foil at the glass covers are shown in Table 2.3 and Table 2.4.

Table 2.3: PID testing outdoors in different environments

Module type	Condition and Location	Characterization and Remark	References
Standard mc-Si module with water film	Series string voltage 160V within several months, Germany	I-V, 35% power drop	(Swanson et al., 2005)
60-cell mc-Si module	-600V one month Florida Solar energy centre, Cocoa, USA	Leakage current, At 1000 W/m^2 about 400nA	(Dhere et al., 2014c)
60-cell mc –Si modules	-600V Six months Florida Solar energy centre, Cocoa, USA	I-V/EL, Maximum 50% power drop	(Schneller et al., 2014)
P-type mc-Si module	-1000V 690 day, Vienna, Austria	EL, IR, IV, 35% power drop	(Schwark et al., 2013)
60-cell standard modules	-600V Freiburg, Germany.	I-V, EL, Leakage current 3µA below 30°C	(Schutze et al., 2011a)
60-cell commercially available modules	-600V, RH varied 10% and 95%, temp 10°C to 90°C, Freiburg, Germany	Dry day Leakage current 150nA, at 16°C and rainy day leakage current 3000nA	(Hoffmann & Koehl, 2013)
mc-Si solar modules	-1000 V at daytime, within 178 days, at Alzenau, Germany	I-V, Maximum power drop 51%	(Nagel et al., 2011)
mc-Si modules	applied -600V logarithmically with irradiance, within ~10 months, Florida, USA	I-V, EL Power drop 11%	(Hacke et al., 2013)
mc-Si modules	under -1500 V after one year, in Florida, USA	I-V, Power drop 25.7%	(Dhere et al., 2011)
mc-Si modules	100 hours, -1000V Berlin, Germany	I-V, EL, 12% power degradation	(Pingel et al., 2014)

From the Table 2.3, it is observed that different researchers have tested the PID of p-type polycrystalline Si modules made of various manufacturers at different places

outdoors. The maximum power drop of 51% was found by Nagel et al. (2011) in Germany and a minimum power drop of 11% was reported by Hacke et al. (2013) in the USA.

Table 2.4: Indoor/laboratory testing of PID in different conditions

Module type	Conditions	Testing	Remark	Reference
P-type Si poly crystalline 60-cell	−1000V, 100 h, 85°C, environmental chamber	I-V, high resolution EL camera	Power loss 32% (RH)50% 99% (RH 100%)	(Berghold et al., 2010; Pingel et al., 2010)
P-type Si polycrystalline mini module	− 600V, 50°C, RH 50%, 72 h, laboratory conditions	LIT, EL, ToF-SIMS) and SEM with EBIC	Parallel resistance $R_p < 1\ \Omega$.	(Naumann et al., 2012)
Si polycrystalline with PID resistant EVA	−1000V,60°C, RH 85% for 96 h, environmental chamber, Al-foil wrap for grounding the entire module	I-V, (LA-ICP MS)	Power drop 73%	(Kapur et al., 2015)
Commercial scale Si polycrystalline	−1000V, 85°C, RH 85%, 192 h, without Al-foil	I-V	88.5% power drop	(Kapur et al., 2015)
4-cell p-type Si polycrystalline	−1000V, 60°C, RH 85%, 40 h, Al plate pressed on the glass face	I-V, SIMS	20% power drop	(Kambe et al., 2013)
P-type Si polycrystalline 60-cell	− 600V, 57 h, 25°C, wet glass surface	I-V, EL, DLIT	Around 55% power drop	(Schutze et al., 2011b)
Si polycrystalline 30-cell standard module	− 600 V/, 25°C halogen lamp, illumination with water cover	I-V, EL	Power drop 9.4% (76h) 46.8% (372h)	(Schutze et al., 2011a)
poly and mono p-type	−1000V, 60°C, RH 85%, 96 h, Vienna, Austria	EL, Si-CCD camera, IR image	Maximum 94% power drop	(Schwark et al., 2013)
P-type Si polycrystalline (one-cell mini module)	− 600 V, RH 85%, 24 h, 85°C	I-V, DLIT, EBIC, SIMS	Steep decrease of R_p (from 240 Ω to 1 Ω) during the first hour	(Bauer et al., 2012)
One-cell mini module with various encapsulants	− 600V, 85°C, RH 85%, 48 h, at STCs	I_{sc}, P_{max},	Power loss 95.5% for EVA,7.23% for ionomer and 12.5% for TPSE	(Koch et al., 2012a)
Monocrystalline p-type Si 60-cell module	−1000V, (1) 85°C, 85%, 48 h (2) 60°C, 85%, 96 h	I-V, EL, IR images	Power drop 74.82% (1) 74.83% (2)	(Koch et al., 2012b)

Table 2.4: Continue

Module type	Conditions	Testing	Remark	Reference
Monocrystalline p-type Si one-cell module	− 600V, 88 h, 65°-85°C, RH 0%, adhesive Al-tape	Light I-V, Dark IV, EL, IR, QE	Power drop 70%, R-shunt = 0 Ω	(Jaewon et al., 2014)
Single cell coupons and panels	−1000V, 60°C, 24 h, Al-foil	I-V, EL	− 80% PID for single cell module	(Pingel et al., 2012)
c-Si p-type standard modules	− 1000V, 50°C, RH 50%, 48 h, climatic chamber with Al-foil	I-V	Max 99% power drop	(Rutschmann, 2012)
a-Si p-type standard modules	− 600V, 60°C, RH 85%, 1340 h, environmental chamber	I-V, LC	52.2% power loss	(Osterwald et al., 2003)
Commercial modules (Si-polycrystalline) 60-cell	−1000V, 25°C, RH 100%, 120 h, Na^+ ion rich environment	I-V, EL	5% power loss and 3.4% FF drop	(Liu et al., 2012)
60-cell modules p-type multi-crystalline	−1000 V, 85°C, RH 85%, 96 h	I-V, EL, (LA-ICP-MS)	10 % power drop and 15-20 % after 400 hours	(Pop et al., 2014)
Monocrystalline Silicon module	− 600V and + 600V, 85°C, 35 h for (+)ve V and 5 hours for (−)ve V	Dark I-V Light I-V, EL, IR	< 5% for positive and 85% power drop for negative voltage	(Goranti & TamizhMani, 2012)
n-type single-crystalline Si solar cell with soda lime glass	Al plate (thickness is ca. 0.5 mm), −1000 V, 85°C, 2 h	I-V, EL, QE, D-SIMS	Power drop 15% and QE drop from17.8% to 15.1%	(Hara et al., 2015b)
n-type single-crystalline Si solar cell with CSG	Al plate (thickness is ca. 0.5 mm), −1000 V, 85°C, 2 h	I-V, EL, QE, D-SIMS	QE decrease from 17.2% to 13.9%	(Hara et al., 2015b)
One-cell mini module p-type multi-crystalline	Al foil test, 1000V, 25°C, 68 h	R_{sh} EL	R_{sh} reduced from 100 to near 1 kΩ-cm^2	(Koentopp et al., 2016)
Standard PV modules from 22 companies	−1000 V, 85°C, RH 85%, 100 h	IV	Maximum 58.3% power drop	(Meydbray & Dross, 2016)

Dissimilar weather conditions of different places produce different PID features such as in Florida, USA, the PID rates are 0.036% and 0.070% per day for negative (−) 600 V and negative (−) 1500 V, respectively. In Vienna, Austria, the PID rate is 0.05% per day for negative (−) 1000 V stress. Schneller et al. (2014) reported that the modules

from different manufacturers have different PID rates and they have found a maximum PID rate per day of 0.27% at −1000 V stress in Cocoa, USA. A maximum power drop of 99% and a minimum power drop of 5% in PV modules are revealed in Table 2.4. Laboratory PID testing is highly dependent on some parameters such as the number of cells contained in the module (mini module degraded more rapidly than large 60-cell modules), applied voltage, temperature, humidity, the type of module surface (water film on the module surface or Al foil attached to module surface). The temperature has a much larger effect on PID than humidity. The effect of humidity, water and the metal contact on the rate of PID is in the order:

Humidity < Water film < Al foil contact

A comparison between the different stressing conditions was done using a 30-cell, polycrystalline Si p-type PV module, reported by Schutze et al. (2011a) as shown in Table 2.5. Leakage current and P_{max} are compared for different PID stressing conditions. At the same voltage and temperature, modules with Al metal covers give higher PID stress as compared to modules wetted with a water film. On the other hand, when the voltage and temperature increase, both the power drop and leakage current increase rapidly.

Table 2.5: Comparison of different conditions of PID stressing on a 30-cell, polycrystalline p-type module
(Schutze et al., 2011a)

Conditions	Duration of Stress	Power Drop (%)	Leakage Current (µA)
-0.6 kV / 25°C / wet	372 h	46.8	0.95
-0.6 kV / 25°C / metal	372 h	51.7	1
-12 kV / 25°C / metal	8 h	37.55	55
-0.5 kV / 55°C / metal	7.5 h	38.65	20
-1 kV / 85°C / metal	0.5 h	40.75	360

2.5 Recovery of PID

The whole power loss of a PID affected module cannot be recovered by simply applying the reverse potential; rather the amount of recovery depends on potential and environmental factors such as humidity and temperature (Schwark et al., 2013). The level of degradation is also an important factor because it is reported that the amount and duration of recovery are dependent on the level of PID of a particular module. Koch et al. (2012b) reported PID recovery levels at three different conditions on two different modules as shown in Figure 2.10. Negative (-) 1000V and positive (+) 1000V were applied for PID and recovery, respectively, to each module at conditions of 48 hours, 85°C, R.H 85%; 96 hours, 60°C, R.H 85%; and 168 hours, 25°C, R.H 35%.

The extent of PID of PV module varies according to PID resistance properties of the PV module constituting materials. On the other hand, PID recovery characteristic depends on the level of PID whether it is high, medium or low (Komatsu et al., 2018). A higher level of PID shows a lower the rate of recovery and the original power does not recover in this condition. On the other hand, the PV module contains a lower level of PID shows a greater amount of recovery (Koch et al., 2012b). Table 2.6 shows the various measures taken in PID recovery process which reveal that the extent of PID recovery vary according to PID history and the recovery process.

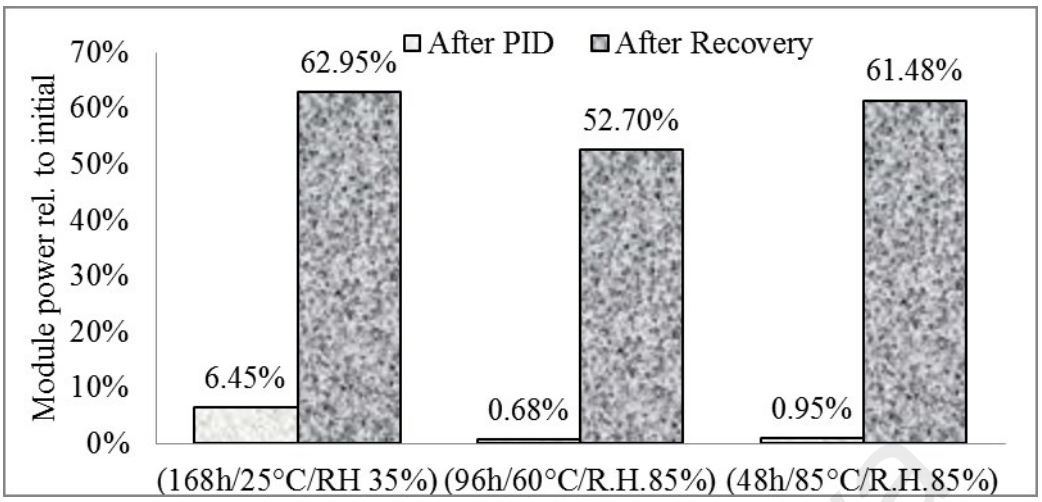

(a)

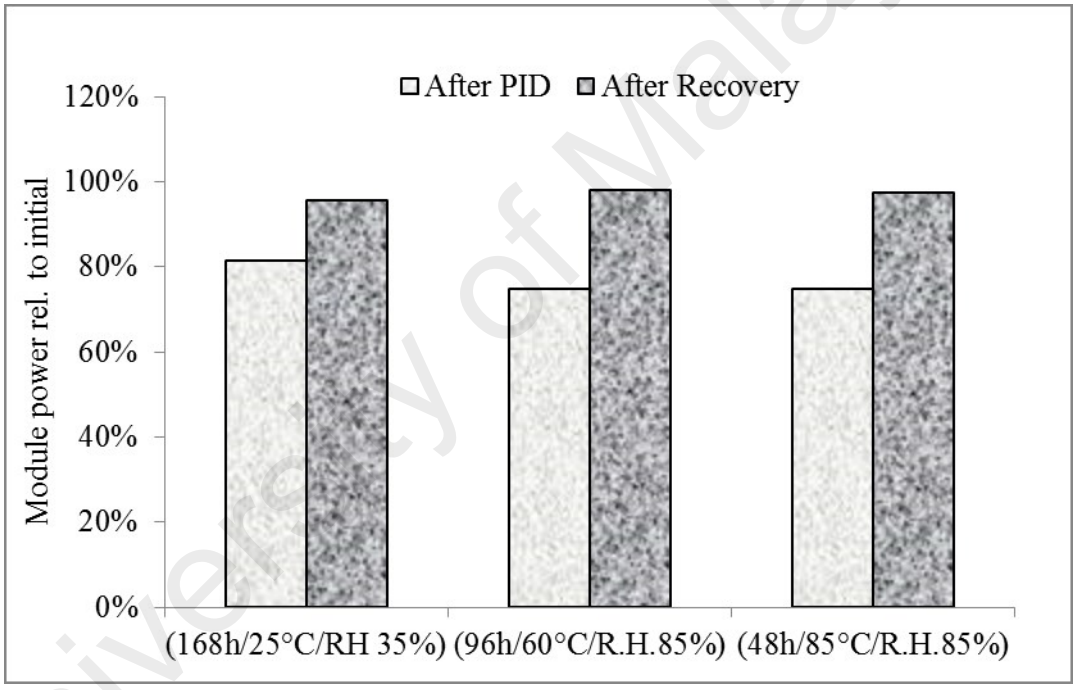

(b)

Figure 2.10: PID recovery behaviour (a) when extent of PID is high and (b) when the extent of PID is low
(Koch et al., 2012b)

Table 2.6: Recovery process of PID affected PV modules

Processes	PID History	Amount of Recovery	Reference
+ 600V/800°C 200 h	− 600V/50h, R_p = 0 Ω	R_p not recovered fully	(Lausch et al., 2014b)
Store at 250 °C /25 h	− 600V/50h, R_p = 0 Ω	R_p not recovered fully	(Lausch et al., 2014b)
+ 1000V, 40°C hot water, 100 h	75% power reduction	95% regeneration	(Pingel et al., 2012)
Store at 18 months	50% power degradation	97% recovery	(Pingel et al., 2012)
+ 600V/88 h/60°C/RH 0%	Power reduced to 30% and shunt resistance almost zero	Power-93%, 40% shunt resistance recovered	(Jaewon et al., 2014)
Store at 75 days	30% power reduced and shunt resistance almost zero	92% power with shunt resistance very poor recovered	(Jaewon et al., 2014)
+ 1000V, 1 , water film	35% power drop in outdoor 160V	100% recovery	(Swanson et al., 2005)
+ 1000V/96 h 60°C, RH 85%	94% power drop at indoor	70% recovery of its original power	(Schwark et al., 2013)
+ 1000V/96 h 60°C, RH 85%	35% power drop at outdoor	Recover 68% of its nominal power.	(Schwark et al., 2013)
+ 600V/35 h /60°C with full carbon on font surface	Power drop 84%	27% recovery of its original power	(Tatapudi et al., 2013)
+ 600V/5h/85°C Previous DH, 1000 h	85% power drop	72% power recovered	(Goranti & TamizhMani, 2012)
Storing/100 °C for 10 h	23% power drop	95% recovered	(Pingel et al., 2010)
+ 1000V/96 h /Al-foil	Cyclic PID and recovery	Maximum 97% recovered	(Jaeckel et al., 2014)

During the PID recovery process, there is a certain PID level from which PID can be recovered 100%, any PID below this level is not fully recoverable. Interestingly, it is also observed that a module can self-recover at room temperature in the absence of high system voltage at a rate of 0.01% per day (Schwark et al., 2013).

2.6 Control and Prevention of PID

Controlling or suppression of PID is now an important issue for manufacturers because the magnitude of PID is increasing day-by-day with the increased string voltage of PV power plants (Hosenuzzaman et al., 2015) and, consequently, the module lifetime is seriously affected by PID (Sharma & Chandel, 2013). The mitigation process of PID can be separated at three different levels: the module level - altering the properties of the cover glass material and altering encapsulant material properties; the cell level - optimizing the antireflective coating, emitter material, and base material properties; and lastly the system level - proper grounding.

2.6.1 Module Level Prevention

Potential induced degradation is generally regulated by altering the properties of module construction materials, for example, glass, encapsulant materials, etc. (Pingel et al., 2010) in such a way that electrical resistivity between the active cells to the ground is increased and the leakage current paths are disturbed.

2.6.1.1 Modification of front glass

The major cause of PID is the migration of metal ions (particularly Na^+) from the front glass materials at HVS (Hacke et al., 2010). Normally, soda lime glass is used due to its low cost, and it contains a lot of sodium ions. By modulating the composition and properties of the front glass, PID can be controlled. It was reported that PID can be suppressed with the replacement of the front glass surface by a Na^+ free font cover (Kambe et al., 2013; Kajisa et al., 2014). A module composed of quartz as a front cover glass shows excellent PID resistance properties due to the absence of Na^+ (Hacke et al., 2010; Hacke et al., 2011; Schutze et al., 2011b). Sometimes, soda lime glass along with the SiO_2 layer below the glass layer act as Na^+ ion barriers. The use of quartz is not reliable due to its high cost and manufacturing difficulties.

Kambe et al. (2013) reports that chemically strengthened glass (CSG) offers better PID resistance characteristics as a substitute of tempered soda lime glass, wherein Na^+ ions are replaced by K^+ ions. The mechanical properties of CSG was also enhanced and an absence of PID at the accelerated condition of 1000V/85°C/2h was reported (Kambe et al., 2013). But it is still a contentious dispute that whether the above-accelerated conditions are satisfactory or not with real field conditions. Hara et al. (2015b) reported that there is significant PID of n-type Si PV module with CSG. Cause of PID resistance behaviour of CSG might be due to the higher ionic radius of K^+ than Na^+ that required higher energy to ionic diffusion. The ionic radius of metal ions within the glass is as follows (Jambon & Carron, 1976; Schubert, 1997).

$$Na << K << Rb << Cs << Fr$$

Metal ion diffusion can be controlled by replacing Na with the element having a higher ionic radius. Recently Oh et al. (2016) has reported a PID controlling process by front glass surface disrupting through applying a Willow flexible glass film. Willow glass can be applied during the manufacturing process PV module and also in the modules existing in the PV plant which prevents further PID. Willow glass flexible film present below the front glass possesses better PID resistant although it reduces the transmittance of the encapsulant and as result, the efficiency of PV module is reduced.

2.6.1.2 Modification of encapsulating material

Encapsulating material has an important role in PID mitigation as encapsulants act as a pathway of Na^+ migration. PID can be prohibited by modifying the encapsulating materials in such a way that ionic migration is barred. Ethylene-vinyl acetate (EVA) is normally used as encapsulant owing to its low cost. PID resistance can be enhanced either by improving the resistivity of existing EVA through cross-linking or replacing

EVA by other alternative materials. It is also reported that by increasing the thickness of encapsulant PID can be inhibited, because thick EVA will reduce the voltage stress on the cell and also delay the Na^+ transfer (Schwark et al., 2014) (de Oliveira et al., 2018). Through the cross-linking using curing agent during the manufacturing, EVA became PID resistant for example. Chen et al. (2014b) reported a PID resistant EVA having tremendous potential induced degradation opposition along with anti-adhesion properties and high impact resistance. The composition is shown in Table 2.7. Some other encapsulate materials have been reported such as polyolefin, polyvinyl butyral (PVB), silicone etc. those exhibit better PID performance (Koch et al., 2012a; Schwark et al., 2013).

Table 2.7: Composition of PID resistant EVA

Material	**Percentage (%)**
Cross-linking curing agent	0.6 − 0.8
Antioxidant	0.3 − 0.4
Mixture of hydroxyl benzophenone and silica in ratio of 3-5:1	0.5 – 1.0
Ethylene-vinyl acetate (EVA)	balanced

Polyethylene-based polyolefin elastomer (POE) in both form either thermoplastic or cross-linking is now used as an encapsulant especially at thin film type solar module due to their excellent barrier of moisture vapour transmission along with high volume resistivity compared to EVA (Nagel et al., 2012; Lin et al., 2013). A typical cross-linked polyolefin material composition having anti-PID properties along with good light transmittance and adhesiveness and shock resistance has been shown in Table 2.8 (Chen, 2014).

Table 2.8: Typical composition of polyolefin

Materials	Weight %
Ethylene-acetylene copolymer	80 − 90
Polyethylene	5 − 10
Ethylene-methyl methacrylate copolymer	5 − 15
Melamine	0.5 − 2
Crosslinking agent	2 − 3
Antioxidants	0.5 − 2

Although POE seems to be a promising encapsulant material Reid et al. (2013) verified that only encapsulant replaced by POE is not sufficient for fully PID prevention because after 96 hours at 1000V/RH85%/85°C showed 60% power reduction. Ionomer, that means an ionic polymer which is partially neutralized e.g.(partially neutralized polyethylene co-methacrylic acid) also reported as an alternative encapsulant for PV module and shown excellent PID resistance (Kapur et al., 2013). Fully replacement of EVA by ionomer enhanced the cost of the module. Ionomer film laminated with standard EVA may be a cost-effective encapsulate with quite similar PID resistive properties (Kapur et al., 2013; Fujioka, 2014). Different layer thicknesses of ionomer and EVA were reported such as 100 μm ionomer/460 μm standard EVA show <<5% PID at up 400h testing (Pop et al., 2014). Ionomer/EVA bilayer module, having 50μm ionomer and 450 μm standard EVA with very little sodium accumulation at 85°C/85%/1000V/425h PID stress (Kapur et al., 2015). Recently it is also studied on the ionomer encapsulant for the n-type solar module and excellent PID resistance is reported (Hara et al., 2015a).

A comparison between the different encapsulant has been depicted in Figure 2.11. Relative power degradation of one cell mini-modules composed of different encapsulant such as Ethylene-vinyl acetate (EVA), Polyethylene (PE), polyvinyl butyral (PVD), thermoplastic silicone elastomer (TPSE), ionomer and polydimethylsiloxane (PDMS)

etc. material after PID testing in condition of -600V /48h/85°C/RH85% were measured (Koch et al., 2012a). PE exposes best PID resistance behaviour, and then followed by Ionomer, TPSE, PVB, PDMS and lastly EVA display the highest degradation.

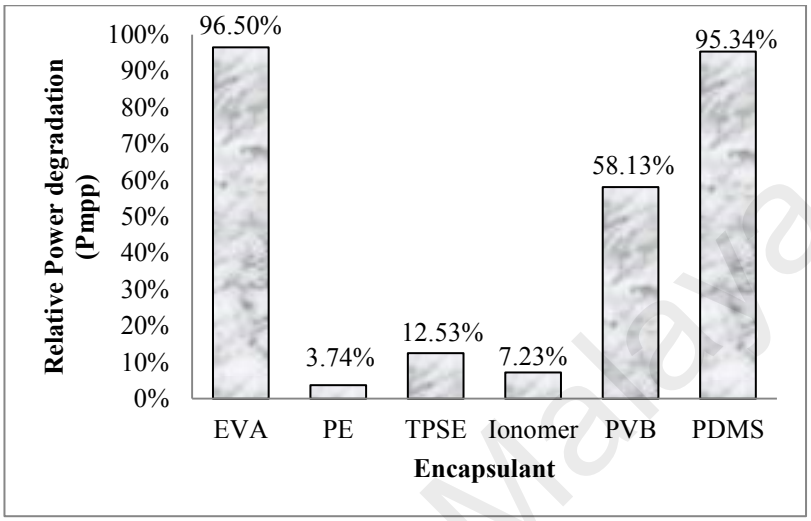

Figure 2.11: PID resistance behaviour of different encapsulant at (-600V /48h/85°C/RH85%) stress condition

2.6.1.3 Use of thin film coating

Although there are different alternative PID shielding encapsulant material to EVA, some other criteria need to account for, viz., cost, longer stability, and accessibility etc. Hydrophobic coating on the glass surface can be used to protect the cell from PID (Hwang, 2014). These coatings create passivation of electrical connection between the grounded frames to the glass surface by the exclusion of water on the surface of the glass. A thin layer such as SiNx, SiO_2, and TiO_2 etc. have Na^+ diffusion barrier capability and can be used to prevent PID of the solar module (Zita et al., 2010; Aubry et al., 2012). It is reported that the TiO_2 thin film undercover glass has a noble suppression effect of Na^+ diffusion and PID performance enhanced with the increase of the thickness of the TiO_2 film (Nehme et al., 2014). But their testing period is not adequate. Recently, it is found that the polyethylene (PE) thin film has superior Na^+

diffusion barrier property than the TiO_2 and only 30μm thickness along with standard EVA can prevent PID for long period of DH test (Hara et al., 2015a).

2.6.1.4 Modification of sealing materials

By increasing the electrical insulating properties of the edge sealing material in between the solar panel and frame, PID can be controlled. Generally high industrial graded silicone seals or polyolefin based seals are used in PV modules (Hong et al., 2014). Copolymerizing polyolefin resin with cyclopentenedione derivative also reported as good sealant for PID resistance (Oka et al., 2015). Some recently developed sealant materials are denoted in the below Table 2.9.

Table 2.9: Different sealant materials composition used as PID resistance

Composition	Feature	Reference
Polyethylene-type resin, and has layers containing 4-10 %mass white pigments.	The water-absorption rate 0.2% or less	(Moriyama & Yamazaki, 2014)
Ethylene-(alpha)-olefin copolymer, with 0.05-2 wt. % epoxy group-containing silane coupling agent, and 0.6-2 wt. % acid acceptor.	Excellent adhesiveness at high temperature, high humidity with suppressed potential induced degradation	(Ikenaga & Ito, 2015)
100 wt.% ethylene- alpha-olefin copolymer, an organic peroxide, and crosslinking adjuvant chosen from divinyl aromatic compound, cyanurate, diallyl compound, triaryl compound, oxime, and maleimide, and 0.1-5 wt.%. (meth) acrylate type monomer.	Venerable PID suppression at high voltage	(Ikenaga et al., 2015)

2.6.2 Cell Level PID Prevention

Both p-type and n-type solar cells are prone to PID but their material composition and thickness of antireflection coating (ARC) have a great influence on the PID modulating aspect. Several parameters such as emitter sheet resistance; base resistivity

etc. can be controlled by doping concentration. It is reported that PID confrontation of the solar cell is enhanced by decreasing the emitter sheet resistance and increasing the base resistivity (Pingel et al., 2010). An anti-reflection coating (ARC) has the capability to prevent PID and a highly PID suppression property is found for ARC with refractive index higher than 2.2 (Pingel et al., 2010). Actually, the polarization of solar cell will be extinct due to a conductive layer over the ARC which will be connected with the base of the solar cell (Swanson et al., 2009) through which PID will be arrested. It is believed that driving force for the ion migration towards the silicon nitrides and then silicon can be eliminated by removal of electrical potential by using a conductive coating on ARC (Hacke et al., 2012). For example, with the increase of refractive index, the electrical conductivity of SiN_x layer also increases, and the conductive layer can be also neutralized the Na^+ ions that are the possible reasons of PID resistance of SiN_x anti-reflection coating with high refractive index. Unfortunately, SiN_x with higher refractive index deteriorates the conversion efficiency due to an increase of unfavorable light absorption (Shirazi et al., 2009). However, ARC layer of SiO_yN_x/SiN_x exhibits better PID resistance compared to the stack as $x SiN_x$ single layer coating for multi-crystalline silicon (mc-silicon) silicon solar cell with the same efficiency (Zhou et al., 2015).

Alterations of emitter diffusion and ARC layer have a large impact to reduce the cell efficiency relatively low impact on PID suppression. Insertion of a thin film between the emitter and ARC suppresses Na diffusion into emitter, which can be an effective way of PID prevention although this layer may reduce the transmittance of the encapsulant, thereby hampering the cell efficiency. Nagel et al. (2014) have explored a PID suppression path by inserting a SiO_2 layer in between the emitter and ARC layers. They have used two inline oxidation processes such as UV oxidation and thermal oxidation for the formation of the SiO_2 layer. Thermally oxidized layer shows better

PID resistant than UV oxidized layer. Recently it has been reported that the SiO_2 amalgamated with the P_2O_5 layer is more effective to reduce the PID without hampering the efficiency of the solar cell (Du et al., 2015). The amalgamation produces a phosphorous silicate glass (PSG) layer [P_2O_5+ SiO_2 → P_2O_5· SiO_2 (glass)] in between the emitter and ARC layer.

In the solar cell materials level, it has been reported that an elevation inhomogeneity of doping concentration, the sheet resistance of emitter and base resistivity reduces the PID of the solar cell (Pingel et al., 2010). Processing of solar cell in such a way that defect-free crystal structure obtained that control the PID effect. Texturing of cell materials in case of the monocrystalline cell has a significant influence on PID and a better PID resistance is shown by groove-rounded textured structure (Chen et al., 2014a). Recently, Yamaguch et al. (2016) reported that a crystal orientation in (111) direction reveals more PID controlled rather than (100) orientation. Table 2.10 shows the summary of various reported PID prevention techniques and their respective performance.

Table 2.10: Summary of prevention and control of PID by changing different PV construction materials

Prevention Technique	Before PID	After PID	Reference
Ionomer layer between the front glass and EVA(100µm ionomer + 460 µm std. EVA)	10% power degradation with standard EVA	Retain 99% of initial power after as long as 500 hours PID	(Pop et al., 2014)
Thin ionomer film (partially neutralized polyethylene co-methacrylic acid) placed between the glass and front EVA encapsulant 50 µm ionomer + 450 µm std. EVA)	PID-resistant EVA drops to 11.5% power	retain 98.5% of initial power after 192 h	(Kapur et al., 2015)
CSG replaces soda lime PV font glass	20% power drop within 40 h at -1000V/60°C /RH 85%	Retain > 95% of initial power after 96 h	(Kambe et al., 2013)
Replacing with a strong PID susceptible EVA	55% PID at -600V/25°C/57h at wet surface condition	Net zero degradation wet condition (25° C, -600V) 1000 h	(Schutze et al., 2011b)
Encapsulant compose of polyethylene (PE) thin film (30 µm) with the copolymer of ethylene and vinyl acetate (EVA)	almost degradation for without film	DH test for 4000 h (85°C/RH 85%) with a decrease of below 2%,	(Hara et al., 2015a)
Coating of TiO_2-thin film inner side of cover glass	applying -1000 V at 85ºC for 2 h 97% power drop (without coating)	3% Power drop at a 200nm thickness of TiO_2	(Nehme et al., 2014)
Plasma enhanced chemical vapor deposition (PECVD) of SiNx thickness 80 nm.	85°C/RH 85% /-1000V /48 h	Only 5% PID and no EL darkened area with cell efficiency gain by 0.3% abs	(Kuan et al., 2013)
SiO_yN_x layer at the interface of SiN_x / Si	−1000 V, 60°C/ 24 h, 30% PID with only SiNx/ Si	Nearly zero degradation after PID testing for 24 h	(Zhou et al., 2015)

2.6.3 System Level PID Control

Biasing of the PV solar cell at a certain polarity (negative bias for standard solar cells) is main cause to occur PID on a system level. By proper grounding scheme, this polarity can be prevented (Schutze et al., 2011b). However modern inverter technology does not allow the grounding of the negative pole due to their transformerless characteristics (Berghold et al., 2010). By installing grounded micro-inverters to each module PID can be prevented. High negative voltage bias to the cell is excluded by using micro-inverters, which are significantly more expensive to install and notoriously difficult to maintain and increases the installation and maintenance cost. PV power plant should be installed in places where the weather conditions having relatively low moisture and temperatures. Module inclination is also important; it is said that more than 15° incline is favourable conditions for draining water away and washing off a portion of the dirt that contributes to the surface conduction (Jaeckel et al., 2013).

2.7 Research Gaps

Potential induced degradation of PV module is a challenging issue for module manufacturers and PV power industry, because there are great financial risks due to anomalous and unexpected reduction of module lifetime. Researchers on this issue are splitting as related to mechanism, characterization, and prevention level. The key findings and possible further researches are needed to address are as follows:

- An investigation of compositional and microstructural changes of PV cell materials degraded in real field is very much essential to understand the actual mechanism of PID.
- An investigation is required to clarify the partial recovery of PID of shunting type.

- A comparative investigation in-between the laboratory PID test standard and on-site PID of similar modules is readily needed.
- A comparative investigation on the PID behaviour different type of PV cells such as (i) polycrystalline Si solar cell, (ii) monocrystalline Si solar cell (iii) amorphous Si solar cell and (iv) other thin film type solar cell is necessary.
- A cost-benefit analysis of recovery process of different types PV modules is also required to find the best cost-effective PV module among the rest of others.
- Appropriate prevention process for PID in cost effective and sustainable way is still an issue.

In the light of literature review and the research gaps detected, it may be concluded that extensive research is still required to understand the PID phenomenon and an apposite protocol for its prevention and recovery is eagerly awaited.

CHAPTER 3: POTENTIAL INDUCED DEGRADATION: THEORETICAL FRAMEWORK

3.1 Concept of PID in PV module

In PV power plant, a number of modules are connected in series to develop the desired output voltage, while module frames are grounded for safety, producing a high potential difference between the module frame and the solar cell by virtue of which the module experiences a high voltage stress (HVS). On the other hand, inverters used in the PV system may or may not be grounded depending on whether the inverter is transformer based or transformerless. Depending on inverter type used, three different types of PV string configurations are possible, such as (i) grounded either only positive pole or (ii) only negative pole of PV system and (iii) both poles are ungrounded which creates floating potential difference as shown in Figure 3.1.

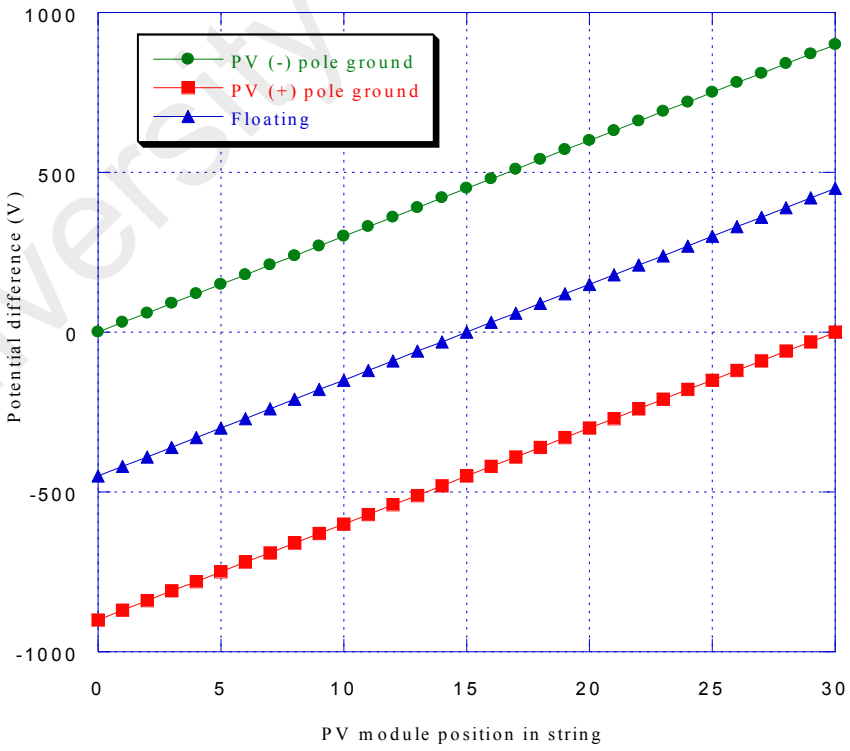

Figure 3.1: Three types of voltage stressing on PV modules in a string depending on the pole grounding
(Pingel et al., 2010)

In positive pole grounding system, PV solar cells are stressed by negative potential relative to module frame, while opposite happens in case of negative pole grounding system. In the latter case, one part of the string has a negative and the other part has a positive potential towards the ground (Pingel et al., 2010). The performance of PV module decreases unexpectedly within several months or few years due to HVS which is known as potential induced degradation (PID). Both types of potential difference can degrade the PV module performance depending on the module and cell materials (Luo et al., 2017). The root cause of PID may be different for different types of module technologies. The real causes in microscopic level are still under investigation. Nevertheless, some explanations have been proposed in the literature to understand the aetiology of PID. Ion migration process as a result of leakage current is one of the prevalent theories to understand the PID of silicon solar cell. The HVS instigates leakage currents to flow either from module frame towards the solar cell or from cell towards the frame depending on the positive or negative voltage stress. In the presence of negative HVS in silicon PV module, positive ions migrate towards the cell surface as shown in Figure 3.2. Migrated ions hamper the emitter performance of the solar cell by creating a charge double layer in the way that positive charges (Na^+ ions) attract or create a layer of negative charges between the layer of positive charges and the n+ emitter. So in the vicinity of the cell, negative charge layer creates an electrical field which repels the emitter electrons (Raykov et al., 2014). The HVS also causes an electrochemical corrosion mainly in thin film module which is nonreversible (Fjallstrom et al., 2013).

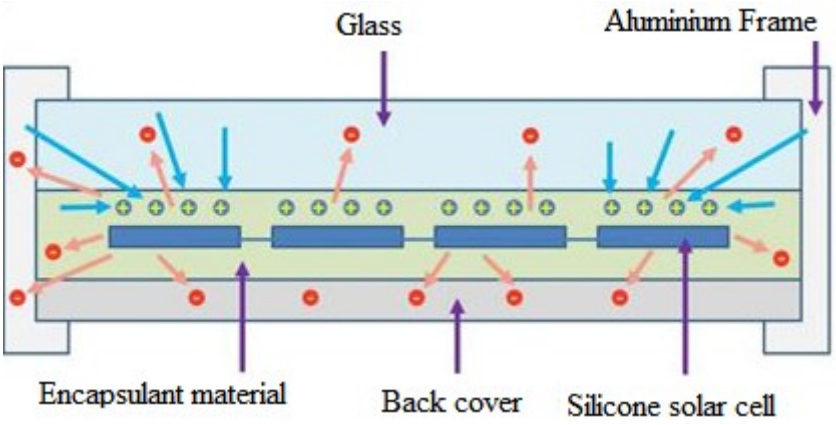

Figure 3.2: Positive and negative ions migration in presence of high voltage stress in PV module
(Vigdu, 2017)

3.2 PID Characterization Techniques

Assessment of the extent of the PID of a solar module is imperative, especially for large solar power plants. The evaluation of the degradation level of each module within the string and each cell within the module are both necessary. The extent of PID of a PV module can be detected by either measuring the different module parameters (such as open circuit voltage (V_{oc}), operating voltage (V_{op}), I-V curve and dark I-V curve measurement, etc.) or surface imaging such as electroluminescence imaging, thermal imaging, and lock-in thermography.

3.2.1 PID Detection by I-V Characterization

The shape of the I-V curve alters due to PID and sometimes I_{sc} and V_{oc} values also change. The change in shape of I-V curves of c-Si PV module does not always predict the PID, especially when the level of PID is low. So at a low PID level, the maximum power point (P_{max}) measurement of each module in the string at STC is an effective way to detect PID (Moreno et al., 2013). P_{max} measurement at low irradiance is a more effective way to predict PID because the efficiency of solar at low irradiance is markedly reduced due to PID interrupt (Berghold et al., 2013; Braisaz & Radouane,

2014). The sequence of the PID affected parameters of crystalline Si PV modules is (Schwark et al., 2013):

$$I_{sc}<V_{oc}<I_{max}<\text{FF}<P_{max}$$

Due to PID, the shunt resistance of a PV module decreases and the module has to operate at a lower voltage than the remaining, non-PID affected modules within a string to maintain the same current. Degradation is easily detected by measuring the operating voltage (V_{op}) under the loaded condition of a PV module. The change of different PV module parameters used to observe the extents of PID are listed in Table 3.1.

The quality of a junction can be easily estimated through its dark characteristics (Bouzidi et al., 2012). To represent the PID of a PV module, sometimes dark IV characteristics taken in dark conditions (without illumination) cause the PV module to act as a diode. During dark IV measurements, modules are biased with about 20% of their datasheet I_{sc} and current flow in the reverse directions to that of light. I-V measurements are usually normalized as $V_{bias}/V_{oc\ nom}$ (Moreno et al., 2013).

The ability to detect PID by measuring V_{op}, V_{oc}, P_{max} and V_{bias} etc. is shown in Figure 3.3 depicting PID behaviour of 24 modules connected in series within a string. The 1st and 24th modules are positioned at the negative and positive terminals, respectively. Values of each of the module parameters (V_{oc}, V_{op}, P_{max}, and V_{bias}) are normalized by dividing them by their respective nominal values from a data sheet given by the manufacturer and are plotted according to the position of each module within the string. However, the 1st and 2nd modules were previously replaced by new modules due to severe PID. Modules positioned near the negative terminal had a greater PID level and lower values of $V_{oc}/V_{oc\ nom}$, $V_{op}/V_{max\ nom}$, $P_{max}/P_{max\ nom}$ and $V_{bias}/V_{oc\ nom}$ as compared to modules not positioned near the negative terminal. In Figure 3.3, it is clear that the P_{max}

and V_{op} values provide more efficient information to detect PID than the V_{oc} and V_{bias} values.

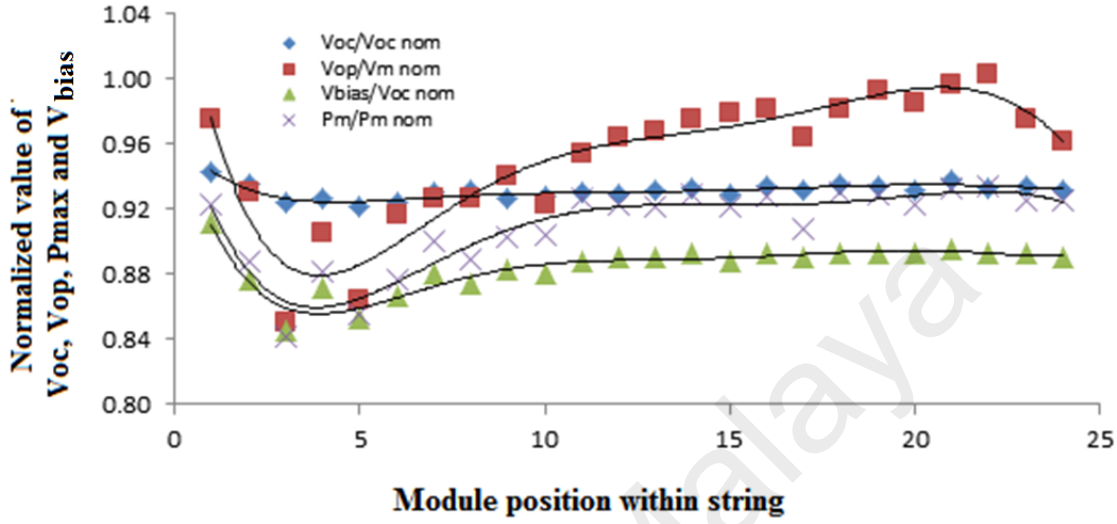

Figure 3.3: Normalized values of V_{oc}, V_{op}, $V_{bias,}$ and P_m of the 24 modules connected in series in a string affected by PID. Module 1 and 2 are newly exchanged (Moreno et al., 2013; Martínez-Moreno et al., 2018)

Table 3.1: Nature of different PID detection techniques

PID Detection Techniques	Operating Process	Amenities	Conditions
Measuring operating voltage (V_{op})	Reduction of V_{oc} due to PID is measured by simple voltmeter	Simple	Reduction is only noticed when the effect of PID is high (Moreno et al., 2013).
Measuring open circuit voltage (V_{oc})	Normalized operating voltage (V_{op} /$V_{maxnominal}$) is measured	PID detection capability is higher than V_{oc} measurement technique	Measurement under loading condition
Maximum Power (P_{max})	Measuring through an I-V curve	More efficient than V_{oc} and V_{op}	At low irradiance, is more effective at detecting PID

3.2.2 PID Detection by Surface Imaging

The electrical characterizations show the PID level of each PV module within strings, nevertheless, the PID of each cell within the module is quite difficult to identify.

Imaging of the module surface with a specialized technique is one of the reliable and fast tools used to identify the PID and possibly to detect the PID of each cell within each module. The surface imaging processes are 1) Thermal (IR) imaging, 2) Electro Luminescence (EL) imaging, and 3) Lock-in thermography (LIT). These are described briefly in the following sections.

3.3.2.1 Thermal (IR) Imaging

Detection of PV module degradation (especially, on-site during operation) through IR thermography is a fast and reliable technique (Buerhop et al., 2012). Although IR imaging can be done without interference of the operation of the PV plant, sometimes the detection of temperature differences between the PID affected and the unaffected cell is hampered at low irradiation; that is why IR imaging has to be done at higher irradiation during sunny days (Moreno et al., 2013). A typical IR image of PID affected modules is shown in Figure 3.4. The bright cells are highly degraded and possess high temperature.

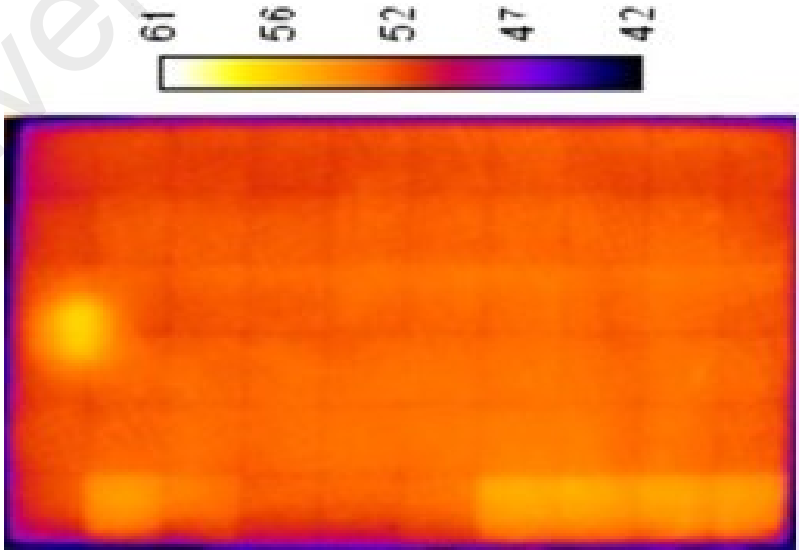

Figure 3.4: Typical thermal image of a PV module with PID (Tsanakas et al., 2016)

3.3.2.2 Electroluminescence (EL) Imaging

Electroluminescence (EL) imaging is one of the most reliable methods to accomplish a detailed characterization of PID affected module (Moreno et al., 2013). A dark environment is requisite for EL imaging; hence, EL imaging is carried out at night for on-site PID characterization. A comparative view of EL and IR imaging is presented in Figure 3.5. In the EL image, healthy cells show a bright appearance due to a high recombination rate, while degraded cells look dark. A module produces a PID pattern depending on the degradation level of each cell within the module. The IR image is in reverse contrast and dark cells possess a higher temperature due to a higher PID level. Both EL and IR images show similar patterns of PID. The immensity of EL imaging over thermal imaging is that EL imaging does not interfere with thermal distortion.

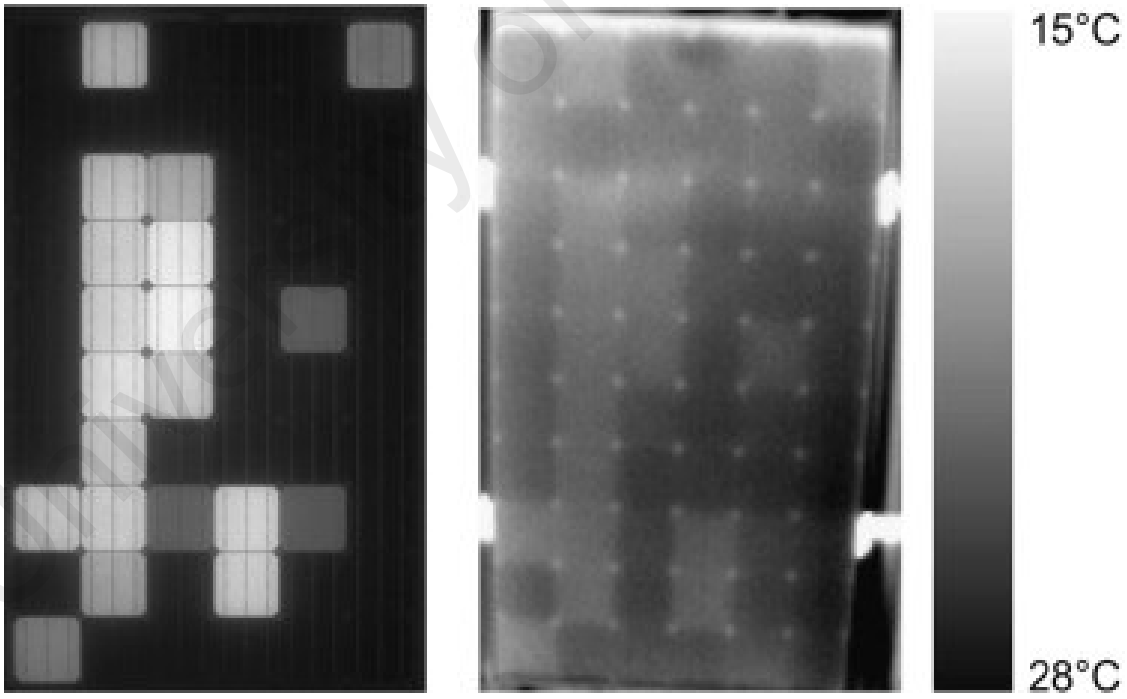

Figure 3.5: EL image (left) and thermal (IR) image (right).of a PID affected module (Kaden et al., 2015)

3.3.2.3 Lock-in Thermography (LIT)

Lock in thermography (LIT) is sometimes used to sense the localized shunting distribution of the PID affected cells (Schutze et al., 2011b). Normally, for PID characterization, LIT is performed in a dark environment (Breitenstein, 2012; Breitenstein et al., 2015). The PV module, without backside foil, improves the resolution of LIT by reducing the lateral temperature gradient extension (Naumann et al., 2012). EL imaging takes some minutes to perform, while LIT takes only a fraction of a second. Nonetheless, a common drawback of LIT is its disturbed three-dimensional resolution due to thermal distortion (Breitenstein et al., 2011).

3.3 Recovery Processes of PID

The degeneration caused by PID can be recovered where the extent of recovery is contingent on the level of degradation (Koch et al., 2012b; Pingel et al., 2012) and on the manner of the recovery system (Fjaellstroem et al., 2015). It was reported that the PID phenomenon is partially reversible excluding electrochemical corrosion or other heavy damages (Berghold et al., 2013). Therefore, by reversing the cause of PID, the degradation extent of a module can be recovered (Pingel et al., 2010). It is assumed that the recovery generally arises through regeneration of the p-n junction of the degraded cell and out-diffusion of Na^+ ions from the vicinity of the p-n junction. The structural view of the PID recovery process is shown in Figure 3.6. During the recovery process, the metal atoms diffuse out of the SFs of the p-n junction to the oxide layer and SFs become free of metallic conduction. Hence, shunt resistance is recovered gradually (Lausch et al., 2014b). Since the PID regeneration process is a diffusion control phenomenon, it occurs at PV plants at night, when harmful high voltage stress is absent, but the process is very slow and the amount is negligible (Schwark et al., 2013). Generally, the diffusion process is accelerated by applying a voltage or increasing the

temperature, similarly, the PID recovery rate can be enhanced by applying a voltage or increasing the temperature. The recovery system can be separated as potential induced recovery and thermal induced recovery, which are briefly discussed below.

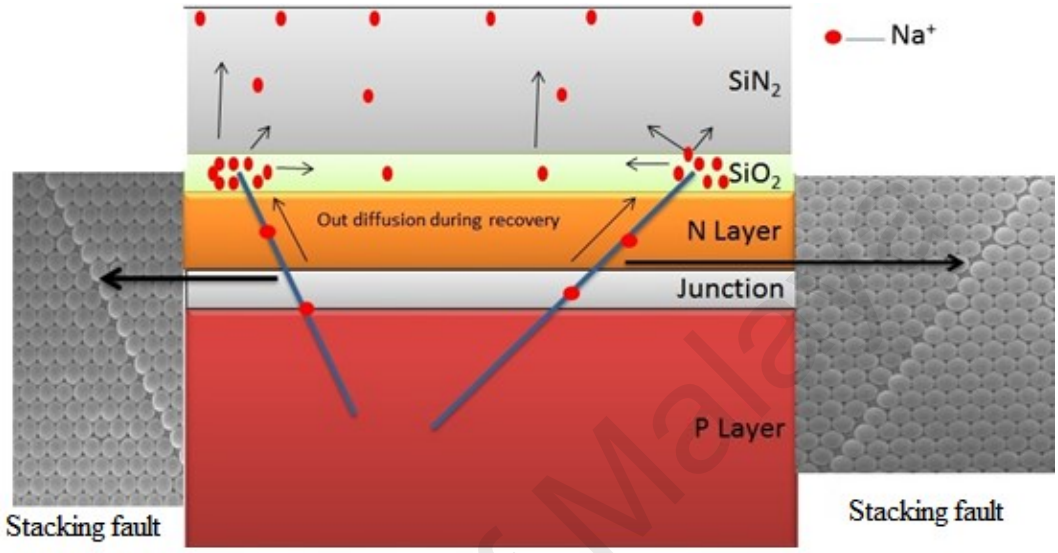

Figure 3.6: Structural view of the PID recovery process (Lausch et al., 2014b)

3.3.1 Potential Induced Recovery

Degradation of module due to PID can be recovered by applying a voltage to a reverse track of the high voltage stressed direction of the PV module; through the application of a negative voltage at the frame to the cell. Potential induced recovery can be done in the field or in the laboratory. In field recovery, a device is used that applies positive voltage during the night. There are several commercially available apparatus from different companies such as SMA solar technology, Ilumen, Padcon and Pidbull that apply a positive voltage to the PV modules for regeneration of PID affected PV modules. PID of a PV module can also be recovered using a grounding kit, where the negative pole of a PV module is grounded and a self-generated positive recovery potential comes from the string (Pingel et al., 2012). In the laboratory, PID recovery is normally done in an environmental chamber where the module is exposed to +600V to

+1000V. The recovery time can be controlled by regulating environmental factors such as humidity and temperature; at a higher temperature, the rate of recovery will increase (Berghold et al., 2010).

3.3.2 Thermal Induced Recovery

In the absence of high system voltage, positive ions accumulated during PID, then diffuse to the back and this diffusion process can be accelerated by thermal treatment. The junction characteristics of the PID affected cell can be regenerated after thermal treatment by storing the affected module at 250°C for 25 hours (Lausch et al., 2014a). Figure 3.7 shows EBIC images for development and recovery of a shunt site due to PID and the thermal induced recovery process. The shunt has been placed inside the dotted circle; the inset of Figure 3.7 (a) shows the shunt at an SF. The grain boundary is indicated by a dotted line. After recovery, the shunt site is clearly vanished. Nevertheless, it was reported that for generation of the initial power, a large amount of heat and time is needed (Lausch et al., 2014b). The high temperature can decrease the long-term stability of panel material by thermal stressing, a drawback of thermal recovery systems (Pingel et al., 2010).

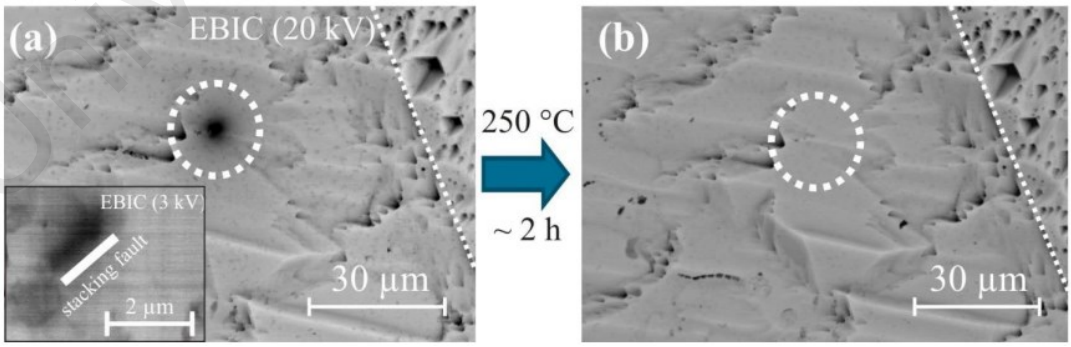

Figure 3.7: PID shunt site before (a) and after (b) a thermal recovery process (Lausch et al., 2014b)

3.4 IEC Standard for Laboratory PID Test

Until July 2015, there was no acknowledged test standard available for PID testing. Recently, the International Electrotechnical Commission (IEC) published standards titled as 'IEC TS 62804-1:2015' for PID testing in laboratory conditions (IEC 62804, 2015). In this standard, the following conditions are assumed:

- In the wet leakage current measurement process, if a wetting agent (such as water) is used, then all faces of the modules shall be immediately and thoroughly rinsed following the wet leakage current test.
- The water of resistivity not less than 0.05 MΩ cm.
- In all cases, all faces of the module should be wiped dry with a clean cotton or paper towels and not air dried as the final step.

Each module should characterize only one set of test conditions since PID is history dependent (Schutze et al., 2011b). The summary of the IEC standards for PID testing methods is given in Table 3.2 and the detailed procedure is shown in Figure 3.8.

Table 3.2: IEC TS 62804-1:2015 standards for PID lab test (IEC 62804, 2015)

	IEC TS 62804-1 (Method A)	**IEC TS 62804-1 (Method B)**
Test environment	Environmental chamber	Temperature controlled laboratory room
Test conditions	Temperature: 60°C Relative humidity: 85%	Temperature: 25°C Relative Humidity < 60%
Contacting method	Frame grounding	Front glass surface is covered with aluminium foil
Test duration	96 h	168 h (7 days)
Test voltage	±1000 V	±1000 V
Pass-fail criterion	< 5% power degradation	< 5% power degradation

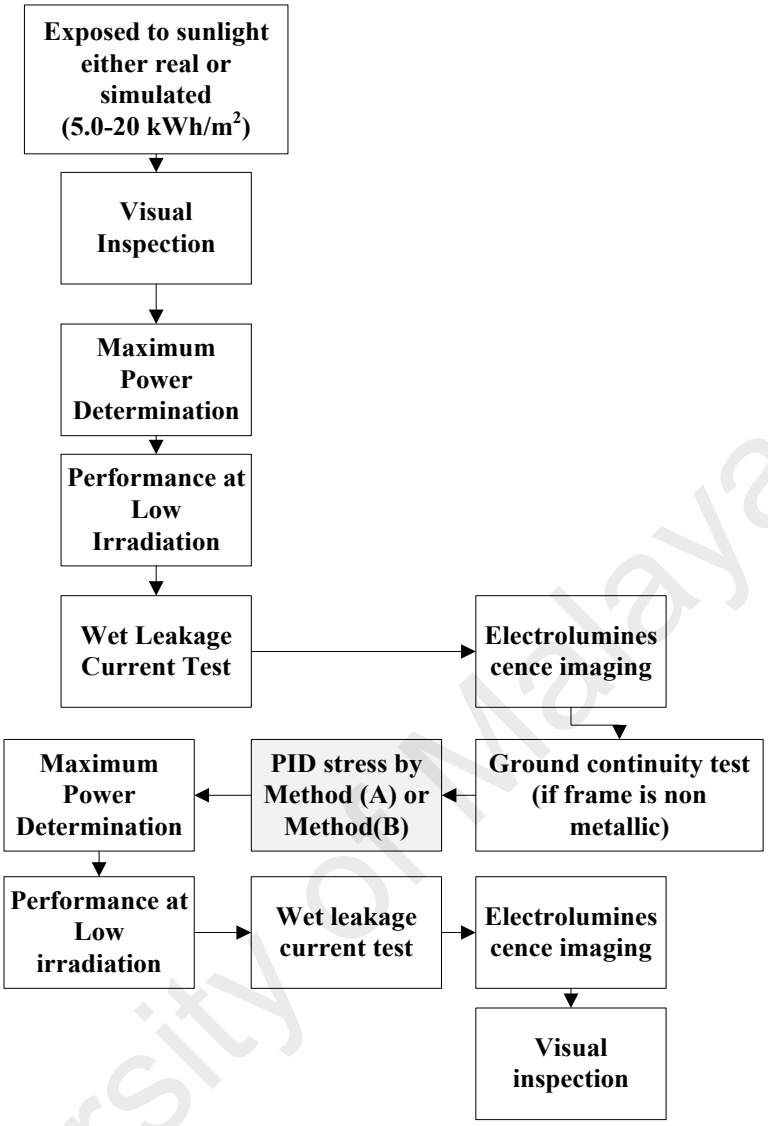

Figure 3.8: Flowchart of IEC 62804 PID characterization process (IEC 62804, 2015)

3.5 Relation between EL Image Intensity and PV Performance

Electroluminescence imaging is a useful and functional method for analyzing different degradations phenomena PV module. Several reports are available in literature regarding the characterization of PV module performances through EL imaging; for example, EL imaging was used for detecting series resistance and shunt resistance (Breitenstein et al., 2008), microcrack (Kajari-Schröder et al., 2011), p-n junction minority carrier's diffusion length (Takashi et al., 2005; Würfel et al., 2007). The diffusion length of minority carrier determines the performance of individual PV cell (Würfel et al., 2007). Takashi et al.

(2005) reported a relationship between the minority carrier diffusion length and electroluminescence image intensity. From this relationship, a measurable investigative technique for the finding of degradation of photovoltaic cells has been introduced (Takashi et al., 2005). Mochizuki et al. (2016) suggested the measurable open circuit voltage representing technique by means of electroluminescence image intensity of PV module. Rajput et al. (2018) reported the possibility of series resistance and dark saturation current extraction of individual cell of PV module by EL imaging. Recently, Bedrich et al. (2018) proposed a quantitative electroluminescence imaging process for performance estimation of PID-influenced PV modules. Electroluminescence intensity depends on the effective diffusion length and number of minority charge carrier and the photovoltaic cell performance likewise rely upon these parameters. So, therefore, the summation of entire pixel's electroluminescence intensity of a PV module is correspondence to the power output of that PV module. The total number of pixels is equivalent to the cell area of the PV module. The average value (mean) of EL intensities of all pixels within the PV module is proportional to the power output (P_{max}) per unit cell area. The relationship is expressed as follows:

$$E_{mean} \propto \frac{P_{\max}}{A_{cell}} \tag{3.1}$$

$$E_{mean} = C \times \frac{P_{\max}}{A_{cell}} \tag{3.2}$$

where the mean of all pixels' intensities is E_{mean}, the maximum power output is P_{max} and C is a calibration factor. The entire area of PV cell is A_{cell}. From the electroluminescence images of new and non-degraded PV modules, the C value can be is determined.

CHAPTER 4: RESEARCH METHODOLOGY

4.1 Introduction

The underlying objectives of this research are to investigate the on-site PID behavior and its relationship with the laboratory standard test condition. To accomplish these purposes, two-fold research methodology has been adopted, viz., exploratory and experimental research technique. As the root cause of PID is still to be resolved, in order to gain further insight into this rather newly detected phenomenon exploratory research is essential. On the other hand, in order to examine the cause-and-effect relationships among various parameters that are involved with PID an experimental research method has been followed. Moreover, in order to facilitate extrapolation of laboratory-based experimental results to natural settings, field experiments have been carried out along with laboratory investigations. The following sections of this chapter contain the details experimental procedure along with the experimental setup, instrumentation, testing conditions and data collection processes.

4.2 Meteorological Conditions and Module Specification of PV Plant Site

The PV module degradation behaviour due to real field aging has been investigated by taking several PV modules aged in real field condition at different time of periods. The sample modules are taken from the 4 kW PV power plant. The plant was situated at the solar garden of UMPEDAC, University of Malaya and comprising of both mono- and polycrystalline types PV modules, which have been field aged for different spans of time. Features of PV module qualifications at standard testing conditions have been showed in Table 4.1. The climate conditions data of the PV plant site is shown in Table 4.2.

Table 4.1: Different PV modules' specification

Module specifications	Module A	Module B	Module C	Module D
Manufacturer	SHAIYANG	ENDAUPV	MITSUBISHI	SHELL SOLAR
Cell material	Monosilicon	Polysilicon	Polysilicon	Monosilicon
Number of cells	36 (4×9)	60 (6×10)	36 (4×9)	36 (4×9)
Size (mm)	1200×545×35	1666×997×42	1495×674×46	1200×527×46
P_{max} (W)	90 W	250 W	125 W	85 W
V_{oc} (V)	22.03	36.96	21.8	22.2
I_{sc} (A)	5.30	8.8	7.9	5.45
V_{mp} (V)	18.36	31.26	17.3	17.2
I_{mp} (A)	4.90	8.0	7.23	4.95
Size of cell (mm)	125×125	156×156	156×156	125×125
Temp coefficient, P_{max} (%°/C)	0.549	0.45	0.452	0.43

4.3 Experimental Setup

The Cell Solar Testing Laboratory at UMPEDAC, University Malaya, was used to carry out the experimental investigations. Investigations have been made to study the leakage current behaviour of PV module at different high voltage stresses and different environmental conditions, to carry out the laboratory PID testing, and to determine the different light and dark IV parameters of degraded PV modules.

4.3.1 Leakage Current Measurement

Different types of PV modules (A, B, C and D as given in Table 4.1) have been used in this experiment. Experimental setup for leakage current measurement is shown in Figure 4.1.

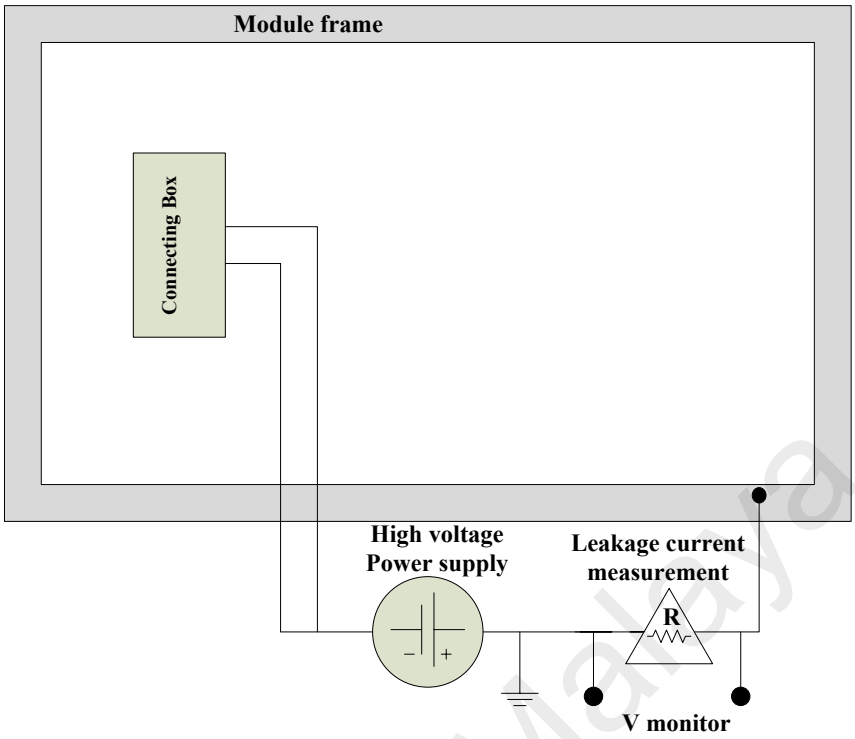

Figure 4.1: Leakage current measurement circuit
(Kang et al., 2015)

In between DC power supply and the PV module frame, a resistor of 10kOhm was inserted in series. The leakage current was measured based on the determination of voltage developed across to the resistor.

Table 4.2: Monthly 22 years average insolation, wind speed and humidity of the PV plant site
(NASA, 2017)

Month	Averaged Insolation ($kWh/m^2/day$)	Average Wind Speed (m/s)	Average RH (%)
January	4.79	3.64	77.40
February	5.37	3.08	73.90
March	5.42	2.68	77.50
April	5.27	1.83	82.20
May	5.11	1.80	83.00
June	4.98	2.58	82.70
July	4.92	2.63	83.10
August	4.87	2.81	83.00
September	4.88	2.25	82.50
October	4.76	2.00	82.10
November	4.36	2.67	83.10
December	4.17	3.66	81.70
Annual	4.90	2.63	81.00

4.3.2 Solar Simulator

A solar simulator made of halogen bulbs, has been used to investigate the PV module performance at different temperatures and irradiances as shown as in Figure 4.2. The halogen bulbs were 50W capacity having voltage and current rating of 12 V and 4.17 A respectively and manufactured by OSRAM. The irradiance has been altered by using variable AC power transformers. This simulator is designed to operate at indoor conditions.

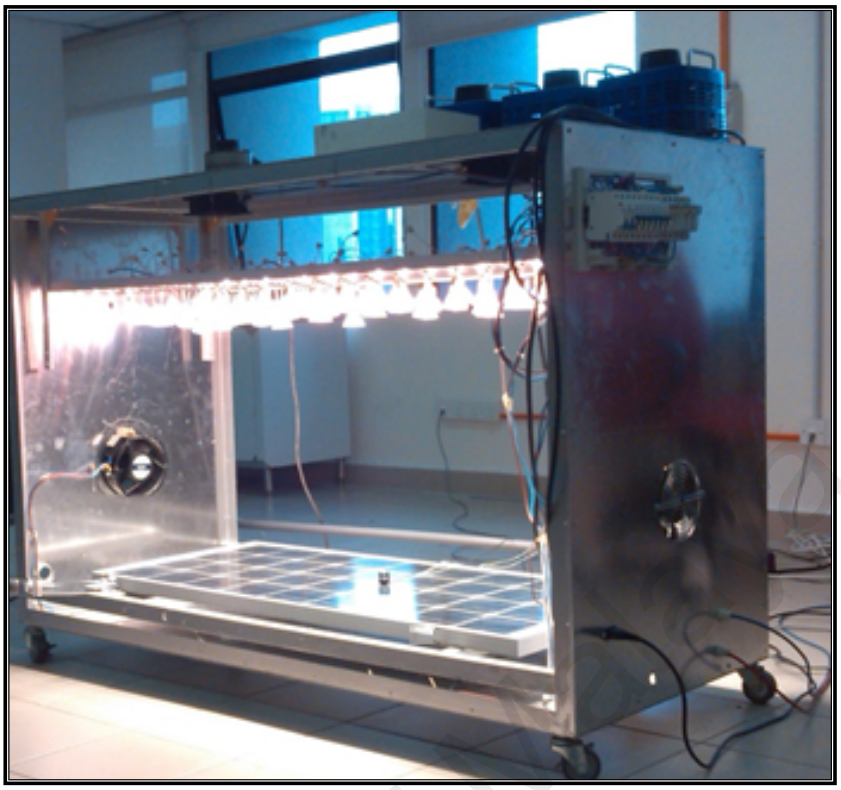

Figure 4.2: Sun simulator used to investigate the effect of temperature and irradiance on PV module performances
(Rahman et al., 2015)

4.3.3 EL Imaging Setup

An electroluminescence (EL) imaging technique has been run to investigate the fitness of PV module's by means of each cell performance as presented in Figure 4.3. The setup consists of components like programmable DC power supply, CCD camera able to sense light in the infra-red range, dark room, and a computer integrated with the control system and EL image analysis software. The block diagram of the EL imaging process is as shown in Figure 4.4.

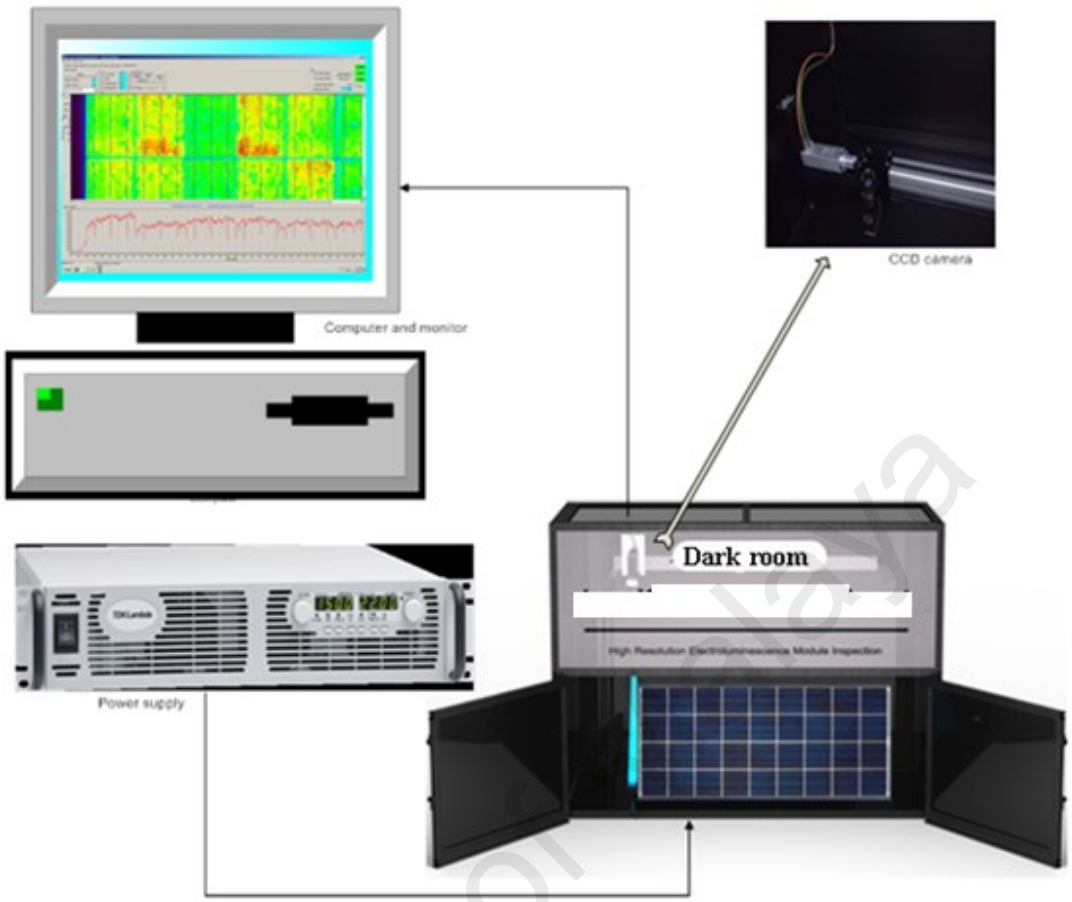

Figure 4.3: EL imaging set up

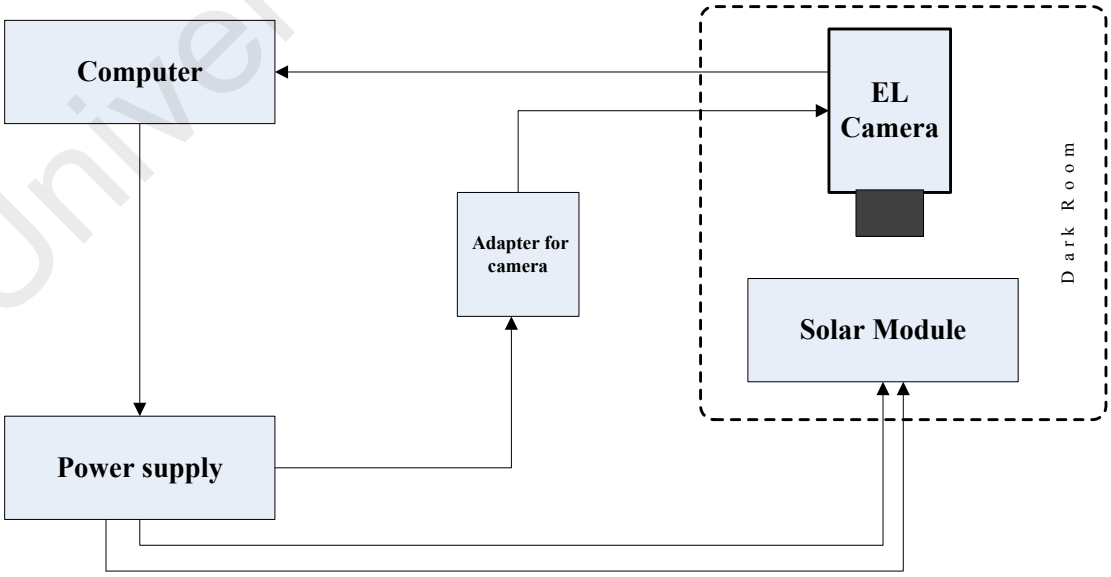

Figure 4.4: EL imaging circuit connection

A Minolta MD W Rokkor objective with a focal length of 35 mm and a maximum F number of f/1.8 is equipped with the CCD camera. The camera is mounted on a tripod which can move freely through a tunnel as shown in the setup in Figure 4.3. The camera scans the entire module by taking several shots. A single shot cover 30 cm distance. Number of shot depends on the PV module length. The camera can move maximum 5.5 m tunnel length allows the measurement of all common panel sizes of up to 2m x 2m. The photovoltaic module is placed inside the dark room and connected with the cable of DC power source for forward biasing. Doors of the darkroom are closed during the imaging process.

4.4 Instrumentations

In this research, various types of instrument have been used for example high DC power source (Hi-Pot Tester), multi-meter, thermos-couple, data logger, conductivity meter and digital high precision electric balance etc.

4.4.1 High Voltage DC Power Supply

A programmable high DC power supply has been used to measure the HVS PV module's leakage current. The brand name of DC power supply is Hi-Pot Tester with the model number of DU-332 manufactured by Delta Instruments, Taiwan as shown in Figure 4.5. The capabilities of the power supply are 0 to 6kV DC and from 0 to 5kV AC. The cut-off current range of the device is from 0.0 to 15 mA for AC and from 0.01 to 7.5 mA for DC system.

Figure 4.5: Programmable DC power supply (Hi-Pot Tester)

4.4.2 Data Logger

A data logger, Brand name: DataTaker; Model; DT80 Thermo Fisher Scientific Inc.) is used to measure different temperatures and solar irradiation. Its web-based dEX graphical interface can trace data rapidly and easily. The recorded data can be retrieved from a web browser or copied to any portable USB drive. The data logger uses a programming language that can interface with any complex system and communicate through a serial sensor port and other communication ports. It consumes very low power during operation.

Figure 4.6: DataTaker DT80

The DataTaker DT80 has five analog input channels; depending on the connection outline used, these channels permit the measurement of 5 to 15 separate voltages. Each analogue input channel is a 4-wire input, which allows the measurement of voltage, current, resistance, and frequency. These are the fundamental signal outputs of most sensors.

4.4.3 I-V Tracer

An I–V analyser as shown in Figure 4.7 is used to measure the PV module output of open-circuit voltage (V_{oc}), short-circuit current (I_{sc}), maximum power (P_{max}), maximum voltage (V_m), and maximum current (I_m). The NASA 2.0 I–V tracer, developed by UMPEDAC, can trace power up to 2000 W. The operating specifications of the I–V tracer is provided in Table 4.3.

Figure 4.7: I-V tracer (Model: NASA 2.0)

Table 4.3: Specifications of the I–V tracer

Parameter	Measuring Range
V_{oc}	1.00 – 600 V
I_{sc}	0.50 – 7.00 A
P_{max}	0 – 2000 W

4.4.4 Pyranometer

A LI-COR PY82186 silicon pyranometer, as shown in Figure 4.8, is used in the experiment to measure the solar irradiance. This type of pyranometer is used for PV performance study to measure incident irradiation intensity as well as meteorological and agronomic research. The LI-COR pyranometer has been calibrated with a standard radiometer on a sunny day. This pyranometer can measure irradiance up to 1500 W/m^2 within a spectral range is from 300 to 1100 nm and its operating temperature range is from − 40 to 95°C.

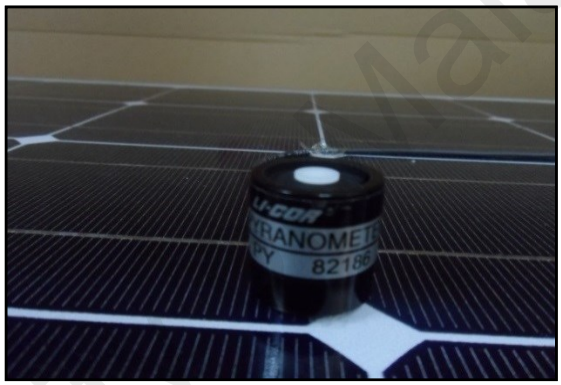

Figure 4.8: Silicon pyranometer (Model: LI-COR PY82186)

4.4.5 EL Imaging Dark Room and Camera

Silicon charged couple device (CCD) camera LumiSolar Professional from Great Eyes GmbH, Berlin, Germany was used for capturing the electroluminescence images of the PV modules (Figure 4.9). The camera is equipped with enhanced VIS sensitivity to infra-red light.

Figure 4.9: EL imaging dark room and camera (Model: LumiSolar Professional)

The specification of CCD camera and the dark room of the EL setup are shown in Table 4.4.

Table 4.4: Specification of the camera and darkroom of the EL-imaging setup

Parameters	Value
Resolution of Image (PPI)	528
Maximum PV module size	Max. 1.1 × 2.0 m
No of camera	one CCD scientific camera
Direction of scan	Single
Dark room size (W;D;H)	2.45×1.4×2.0 m

4.4.6 PID Insulation Tester

A PID insulation tester (Model: TOS7210S, Kikusui Electronics Corp., Japan), as shown in Figure 4.10, has been used for the PID laboratory testing purpose. The device can be to set from of 50 Vdc to 2000 Vdc with 1.0 V resolution. The polarity of applied voltage can be changed instantly by a switch provided on the front panel.

Figure 4.10: PID insulation tester (Model: TOS7210S)

4.5 Experimental Testing Conditions

4.5.1 Measurement of PV module's HVS Leakage Current

Different high voltage stresses within a range of 100 V to 1500 V DC, with a step 100 V have been applied to measure the leakage current. The effect of module temperature on the HVS leakage current of PV module has been investigated by increasing PV module temperatures from 25°C to 60°C with a step of 5 degrees. Both top and bottom surface temperatures of PV module have been monitored and module temperature is the average of these two. The IEC 61215 test standard was followed during the wet leakage current test. By spraying 200ml/m^2 distilled water on PV module surface the wet surface condition has been created. The effect of aqueous salt on the HVS leakage current has been investigated by using purified sea salt aqueous solution. The concentrations of aqueous salt solution are 1, 2, 3, 4 and 5 g in 200 ml/m^2. The temperature during the leakage current measurement was room temperature (25°C). A STARTER 3100C Brand named, conductivity meter has been used to measure the salinity and conductivity of the salt aqueous solution.

The dust deposition effect at on-site on HVS leakage current characteristic of PV module has been investigated by taking three outdoor placed PV modules with duration of near about one year. The HVS leakage current characteristic has been measured at

wet surface and 25 °C temperature conditions. To investigate the effect of different amount of dust particle deposition on the PV module surface, numerous dust weights for example 2, 3, 4 and 5 g/m^2 have been applied on the module surface as possible as homogenously and HVS leakage current characteristic has been measured at wet surface and 25 °C temperature conditions. The PV module was washed with distilled water and dried properly before running each test; so that effect of the previous experiment diminishes. The FESEM and EDX characterization of dust particles have been done by using a field emission scanning electron microscope, Brand- Hitachi, Model SU8220 and an X-ray diffraction machine (Brand: PANalytical Model: EMPYREAN) with Cu-K_α radiation has been used to take XRD. Scanning angle (2θ) range for XRD was 5° - 85°. The effect of aging on the leakage current of PV module has been investigated measuring wet leakage current of PV module field aged at different time of periods.

4.5.2 Laboratory PID Testing

Laboratory PID testing has been carried out rendering to the IEC 62804 test standard (Method B) in a temperature controlled room of 25°C was maintained. PV module front surface and frame were fully wrapped with aluminium foil. The high DC voltage stress was given by using a PID insulation tester. Leakage current in terms of resistance of the PV module was recorded from the of PID tester. DC voltage of +ve 1000 V and -ve 1000 V stresses were applied to the PV modules by changing the polarity of the PID tester for a duration of 168 hours (7 days) at a stretch, while room humidity was maintained below 60%. Before voltage stressing, the PV module was exposed to a real sunlight in outdoor for about 20 kWh/m^2. EL imaging, wet leakage current measurement, and I-V characterization have been conducted both before and after voltage stressing.

4.5.3 Electroluminescence (EL) Imaging

Before taking EL image, the module surface has been rinsed with distil water and isopropyl alcohol. The maximum current and voltage rating in course of EL imaging are set to 3 A and 50 V respectively for the DC bias. The each cell electroluminescence mean intensity value has been determined by selecting complete cell by marquee tool and taking the histogram data as shown in Figure 4.11(Bauer et al., 2017). Rectangle marquee tool is used to mark the EL images of polycrystalline PV modules, while for monocrystalline modules the rounded rectangle has been used.

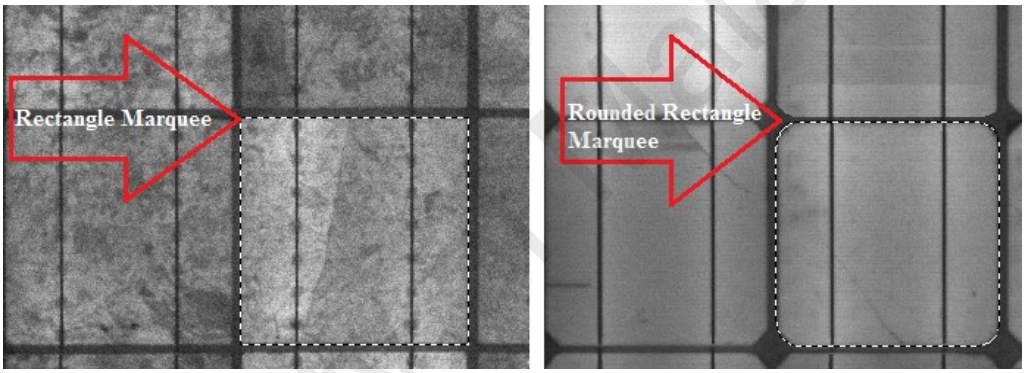

Figure 4.11: EL intensity measurement of individual cells with a polycrystalline (left) and monocrystalline (right) PV module

4.5.4 Light and Dark IV Characteristics

Light I-V (LIV) characteristics of different PV modules have been taken both in indoor and outdoor conditions. In indoor, a solar simulator has been used and different independent variables such as ambient temperature, module temperature (rear and top surface) and radiation are observed through the thermocouples and pyranometer connected with the data logger at a predefined time interval. The PV module outputs in terms of V_{oc}, I_{sc}, V_{max}, I_{max} and P_{max} are also measured by the I-V tracer with the same time interval of the data logger. In outdoor, the PV module I-V characteristics are measured during the sunny days at Solar Garden of UMPEDAC, University of Malaya,

Kuala Lumpur, Malaysia. The PV module surface has been cleaned with water and isopropyl alcohol to eliminate the error due to dust accumulation. At room temperature, 25°C, the dark I-V (DIV) characteristic was tested by biasing the solar modules with a dc power supply. The biasing voltage was increased from 0.1 V up to the rated V_{oc} of respective PV module with a step of 0.1V and corresponding currents were monitored.

4.6 Mathematical Formulation

4.6.1 Photovoltaic Module Degradation from EL Image

The PV module degradation D has been determined as follows:

$$D = (E_{mean\ (STC)} - E_{mean}) / E_{mean\ (STC)} \times 100\ \% \tag{4.1}$$

$$E_{mean\ (STC)} = \frac{P_{\max}(STC)}{A_{cell}} \times C \tag{4.2}$$

where $E_{mean(STC)}$ is mean intensity of non-degraded PV module EL image, A_{cell} is the total PV module's actual cell area, E_{mean} is mean intensity of EL image of degraded module, C is a calibration factor.

The value of calibration factor C has been determined by the several brand new PV modules $[P_{max}(STC)/A_{cell}]$ value and mean value of EL intensity (E_{mean}) from the brand new non degraded module's EL image by Eq.(4.3) as follows:

$$C = E_{mean} \div [\frac{P_{\max}(STC)}{A_{cell}}] \tag{4.3}$$

4.6.2 Temperature of the PV solar Cell and Temperature Coefficient of P_{max}

Solar cell temperature can be calculated by the following equation: (Rahman et al., 2015):

$$T_{sc} = \frac{p_{sc} G\left(\tau_g \alpha_{sc} - \eta_{sc}\right) + \left(U_{sca} T_a + U_t T_b\right)}{\left(U_{sca} + U_t\right)} \tag{4.4}$$

Different parameters and their values for the determination of solar cell temperature is enumerated in Table 4.5 as below:

Table 4.5: Values of the parameters for the calculation of solar cell temperature (Dubey & Tay, 2013; Rahman et al., 2015)

Parameter	Value
Glass transmissivity, τ_g	0.960
Cell absorptivity, α_{sc}	0.90
Coefficient of heat transfer through glass, U_{sca}	7.14 W/m^{2}K
Coefficient of heat transfer from top to rear surface, U_t	150 W/m^{2}K

The temperature coefficient of P_{max} (γ) has been determined as follows:

$$\gamma = \left[\frac{P_{\max}(STC) - P_{\max}(T_{sc}, 1000\ W/m^2)}{T_{sc} - 25\ ^\circ C}\right] \div P_{\max}(STC) \times 100\ \% \tag{4.5}$$

The rate of degradation of γ value (DR_γ) is calculated by Eq. (4.6) where Y_{age} is the aging period in year.

$$DR_\gamma = \frac{\gamma - \gamma(STC)}{\gamma(STC)} \div Y_{age} \times 100\ \% \tag{4.6}$$

4.6.3 Uncertainty and Sensitivity Analysis

Uncertainty of an experiment is very important to determine the consistency of the experimental work. The standard error has been calculated by using following equation as below (Carrillo et al., 2017; Nasrin et al., 2018):

$$\varepsilon = \frac{S}{\sqrt{n}} \tag{4.7}$$

Where

ε is the value of standard error

S is the standard deviation

n is the number of samples

Standard deviation has been calculated by using following equation

$$S = \sqrt{\frac{1}{n}\sum_{i=1}^{n}(Y_i - \overline{Y})^2} \tag{4.8}$$

Where Y_i is the i^{th} depended variable value

$\overline{Y}$ is the mean of dependent variable values.

The sensitivity analysis has been carried out by measuring sensitivity index (SI). The below formula has been used to measure the sensitivity index (SI) as follows (Jakhrani et al., 2013):

$$SI = \frac{Y_{\max} - Y_{\min}}{Y_{\max}} \tag{4.9}$$

Where

SI is the sensitivity index,

Y_{min} and Y_{max} are the minimum and maximum values of dependent variable.

CHAPTER 5: RESULTS AND DISCUSSIONS

5.1 Introduction

An investigation of PID behaviour of PV modules under real field condition and standard laboratory accelerated test condition has been carried out. The effects of different environmental and operating parameters on HVS leakage current of PV module as well as the effect of field aging on the performances of PV modules have been investigated experimentally. The results obtained are examined and analysed along with relevant scientific justifications and elucidations. The inception of this chapter is with impact of different operating parameters on HVS leakage current of PV module. The selected operating parameters are such as temperature of PV module, water film, and dust and salt accumulation on the surface of PV module. Results from the PV module' degradations through different procedures, for example, maximum power detecting, EL imaging, HVS leakage current and dark IV have been detailed in the subsequent section. Finally, the degradation analysis of PV module due to LID effect, cell cracking, EVA discoloration etc. as consequence of different longtime field aging have been enumerated.

5.2 Effect of Different Parameters on Leakage Current

5.2.1 Consequence of PV Module Temperature

The HVS dependent leakage current of PV module at different module temperatures is shown in Figure 5.1. It can be noticed that with the increase of voltage stress, the leakage current increases exponentially. Precise minor increase in leakage current has been observed by reason of module temperature escalation from 25°C to 60°C as shown in Figure 5.1 inset. This can be due to the consequence of resistivity decreasing of glass and EVA at high temperature. It has been reported that resistivity of soda lime glass

declines 0.002/°C (Dhere et al., 2014c). The consequence of module temperature HVS leakage current at 600, 1000 and 1500 V stresses is presented in Figure 5.2. The obtained increasing rates are 0.0295, 0.0125 and 0.0038 µA/°C at 1500, 1000 and 600 V voltage stress respectively.

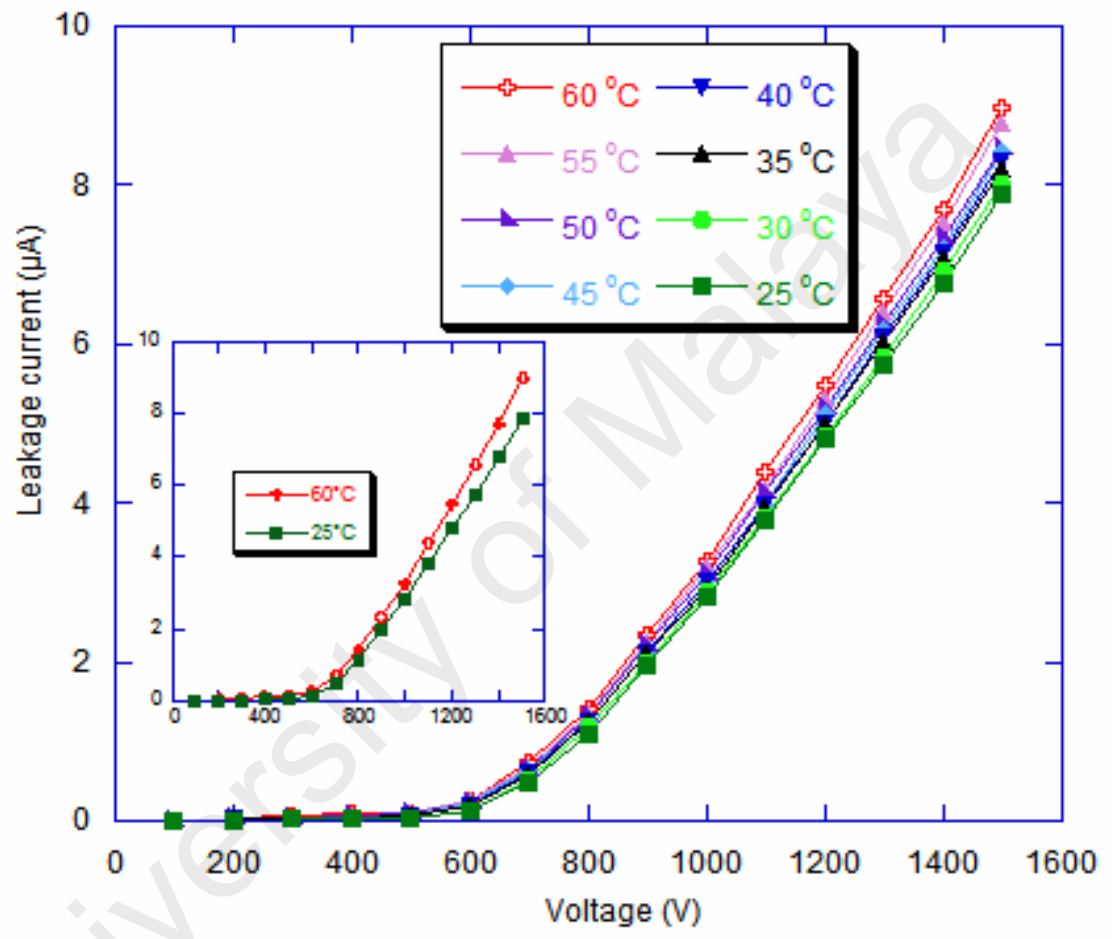

Figure 5.1: Effect of different HVS on the leakage current behaviour of PV solar module at different module temperature

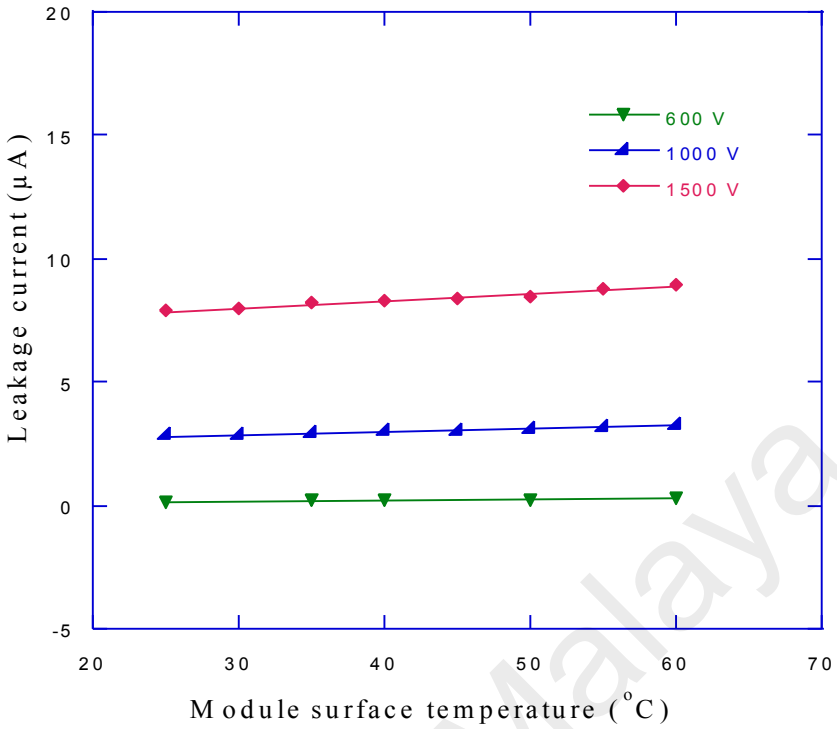

Figure 5.2: Module temperature dependent leakage current of non-wetted PV module at 600, 1000 and 1500 V stresses

5.2.2 Effect of Module Surface Wetting

The surface of photovoltaic module become wet owing to the high relative humidity of the ambient, morning dew or mist and rainfall etc. The effect of wet surface condition at different module temperatures of PV module is shown in Figure 5.3. The leakage current at wet surface condition increases drastically with the a slight increase of module temperature. The inset of Figure 5.3 shows that the value of leakage current at 60°C module temperature and dry condition is less than the leakage current value at room temperature and wet surface condition. In existence of wet condition, the metal content in the glass become ionized according to the following reaction and the surface conductivity increases as result leakage current also increases (Sinton & LaCourse, 2001).

$$(Si-O-R)glass + H_2O \rightarrow (Si-O-H)glass + R^+ + OH^- (solution)$$

where *R* is alkaline metal contains in the glass composition.

The high temperature and voltage stress at wet condition are very detrimental for PV module, because amount of leakage current increases drastically resulting in an escalation in PID rate. Table 5.1 shows a comparative feature of leakage current value obtained in the current investigation with the other published works.

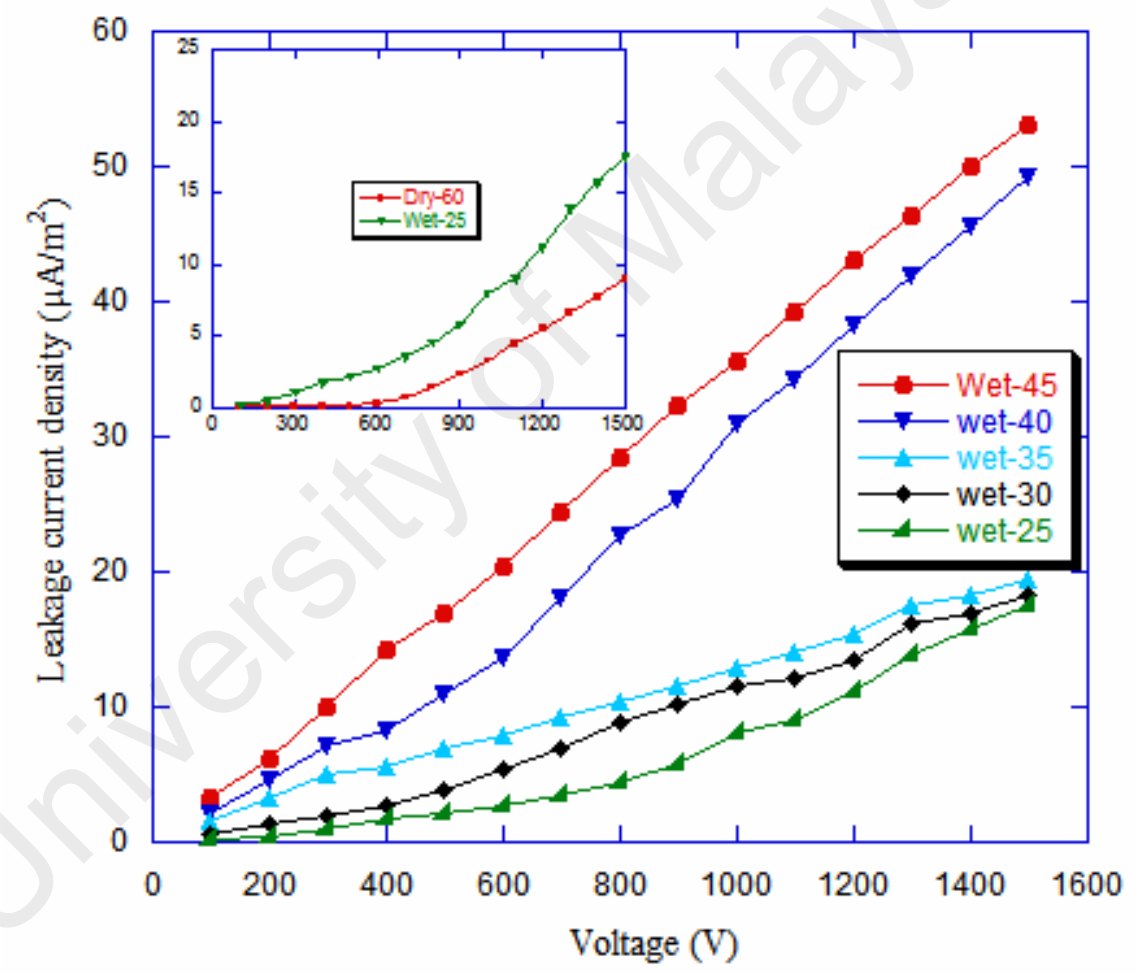

Figure 5.3: Effect surface wetting on the HVS leakage current of solar PV module at different temperatures

Table 5.1: Comparison of leakage current results of the present work with other published works in literature

	Author	Experimental Site	Experimental Condition	Leakage Current
Dry Leakage Current	Hoffmann and Koehl (2012)	Freiburg, Germany	600V, Module temperature: 10°C, Humidity: > 90%	95 nA
	Present investigation (2016)	Kuala Lumpur, Malaysia	600V, Module temperature: 25°C, Humidity: ~ 80%	128 nA
Wet Leakage Current	Schutze et al. (2011a)	Freiburg, Germany	600V, Module temperature: 25°C, Wet surface condition	0.95 µA
	Present investigation (2016)	Kuala Lumpur, Malaysia	600V, Module temperature: 25°C, Wet surface condition	1.5 µA

5.2.3 Effect of Salt Deposition

Near the coastal areas, the deposition of salt on the PV module surface commonly occurs. The effect of different salt concentration of water film of PV module surface at different high voltage stresses leakage current of PV module is shown in Figure 5.4. With the increase of salt concentration, the leakage current of PV module also increases significantly. It has been found that both conductivity and salinity of water film are increased with the increase of salt content as shown in the inset of Figure 5.4 as a result of which PV module glass surface resistivity drops. The ionization of salt content element in presence of water boosts the leakage current by increasing charge carriers. The increasing trends of leakage current due to increase of salt concentration at voltage stresses of 600, 1000 and 1500 V have been presented in Figure 5.5. The rate depends on the magnitude of voltage stress. At high voltage stress, the rate is also high. The leakage current increasing rates at 600, 1000 and 1500 V have been found as 0.469, 0.861 and 0.930 µA/gm respectively.

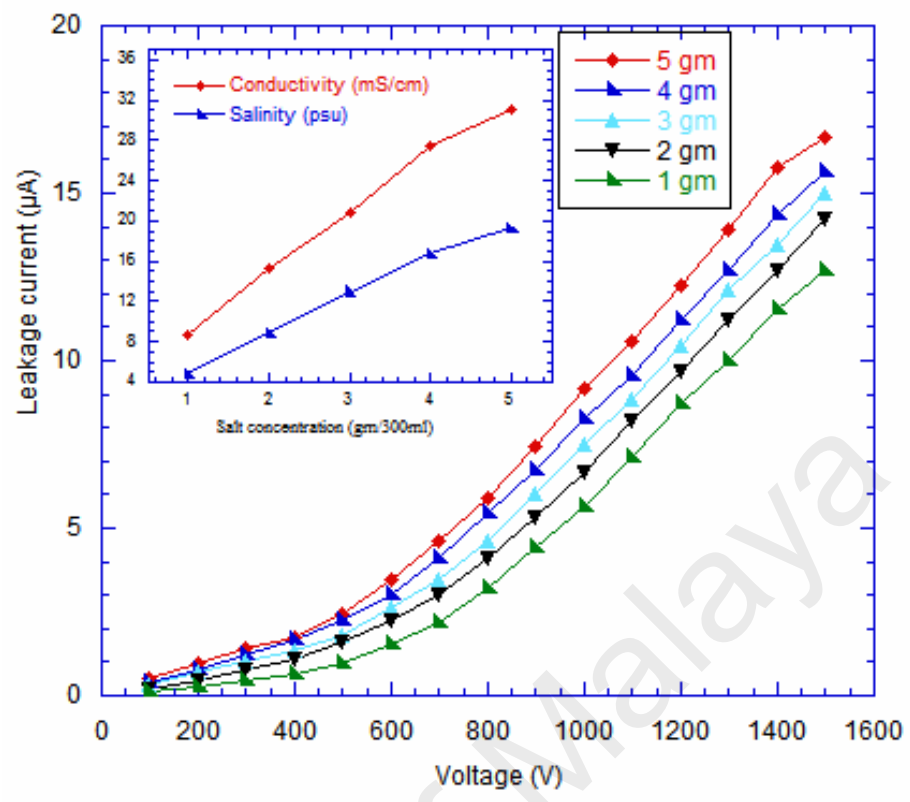

Figure 5.4: Effect of different salt concentration on the HVS leakage current of PV module at wet surface condition

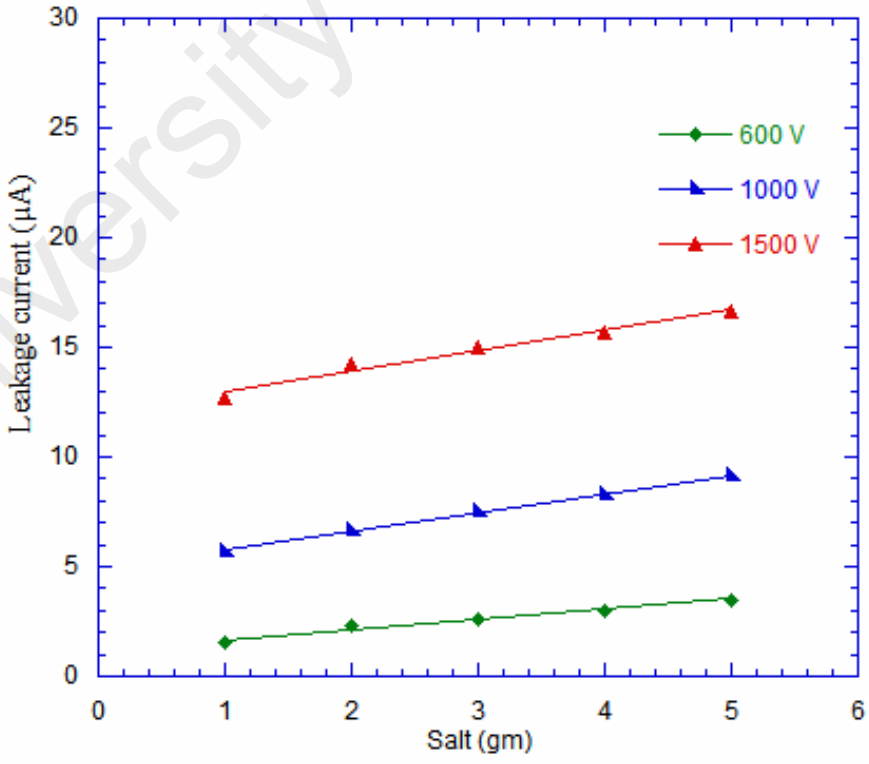

Figure 5.5: Leakage current at 600, 1000 and 1500 V stress at different level of salt on PV module

5.2.4 Dust Deposition Effect

The dust deposition effect has been investigated in laboratory by applying varing amount of dust on the sureface of type 'A' module. The wet leakage current dusty module has been measured. Figure 5.6 shows the HVS dependent PV module's leakage current behaviour in the presence of mud containing different amounts of dust. Figure 5.7 shows the leakage current at 600, 1000 and 1500 V stress at different dust amount on the surface of PV module. Highest leakage current has been found at 3 gm/m^2 and leakage current values are 2.66, 7.88 and 16.06 µA at voltage stress 600, 1000 and 1500 V respectively.

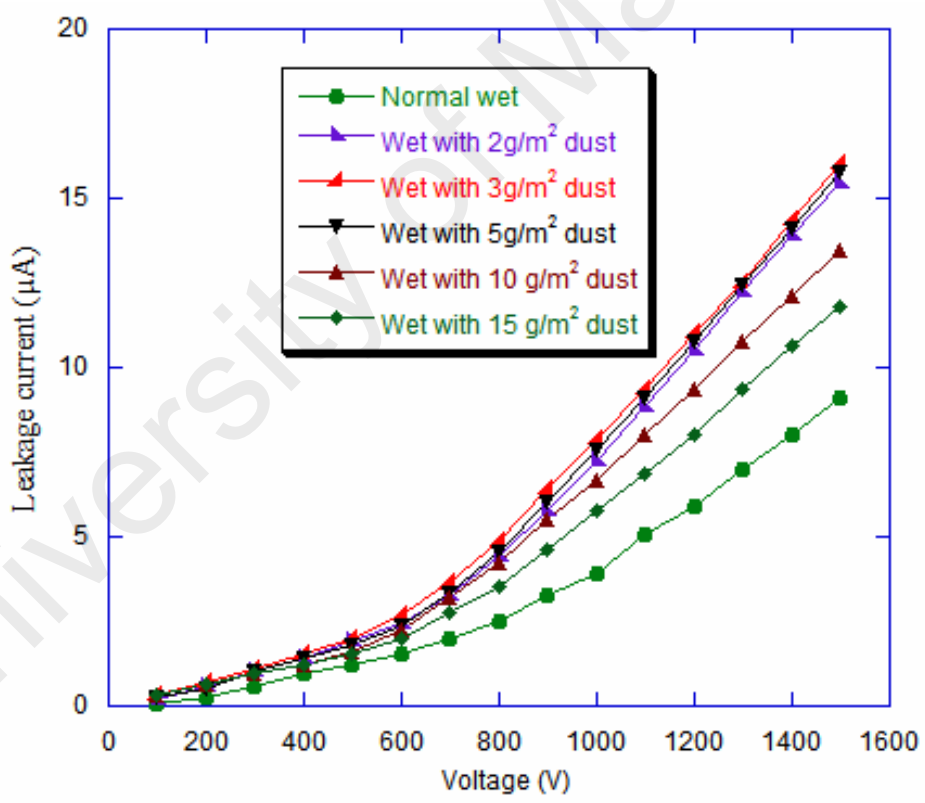

Figure 5.6: Effect of dust deposition on the wet leakage current of PV module

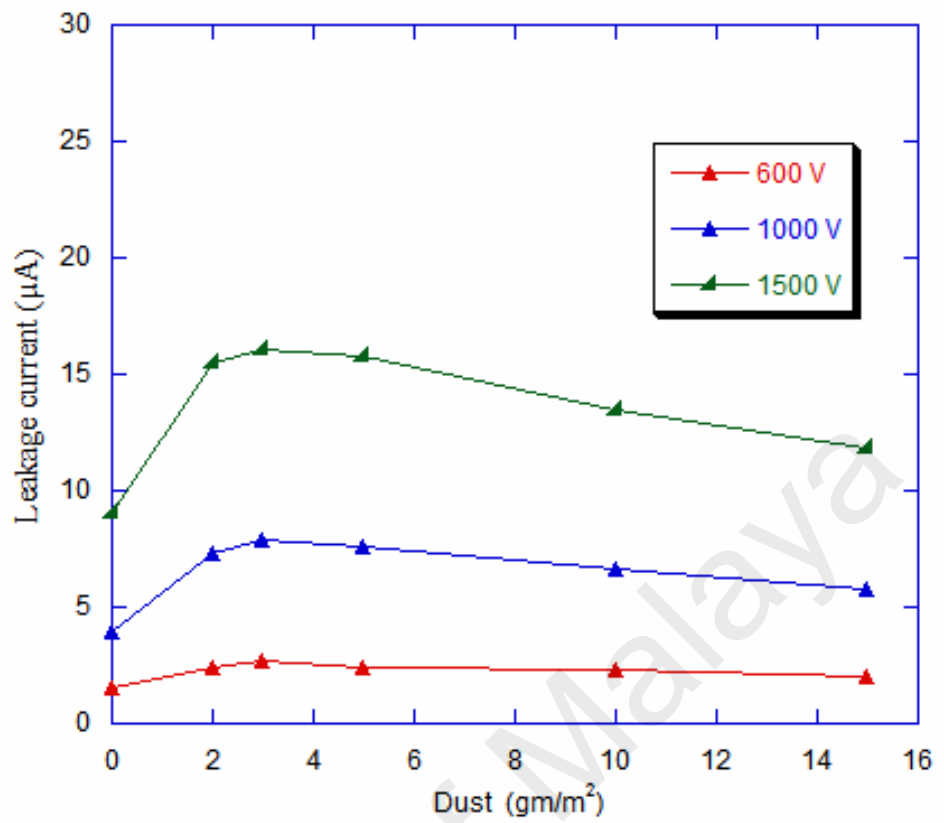

Figure 5.7: Leakage current at 600, 1000 and 1500 V stress at different dust amount on the surface of PV module

The effect of on-site dust deposition is shown in Figure 5.8. The values of wet leakage current of all unwashed modules are higher than that of washed modules. Table 5.2 displays the wet leakage current values at washed and unwashed condition of three different PV modules at voltage stress of 1500V. For module B, C and D, leakage current values are increased by 12.5, 11.14, and 31.39 % respectively due to dust deposition.

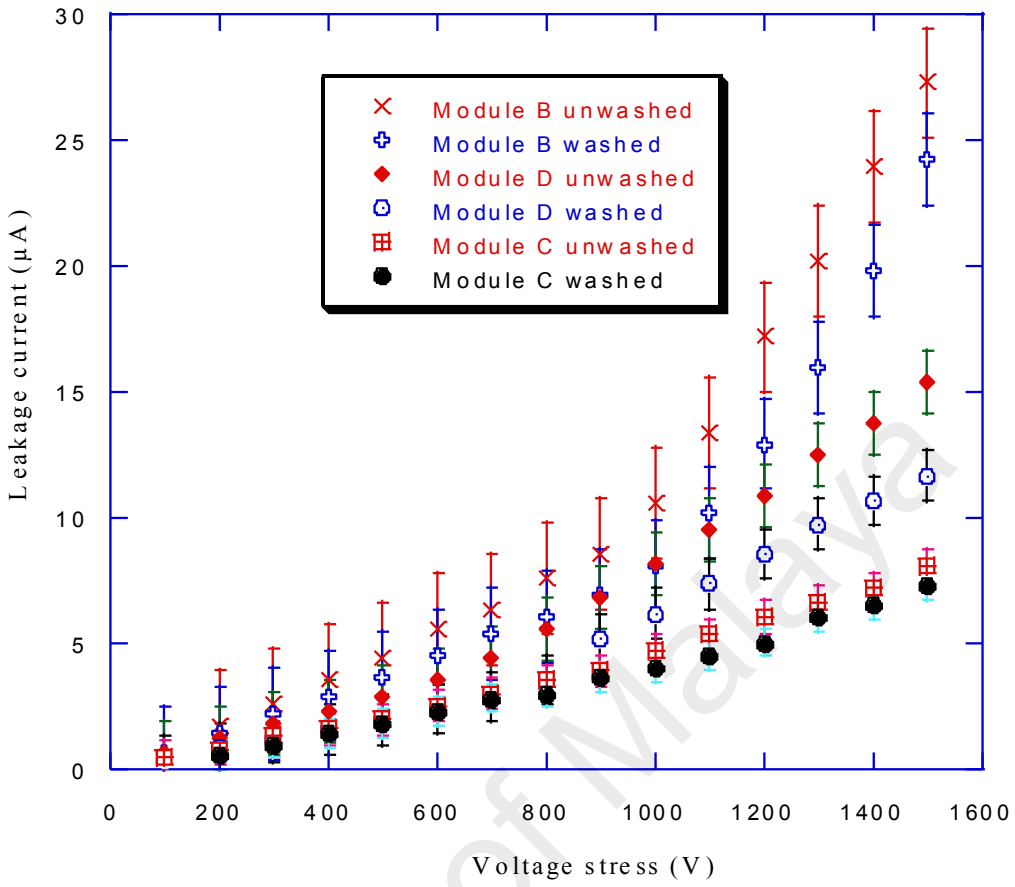

Figure 5.8: On-site dust effect on the high voltage stressed leakage current of different PV modules Module B, Module C and Module D

Table 5.2: Effect of on-site dust on HVS leakage current behaviour of different solar modules

Module Type	Cell Material	Leakage Current with Dust at 1500 V (μA)	Leakage Current without Dust at 1500 V (μA)	Leakage Current Increase (%)
B	Polycrystalline silicon	27.27	24.24	12.5
C	Polycrystalline silicon	8.08	7.27	11.14
D	Monocrystalline silicon	15.39	11.66	31.98

The FESEM images of dust particles at different positions are shown in Figure 5.9. The dust particles are heterogeneous in size distributed from small as 18 nm to large as several micrometres. Tiny dust particles are appended to the bigger dust particle. Small particles are brighter than bigger particles which show electron charging amid imaging. So tiny dust particles have charges that enable them to append to the bigger molecule (Yilbas et al., 2015). In the coastal region, these small dust particles can undoubtedly connect with ionic compound (salt) because of their charging nature. As an outcome, the salt is effectively kept on the PV module surface (Schladitz et al., 2011). The elements contained in the dust particle are shown by the EDX spectra in Figure 5.10 from which percentage of different elements are also revealed. The presence of oxygen, aluminium, silicon, calcium, iron, titanium, magnesium, carbon, potassium, and sodium etc. elements are explicit in the EDX spectrum. Different concentrations of these elements are obtained from different locations of dust which means elements and compounds are non-homogeneously distributed through the dust.

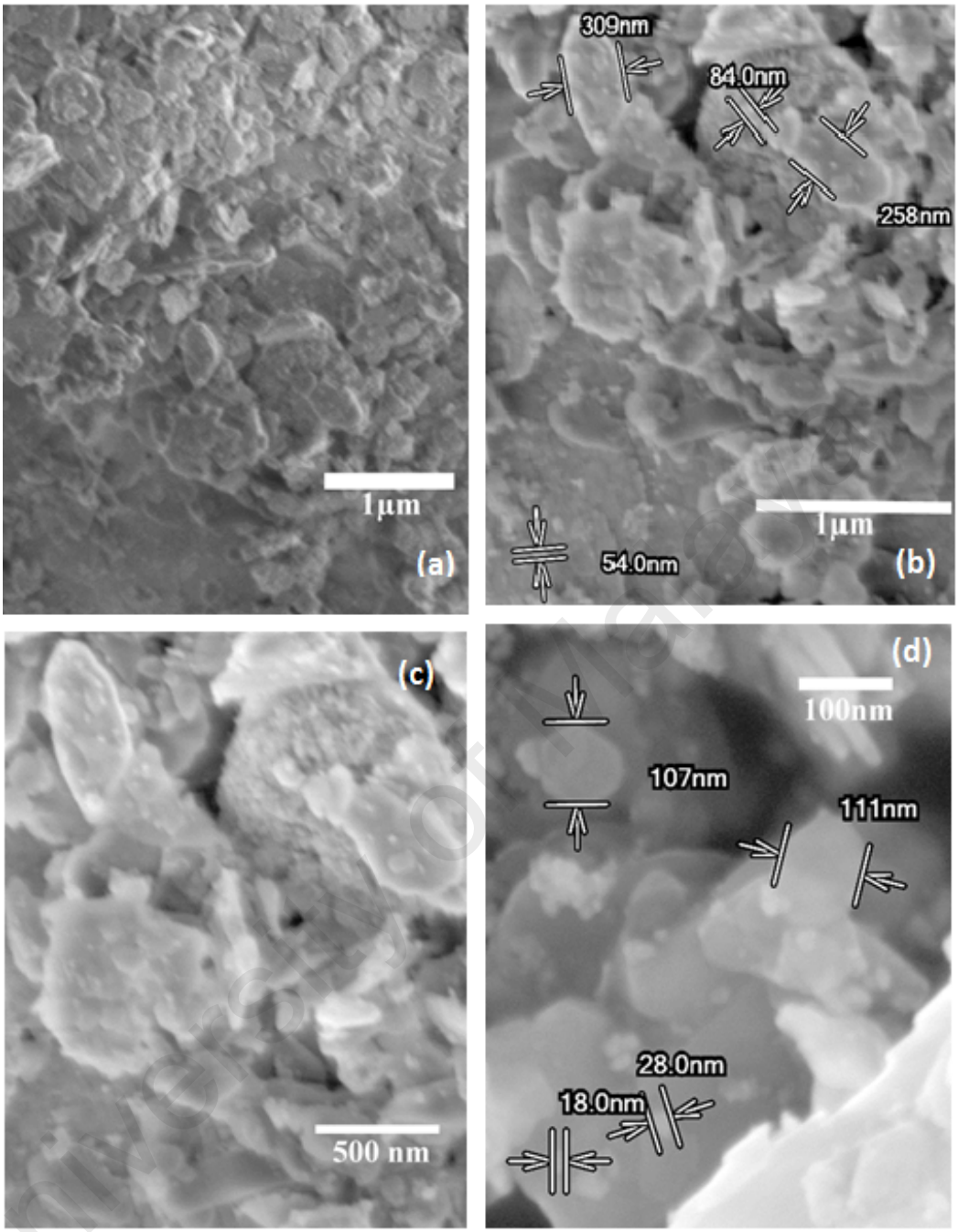

Figure 5.9: FESEM images of dust particles at different resolution of (a) 10k, (b) 20k, (c) 30k and (d) 70k

Figure 5.11 shows the XRD pattern of the dust particles. XRD has done at a temperature of 25°C by using Cu anode. From the diffractogram, some possible compound can be predicted such as SiO_2, $CaCO_3$, MgO, Al_2O_3 etc.

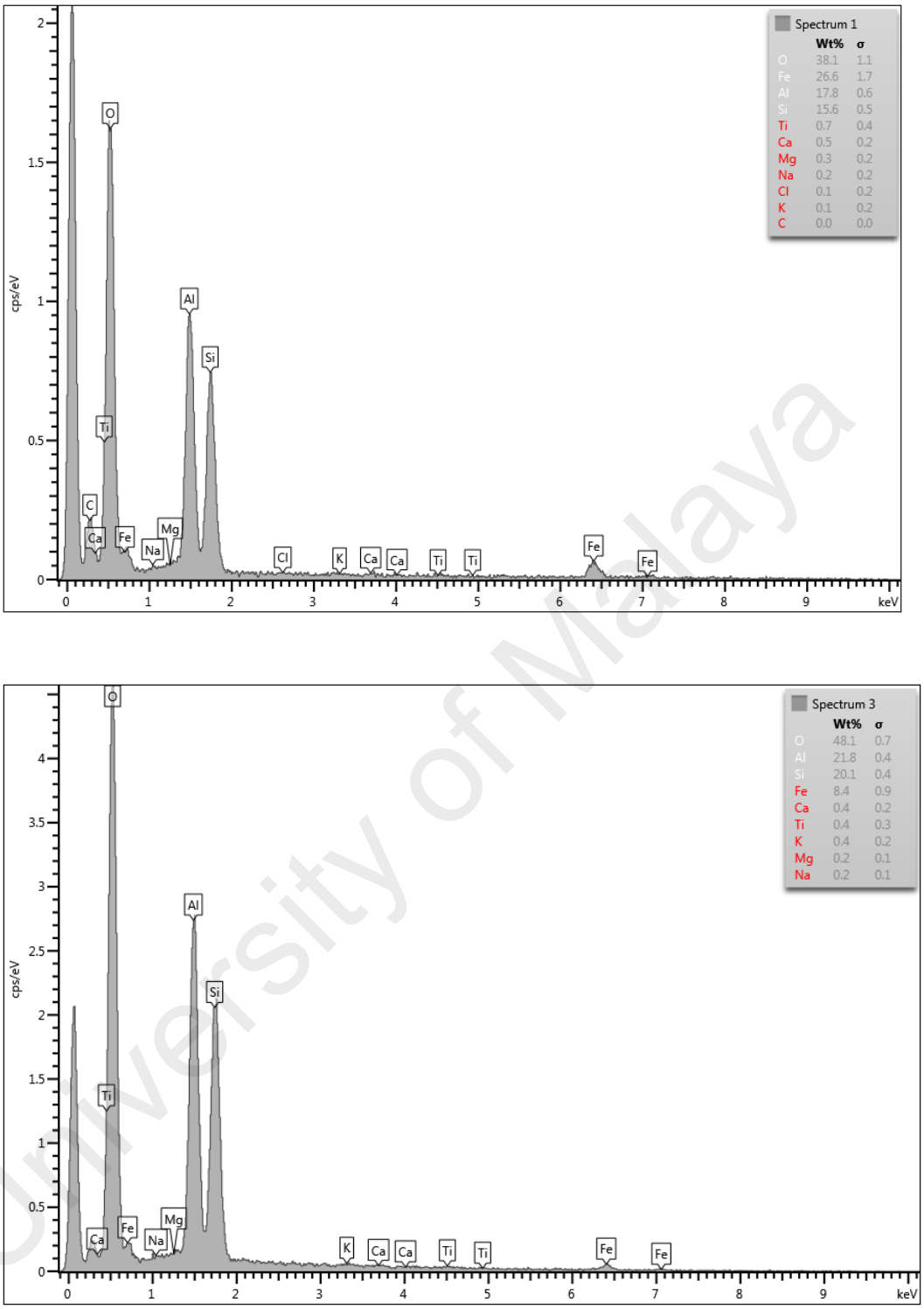

Figure 5.10: EDX spectra at different location of dust

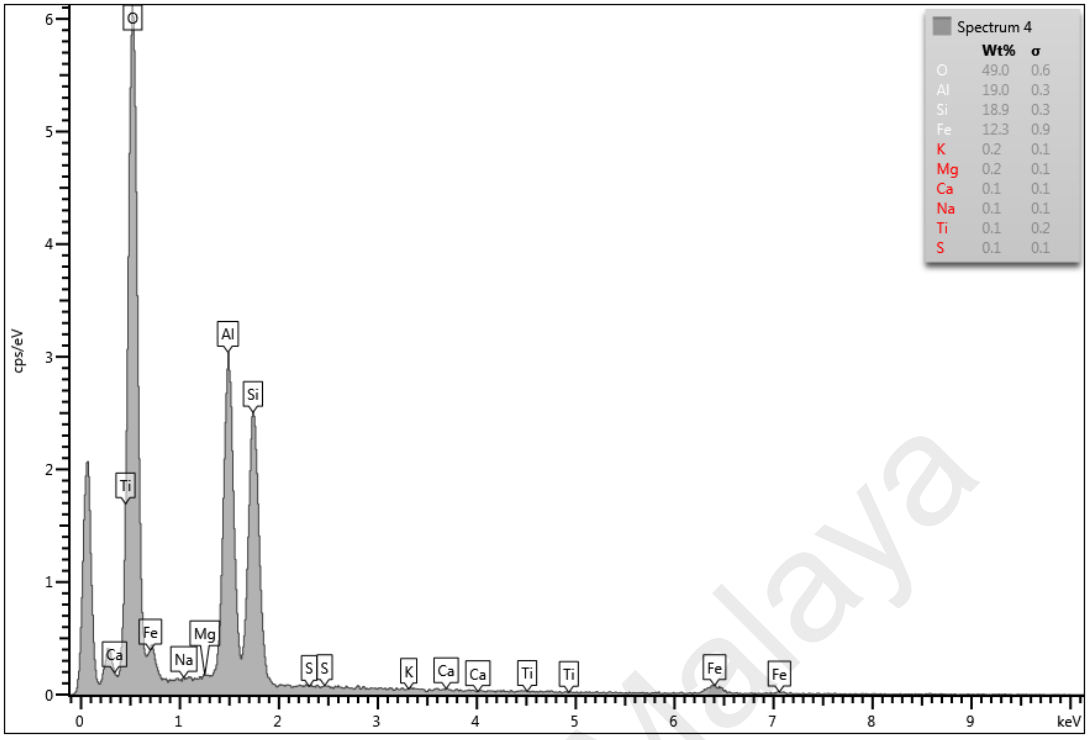

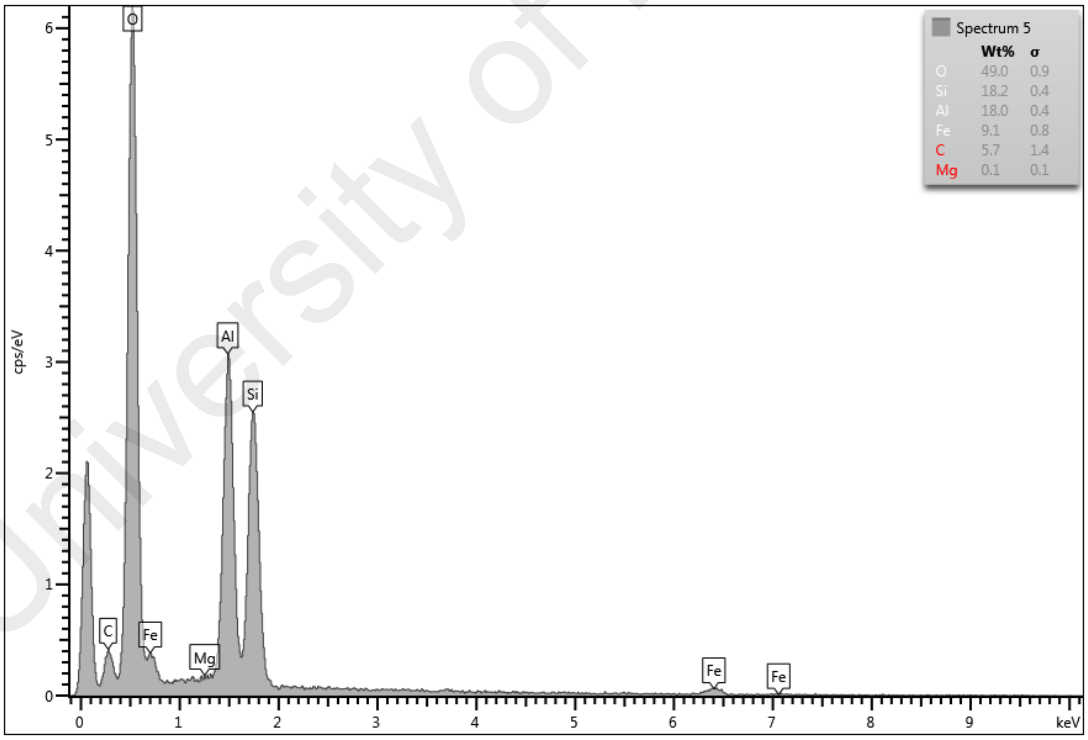

Figure 5.10, continue

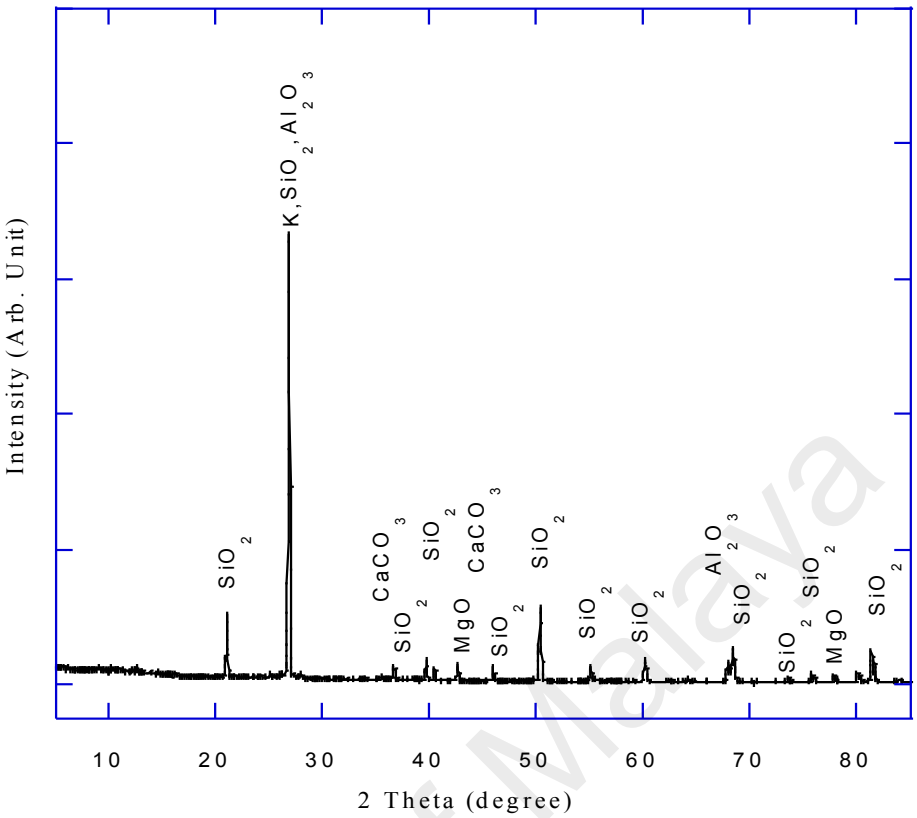

Figure 5.11: X-ray diffraction pattern of dust particles

5.2.5 Aging Effect

The impact of aging on the leakage current conduction of PV module has been investigated by considering PV module of different manufacturers, for example, C and D. Two C type PV modules dissimilar in aging periods (brand new and 8 years aged) and three type D PV modules (same aging period) are selected in the investigation. The aging condition of the selected modules is shown in Table 5.3.

Table 5.3: Aging period of different PV modules

Aging Condition	Type of Module
New unused	C
8 years field aged	C
10 years field aged	D

Figure 5.12 reveals the HVS dependent leakage current characteristics of PV module C type aged at the different time of periods. For the C type module, the new and aged

module leakage current values are 0.30 and 4.04 µA respectively at 1000 V voltage stress. The leakage current of the new module was 84.73% lower than that of the 8 years aged module at 1500 V stress condition. In case of D the type module, the average leakage current values have been executed as 2.9, 6.8 and 15 µA at voltage stress of 600, 1000 and 1500 V respectively (Figure 5.13). Higher leakage current values have been obtained for type C module as compared with type D. This could be due to the higher aging period. Figure 5.15 reveals the ordinary visual appearance of C type module new and 8 years aged. There is a significant amount of EVA yellowing has been observed because of aging. Discoloration of EVA reduces the insulating property of encapsulant that increases the leakage current of the aged PV module (Sinha et al., 2016).

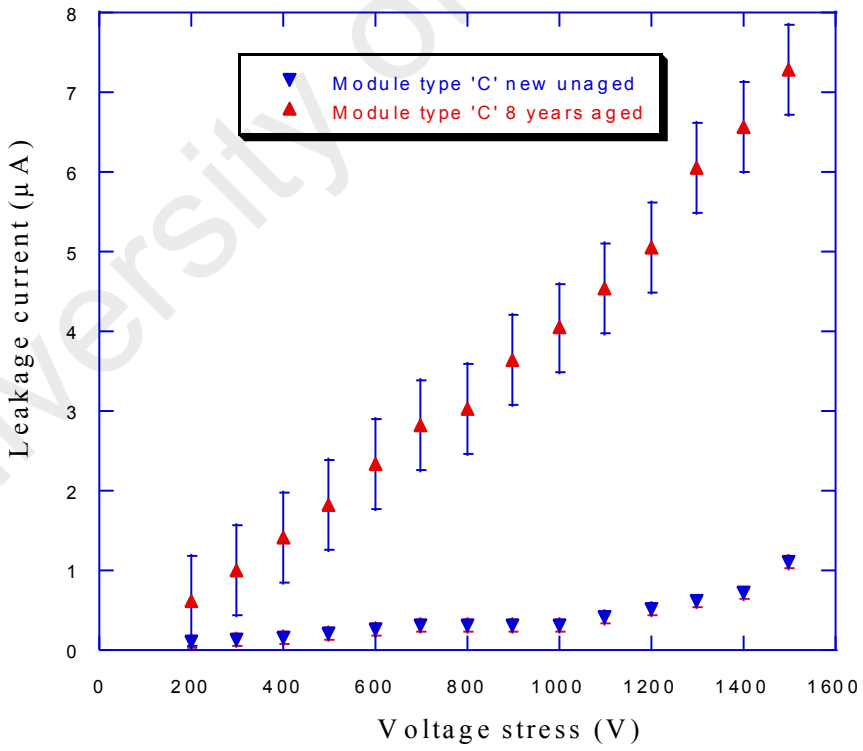

Figure 5.12: Wet leakage current behaviour of 'C' type modules at different aging condition

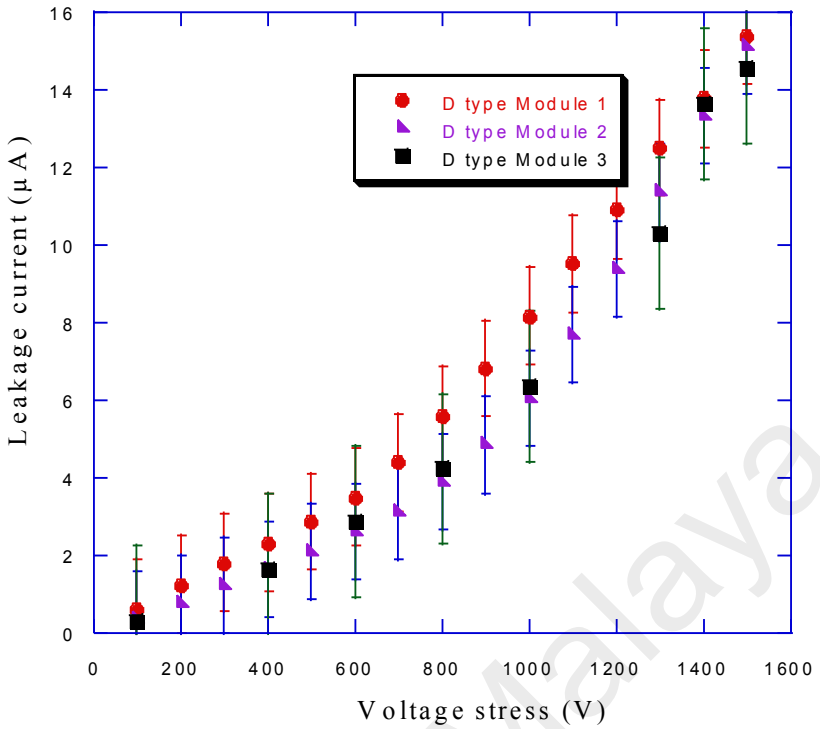

Figure 5.13: Wet leakage current behaviour of 'D' type modules

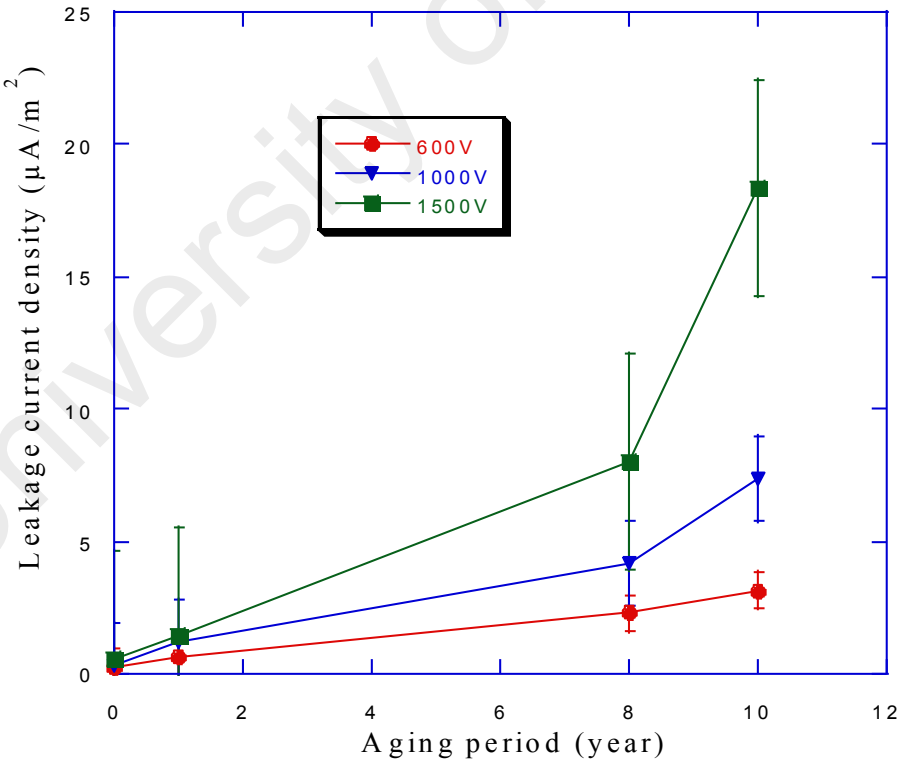

Figure 5.14: Wet leakage current density of PV modules at different aging periods

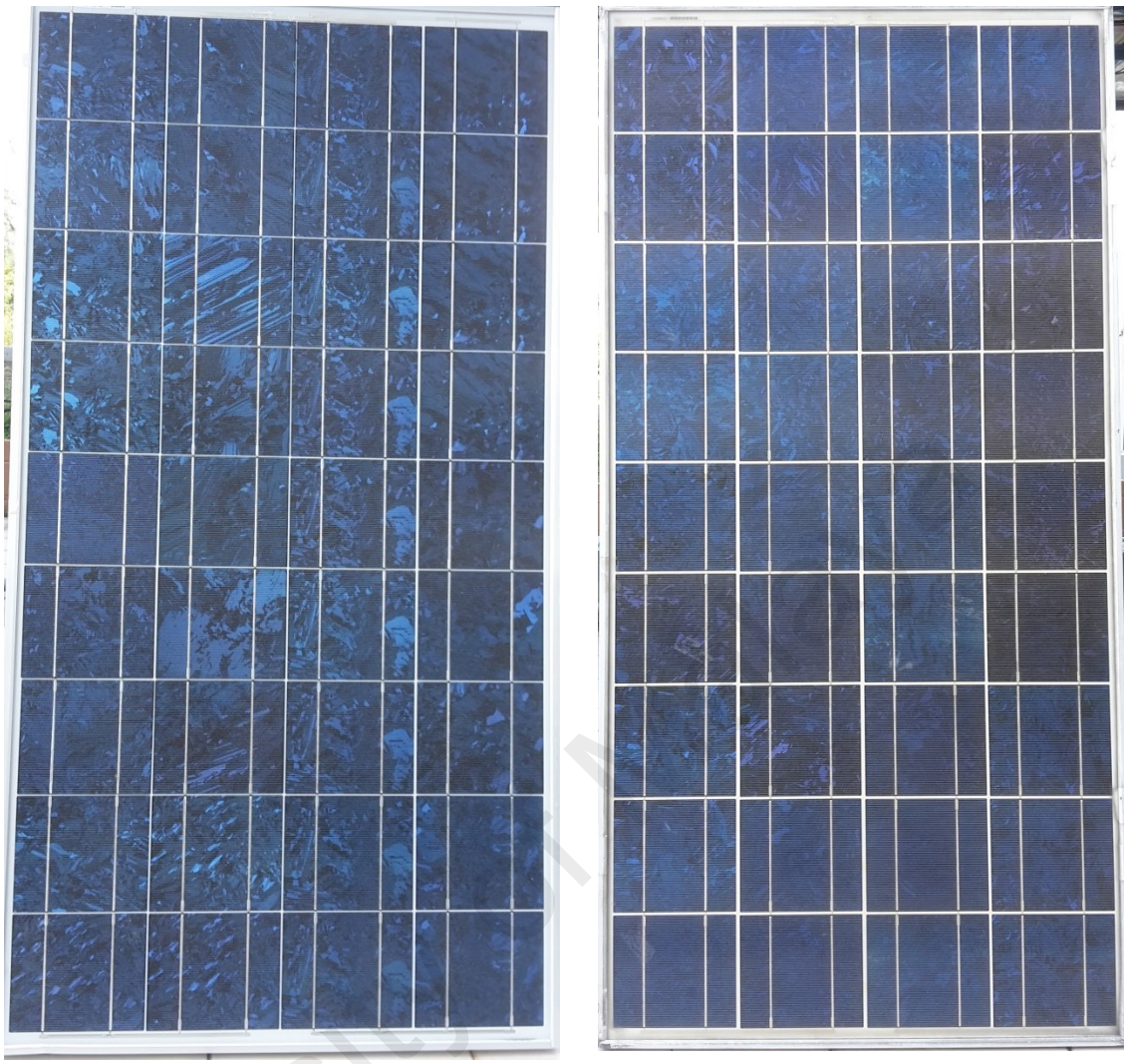

Module C (new) Module C (8 years aged)

Figure 5.15: Visual inspection of C type module new and 8 years aged

The activation energy of wet leakage current has been calculated by using the Arrhenius equation as (Kindyni & Georghiou, 2013).

$$I_{LC} = I_{LC\,0} \times \exp^{-[E_a / k_b T]} \tag{5.1}$$

$$\ln I_{LC} = \ln I_{LC\,0} - (E_a / k_b) \times \frac{1}{T} \tag{5.2}$$

I_{LC} is leakage current, I_{LC0} is the leakage current at temperature 0°K, E_a is the activation energy, k_b is Boltzmann's constant ($k_b = 8.617 \times 10^{-5}$ eV/K), T is the PV

module's absolute temperature in Kelvin. Temperature dependent wet leakage current behaviour of two PV modules of same manufacture and different in aging period (i.e. new and near about 8 years field aged) in Figure 5.16 and Figure 5.17 respectively. Leakage current has been measured under 1500V stress. From the slopes of the curves, respective activation energy has been calculated. The activation energy is increased from 0.763 to 0.856 eV in course of 8 years of aging. This increase in activation energy is comparable to that reported by del Cueto and McMahon (2002) wherein rise in activation energy at high relative humidity (RH 95%) is from 1.0 to 0.8eV and at low relative humidity (RH 10%) is from 0.8 to 0.6 eV (del Cueto & McMahon, 2002).

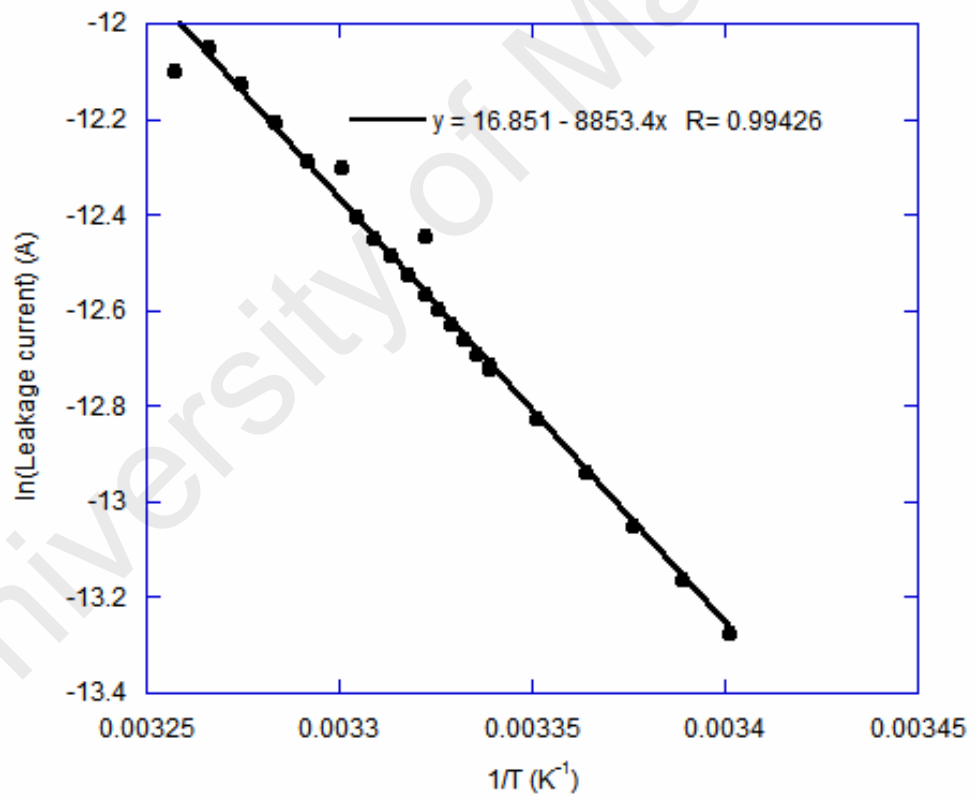

Figure 5.16: Inverse temperature dependent leakage current behaviour of new solar PV module type C

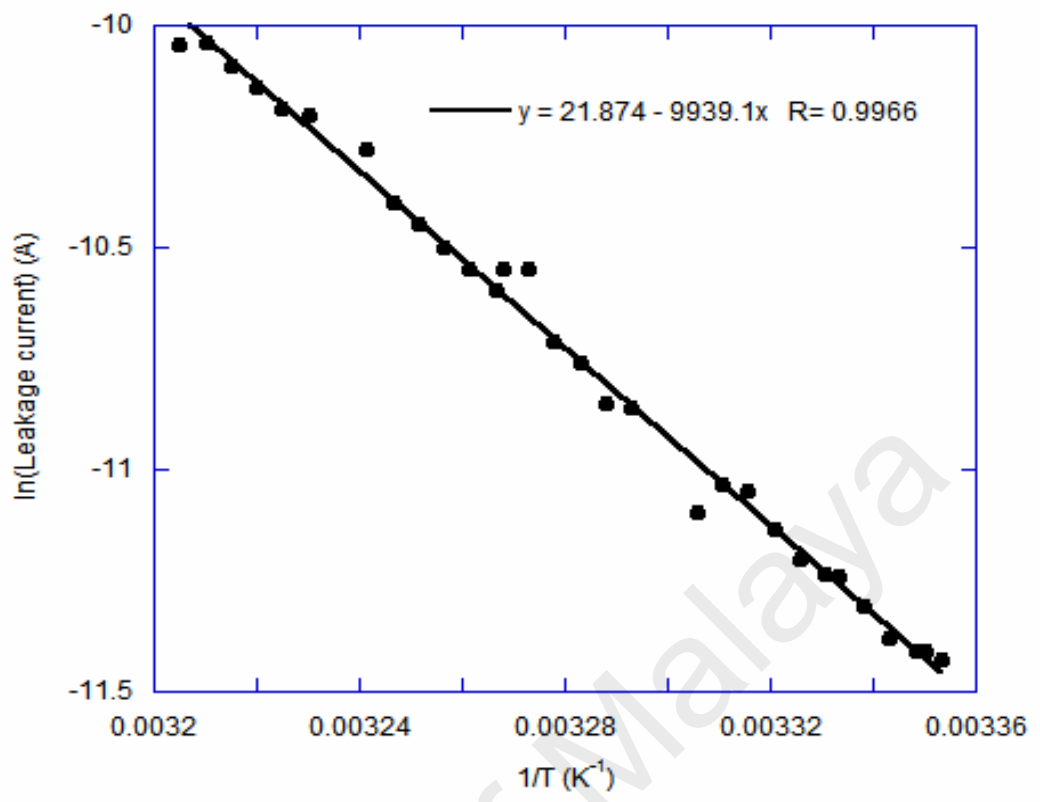

Figure 5.17: Inverse temperature dependent leakage current behaviour of 8 years aged PV module type C

5.2.6 Comparison between different factors and sensitivity analysis

A comparative depiction on the impact of different parameters such as module temperature, surface wetting, dust and salt deposition on leakage current density has been illustrated in Figure 5.18. The wet surface condition is more severe than the dry surface condition although the module temperature is as high as 60°C. At surface wet conditions, module temperature shows higher impact on the HVS leakage current then followed by salt and then dust deposition. Sensitivity indexes of leakage current at 1000V stress with respect to different factors are illustrated in Figure 5.19. The highest sensitivity index has been found for the aging effect with the sensitivity index of 0.95. The second most sensitive variable has been observed for the parameter module temperature effect at wet condition with the sensitivity index value of 0.77. The sensitivity index values of dust and salt deposition effects are observe as 0.50 and 0.38

respectively. The module temperature at dry condition has been found to be a lowest sensitive parameter with sensitivity index value of 0.13.

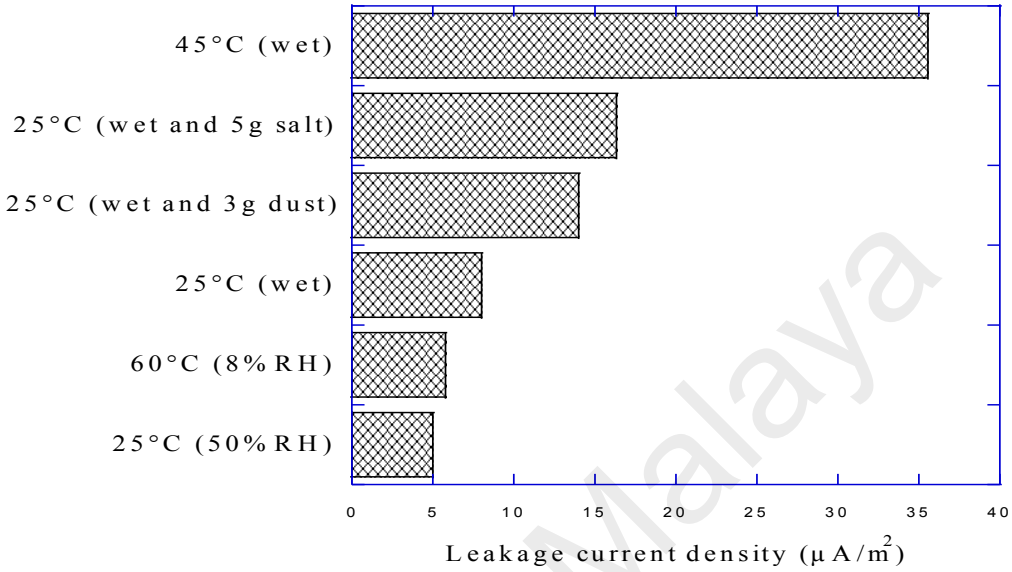

Figure 5.18: Comparative impacts of different operating parameters on HVS leakage current of PV module at 1000V stress

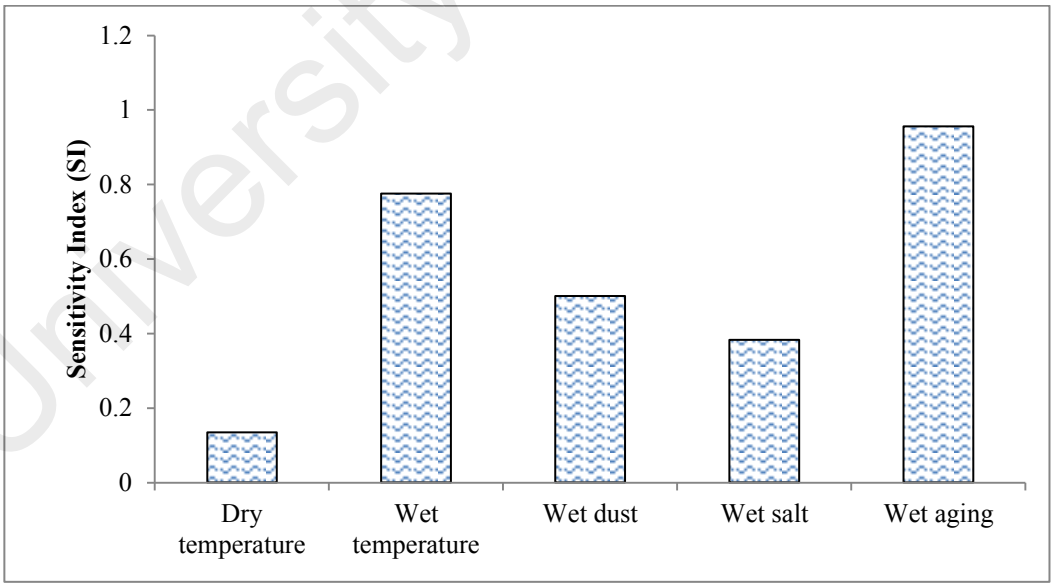

Figure 5.19: Comparative sensitivity index of different operating parameters on HVS leakage current of PV module at 1000V stress

5.3 On-Site Potential Induced Degradation of PV Module

5.3.1 Electroluminescence Images

Electroluminescence (EL) imaging has been employed to examine the degradation of individual cell within a PV module. Degradation value of individual module is ascertained by comparing the mean values of intensity of EL image with that of brand new reference PV modules. To determine the calibration factor *C* in equation 4.3, EL images of three sorts of reference brand new PV modules are considered. The specifications of the reference PV modules have been shown in

Table **5.4:** Three reference new PV modules specification at (STC)

Parameters	**EPV-72P/B3/CF-305**	**EPV 60P/B3/CF-250**	**YL275C-30b**
Cell material	Polycrystalline	Polycrystalline	Monocrystalline
Number of cell	72 (6×12)	60(6×10)	60(6×10)
Pmax (W)	305	250	275
Voc (V)	45	37.8	38.9
Isc (A)	8.85	8.73	9.34
Vmp (V)	37.8	30.6	31.2
Inp (A)	8.34	8.17	8.82
Cell area (m2)	1.46	1.46	1.47

. Electroluminescence images of three brand new solar modules are presented in Figure 5.20.

Table 5.4: Three reference new PV modules specification at (STC)

Parameters	**EPV-72P/B3/CF-305**	**EPV 60P/B3/CF-250**	**YL275C-30b**
Cell material	Polycrystalline	Polycrystalline	Monocrystalline
Number of cell	72 (6×12)	60(6×10)	60(6×10)
P_{max} (W)	305	250	275
V_{oc} (V)	45	37.8	38.9
I_{sc} (A)	8.85	8.73	9.34
V_{mp} (V)	37.8	30.6	31.2
I_{np} (A)	8.34	8.17	8.82
Cell area (m^2)	1.46	1.46	1.47

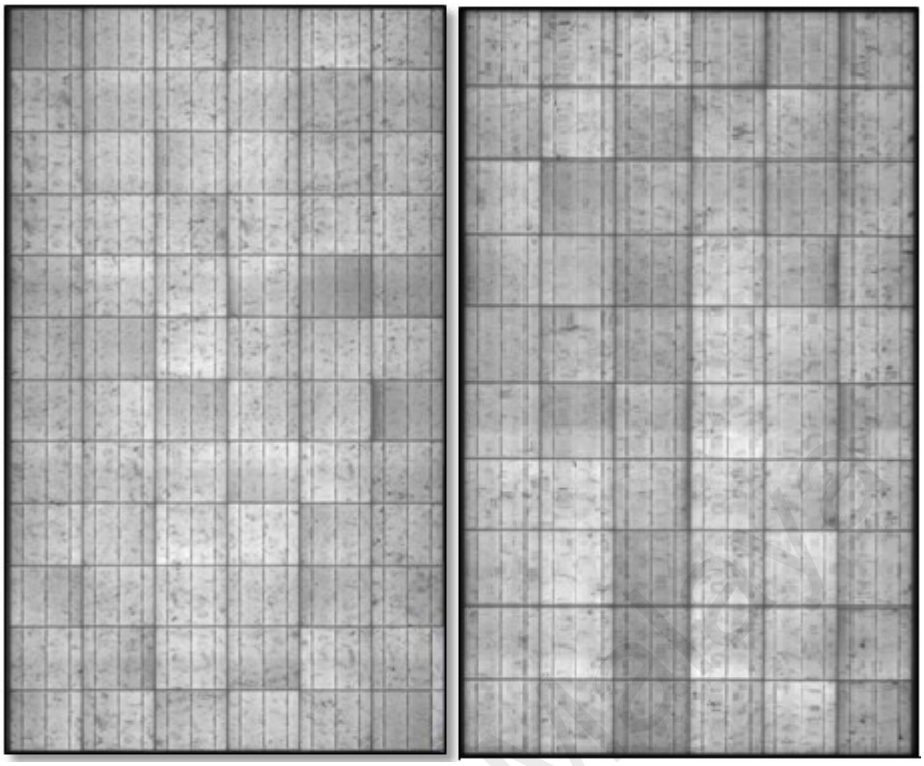

(a) (b)

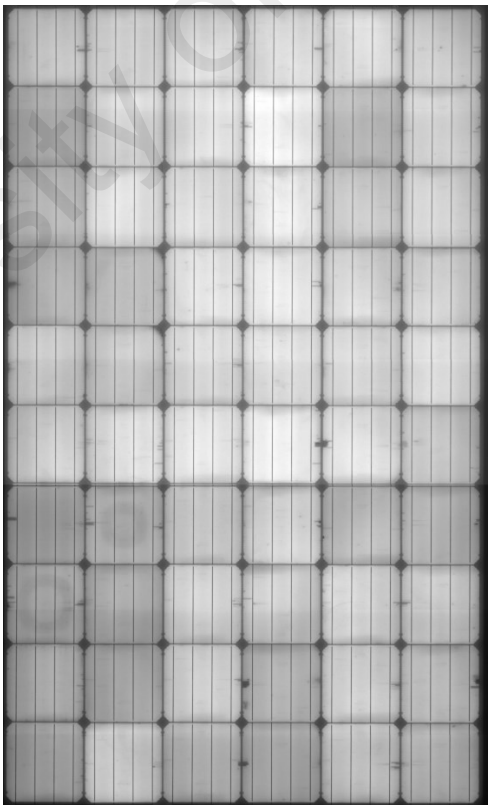

(c)

Figure 5.20: EL images of new reference PV module (a) EPV 305W (b) EPV 250 W and (c) YL 275 W

Table 5.5 displays the EL image characteristics of three reference PV modules. The mean value of electroluminescence intensities of EPV-305, EPV-250 and YL-275 PV modules are 173.69, 169.39 and 186.23 respectively. It is revealed from the Table 5.5 that the calibration factor '*C*' is found to be 0.99 that is almost close to unity.

Table 5.5: Electroluminescence image characteristics of three reference PV modules EPV-250W, EPV-305W and YL-275 W

Photovoltaic module	**P_{max} at STC (W)**	**Total number of pixel**	**P_{max}/total cell area (W/m^2)**	**Mean value of intensity of EL image (E_{mean})**	**Calibration factor (*C*)**
EPV-250W	250	19450 × 32432	171.21	170.36	0.99
EPV-305W	305	19450 × 38919	174.06	173.69	0.99
YL-275	275	19450 × 32432	187.07	186.23	0.99

The EL images of two outermost modules of the string, i.e., S1M1 (negative end) and S1M11 (positive end), are shown in Figure 5.21 and Figure 5.22. Each figure holds three different viewing modes and individual cell performances. As a consequence of long-time field aging, the EL images of both PV modules display lower illumination when matched with the new reference module. Although cracks have been noticed in both modules, the module at negative end contains more cracks compared to that in the positive end. This is due to the fact that crack propagation rate due to cyclic thermal stress is higher at the negative end (Goranti, 2011). In addition, some dark areas have been remarked in negative end modules representing localized shunting. However, localized shunting is not seen in positive end module, demonstrating the influence of PID in the negative end only. Table 5.6 displays electroluminescence image related characteristic of S1M1 and S1M11 PV modules. Amount of degradation of the modules

is calculated using the mean intensity value of EL image (E_{mean}). The mean EL intensity of module S1M1 is 81.35 and that for S1M11 is 117.17. At the non-degraded state, the standard mean value of EL intensity ($E_{mean(STC)}$) is calculated by employing equation 4.2, wherein its value is found 141.25. The degradation value of the PV module has been determined by using Eq. (4.1). The obtained amount of degradation of modules S1M1 and S1M11 are 42.40% and 17.04%, correspondingly. The results are comparable with the other reports in literature. For example, in Italy, the PV module degrades near about 11-22% due to normal aging at outfield after 10 years (Parretta et al., 2005). Normally PV module containing cells' performance is varied due to different doping concentration. The average of all cells' performance is the standard cell performance. The individual cell performances of each PV module are also presented in both figures. The performance is based on the percentage of deviation of cell mean EL intensity from the standard cell mean intensity ($E_{mean(STC)}$) value of 141.25. The negative sign means lower performance and positive sign means higher performance compared to the standard cell performance. For example, in Figure 5.21 the darkest cell shows 90% less performance than the standard cell performance.

Table 5.6: Measuring the PV module degradation by EL imaging

Module	**Total number of pixels**	**Degraded Module's EL Intensity Mean Value**	**P_{max} (STC) /A_{cell}**	**Calibration Factor (*C*)**	**Mean EL Intensity of Brand New Module** [Eq. 4.2]	**Degradation (%)** [Eq. 4.1]
S1M1	10395 ×23389	81.35	142.68	0.99	141.25	42.40
S1M11	10395 ×23389	117.17	142.68	0.99	141.25	17.04

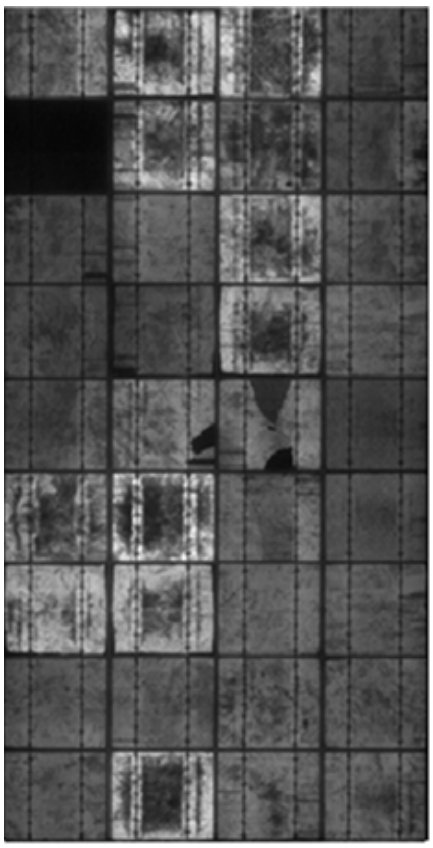

-38.05	-18.70	-28.71	-57.08
-90.93	-28.57	-48.69	-56.45
-59.04	-39.32	-23.11	-50.12
-58.87	-54.95	-31.10	-43.17
-53.71	-33.58	-42.64	-61.06
-37.65	-25.57	-41.36	-53.01
-11.94	-13.16	-37.39	-47.52
-45.59	-43.17	-44.38	-49.01
-46.07	-24.16	-37.74	-45.42

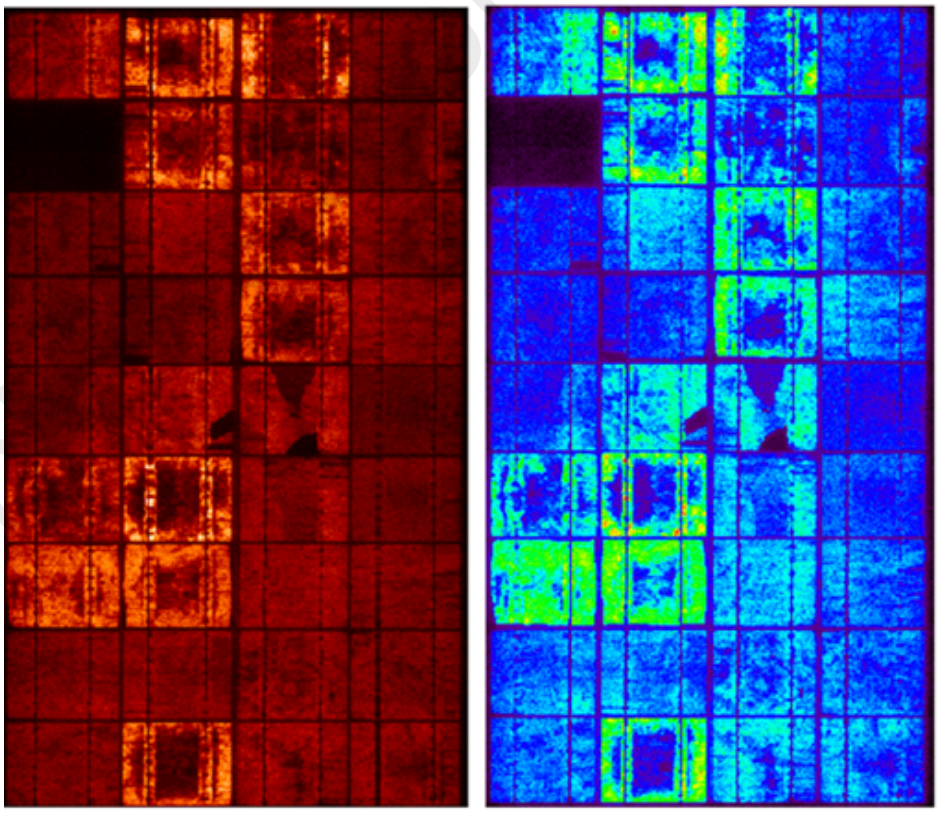

*Note: (+) and (-) value of individual cell performance indicate higher and lower performance than standard cell performance respectively

Figure 5.21: Electroluminescence images in various viewing modes (Grey, Red, Rainbow) and individual cell performance of negative end module (S1M1)

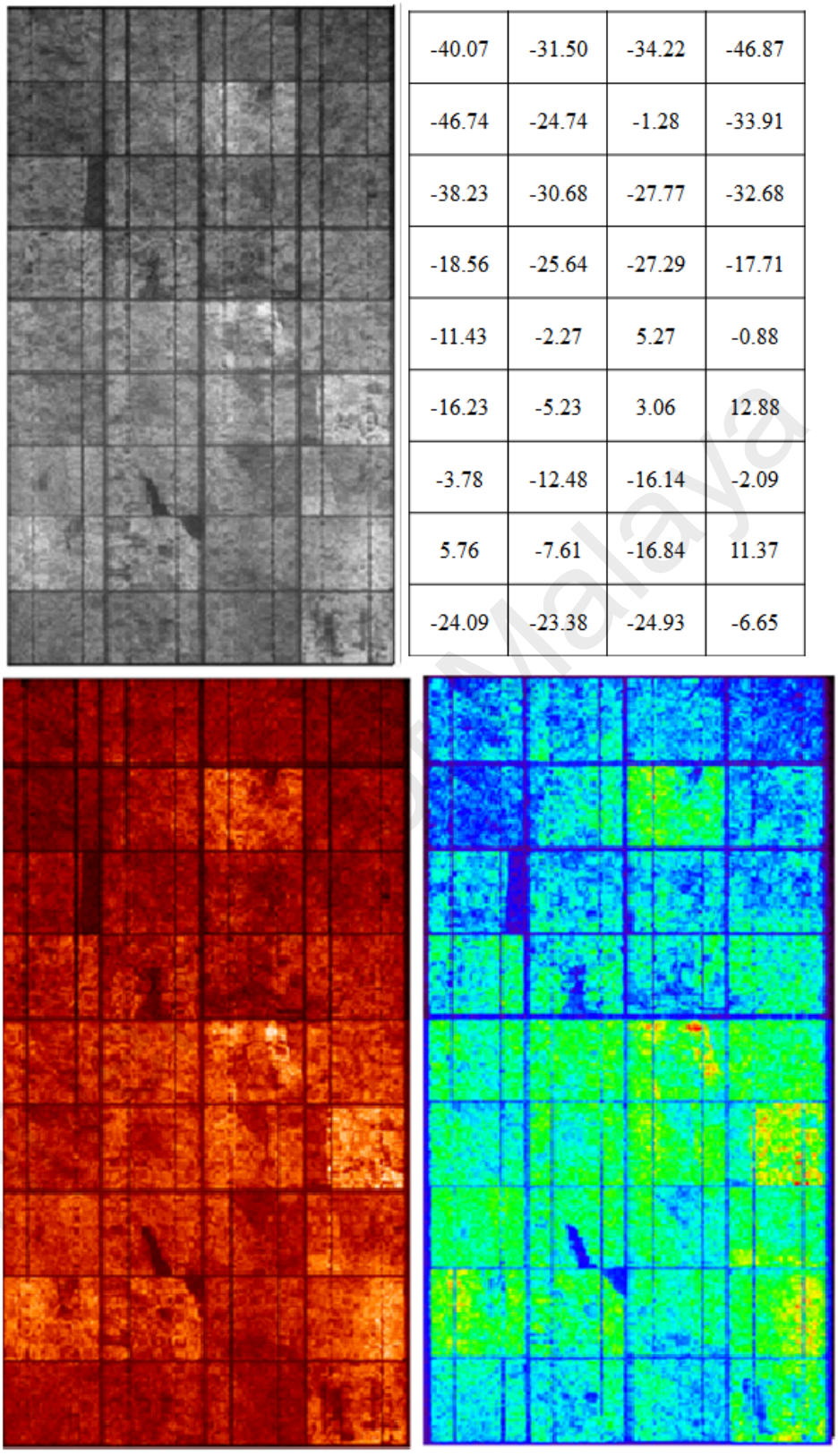

-40.07	-31.50	-34.22	-46.87
-46.74	-24.74	-1.28	-33.91
-38.23	-30.68	-27.77	-32.68
-18.56	-25.64	-27.29	-17.71
-11.43	-2.27	5.27	-0.88
-16.23	-5.23	3.06	12.88
-3.78	-12.48	-16.14	-2.09
5.76	-7.61	-16.84	11.37
-24.09	-23.38	-24.93	-6.65

*Note: (+) and (-) value of individual cell performance indicate higher and lower performance than standard cell performance respectively

Figure 5.22: Electroluminescence images in various viewing modes (Grey, Red, Rainbow) and individual cell performance of positive end module (S1M11)

5.3.2 Maximum Power Output

The output of the PV modules increases with of the intensification of solar radiation. However, in the meantime, the cell temperature of the PV module also increases. As a consequence of high temperature, the band gap of the PV cell decreases and the efficiency of the PV module gradually drops. Maximum power (P_{max}) and cell temperature for modules S1M1 and S1M11 as a function of solar irradiance have been illustrated in Figure 5.23, where both parameters are observed to rise with solar radiation. To calculate the temperature coefficient of maximum power (P_{max}), the P_{max} versus cell temperature curves have been drawn (Figure 5.24) and the temperature coefficient of P_{max} (γ) for S1M1 and S1M11 from the corresponding linear fitted equation have been found to be 1.21% and 1.36% respectively. The temperature coefficient of P_{max} due to longtime field aging experience noticeable upsurge (Figure 5.25), where the γ value of negative end module S1M11 is observed to increase from 0.45% to 1.37% after 9 years field aging which agrees well with results reported in the literature (Kaewkhao et al., 2012). On the other hand, γ value of positive end module is found lower (1.22%) than that of negative end module (1.37%) which also comply well with the results reported in (Spataru et al., 2015).

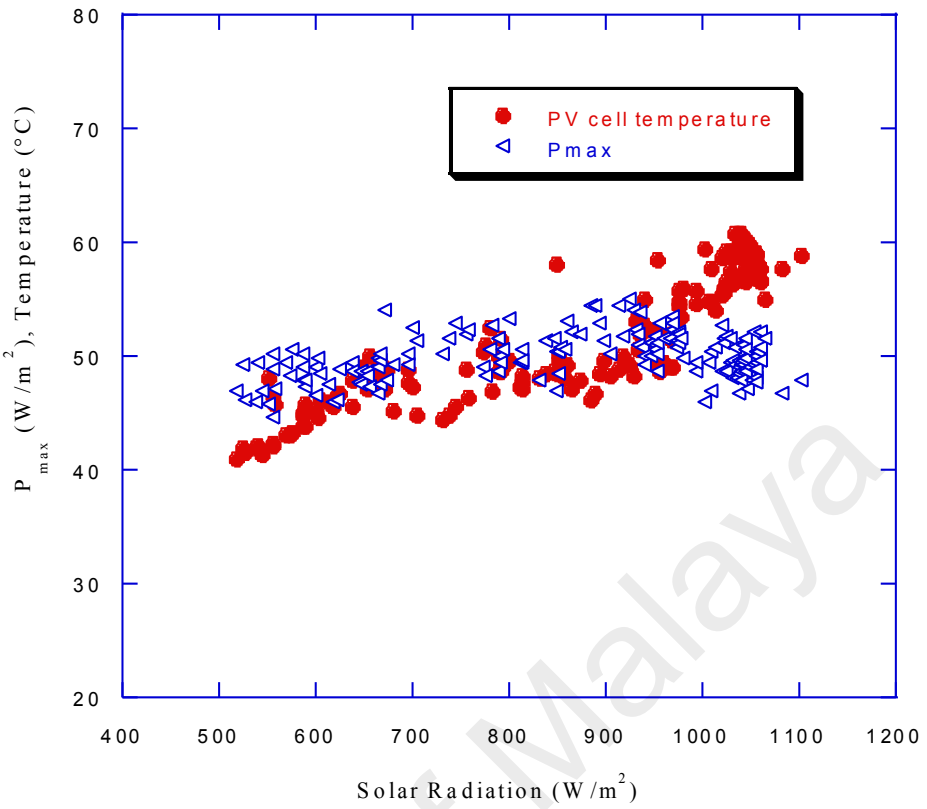

(a)

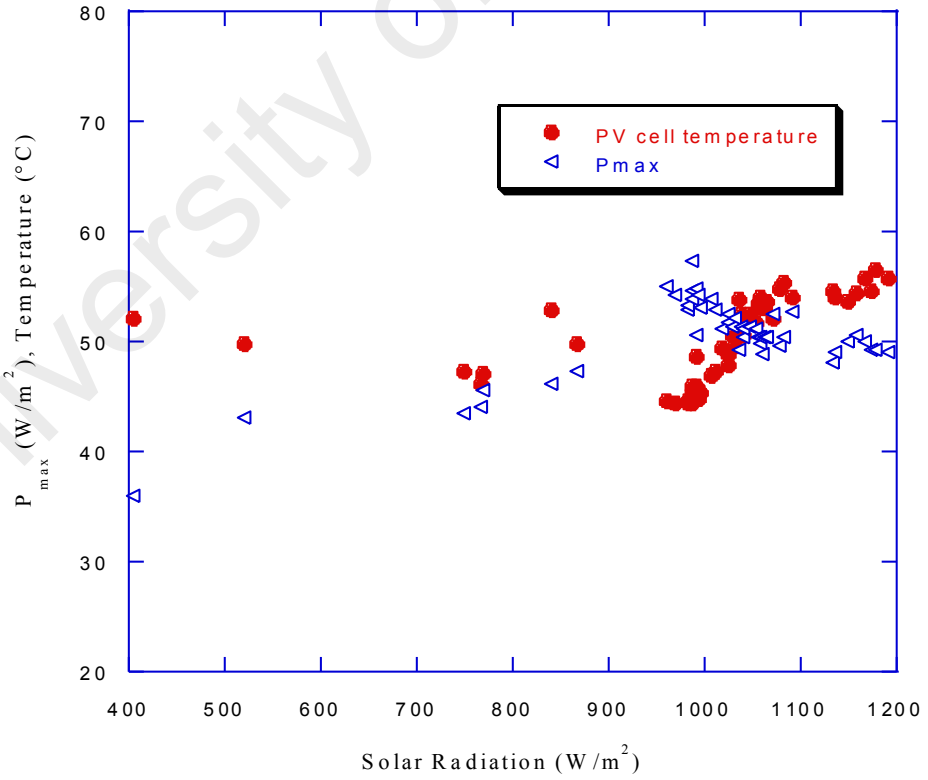

(b)

Figure 5.23: Effect of outdoor solar radiation on the P_{max} and cell temperature of PV modules (a) S1M1 and (b) S1M11

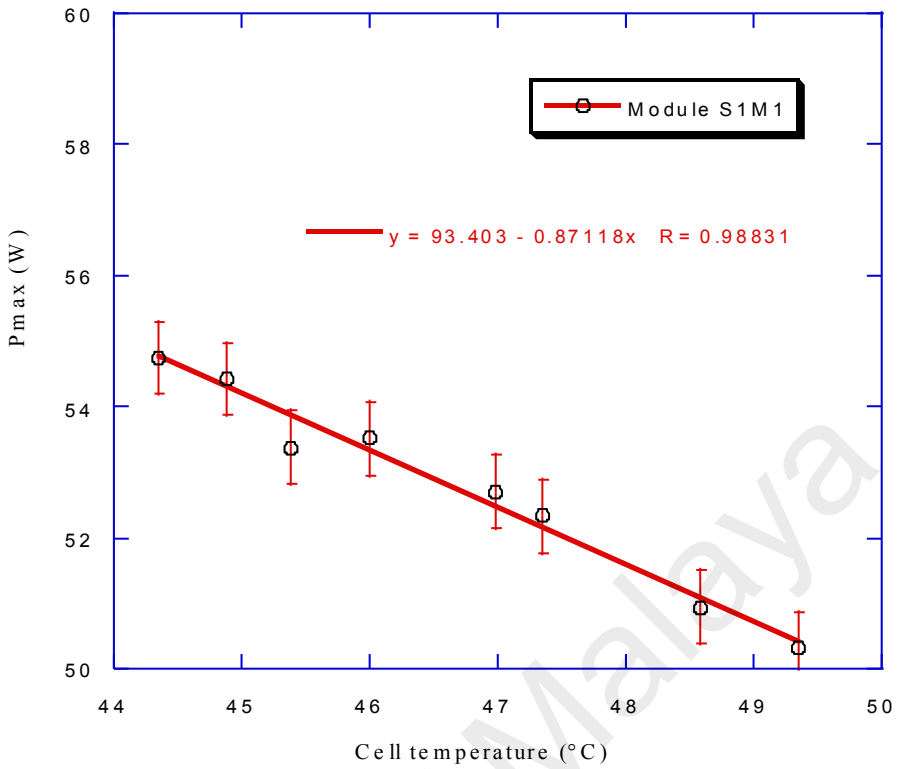

(a)

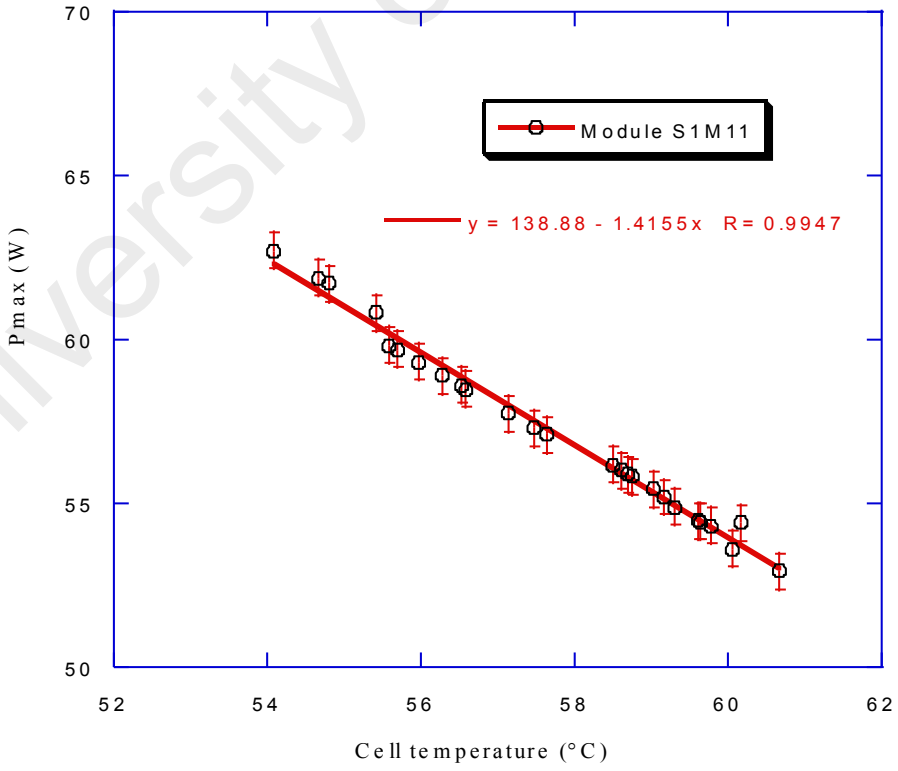

(b)

Figure 5.24: Effect of cell temperature on the P_{max} of PV module (a) S1M1 and (b) S1M11 (at 1000 W/m^2 radiation)

The amount degradation of a PV module is normally determined through light I-V characterization under solar irradiance with 25°C module temperature. In the outdoor condition, module temperature exceeds far beyond 25°C under irradiations of 1000 W/m^2. Therefore, PV power output is adjusted at 25°C according to the following equation:

$$P_{\max,\ 25\,^\circ C} = \frac{P_{\max,\ T_{sc}}}{[1 + \lambda \times (T_{sc} - 25\,^\circ C)]} \tag{5.3}$$

where $Pmax_{25\,^\circ C}$ is the maximum power output at 25°C and 1000W/m^2, $Pmax_{T_{sc}}$ is maximum power at 1000W/m^2 at T_{sc} and γ is temperature coefficient of P_{max}. The degradation of the PV module is then calculated by comparing the P_{max} under 1000 W/m^2 irradiance at 25°C with the rated P_{max} at STC.

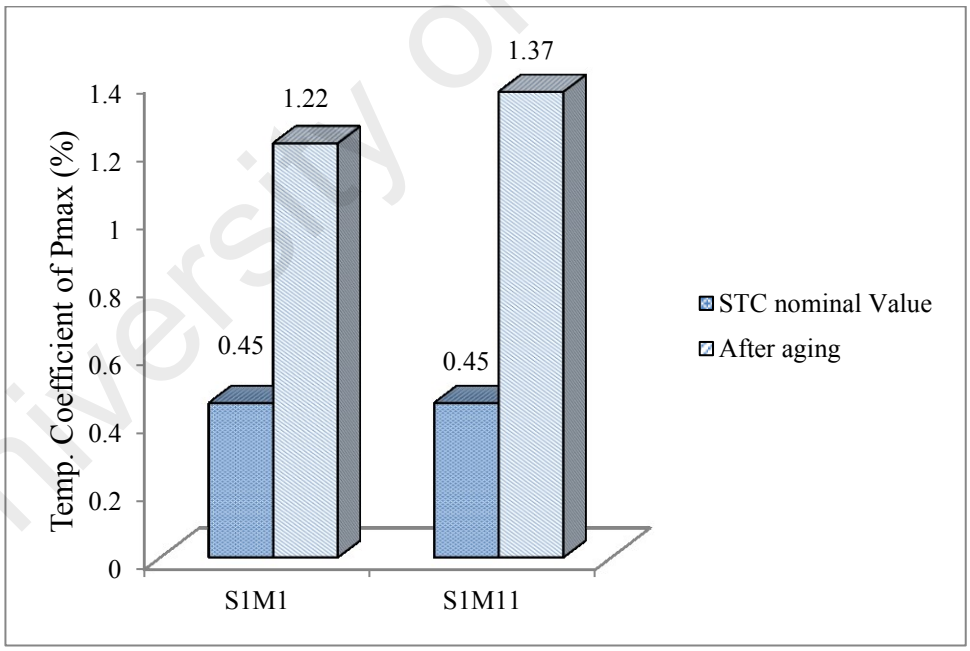

Figure 5.25: Effect of long-time real field aging on temperature coefficient of P_{max} of positive end (S1M11) and negative end (S1M1) modules

Outdoor light I-V measurement gives degradation values for modules S1M1 and S1M11 as 42.70% and 19.83% respectively. The degradations obtained from the light IV characterisation in outdoor and from EL imaging method are presented in Figure

5.26. There are very small amount of differences have been found. This ascertains the reliability of the EL imaging method for PV module performance degradation testing.

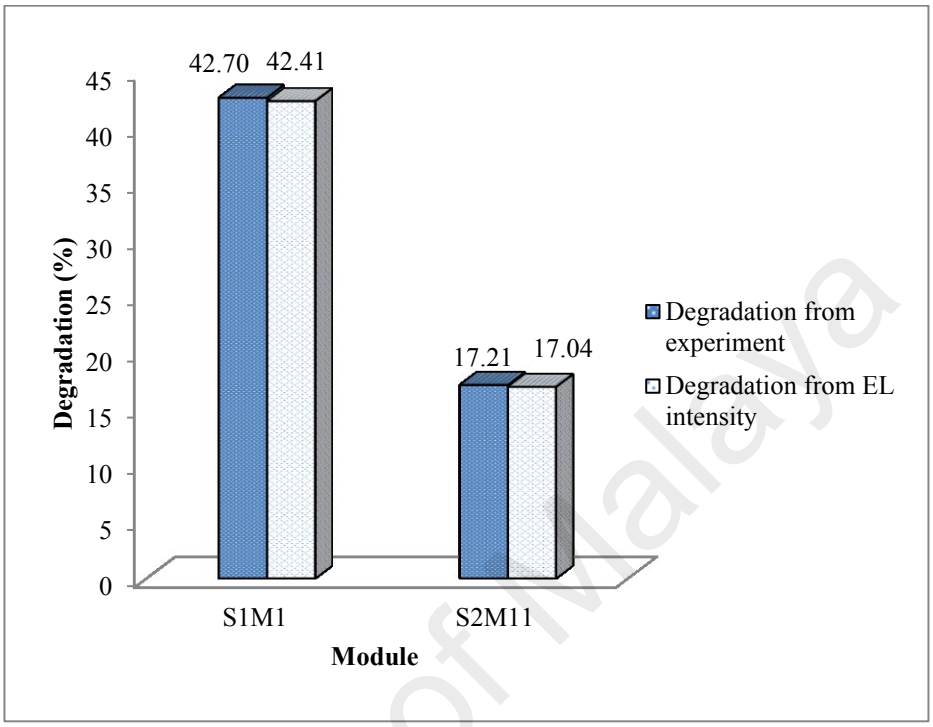

Figure 5.26: PV modules' degradation obtained from EL image method and from outdoor light IV experiment

5.3.3 Dark I-V Characteristics

The dark I-V characteristics have been employed to determine the shunt resistance of the PV module. This is a useful technique because the output results are not influenced by the fluctuation of sunlight irradiance. The shunt resistance has been determined by taking the voltage very nearly zero in the I-V curve where it is almost a straight line. The slope of the linear fit line is ascertained and the inverse of the slope gives shunt resistance. The dark I-V and semi-logarithmic dark I-V of module S1M1 and S1M11 are shown in Figure 5.27 (a) and (b) respectively. The S1M1 PV module shows higher biasing current compared to the S1M11 because of degradation due to PID.

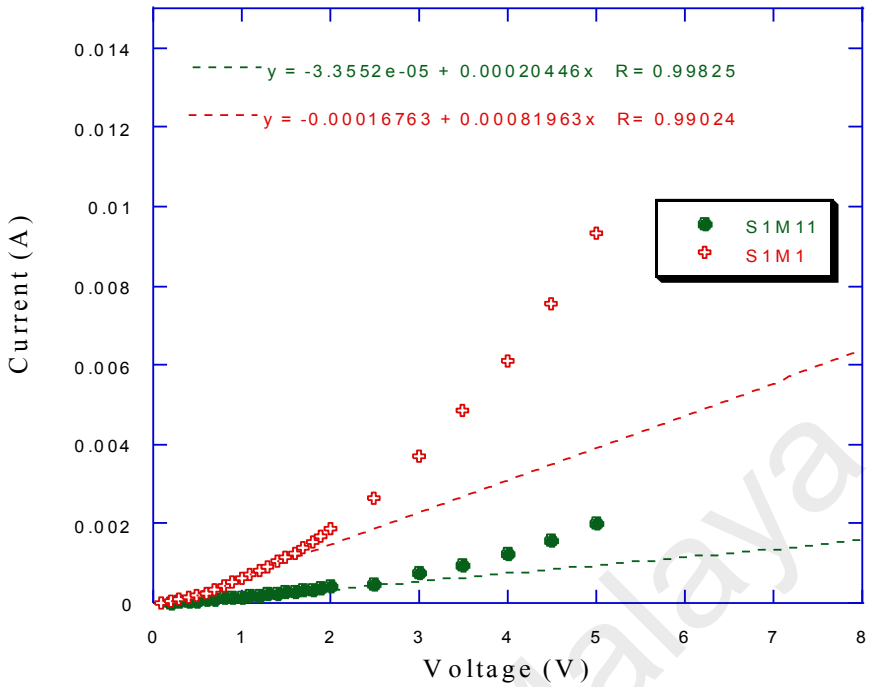

(a)

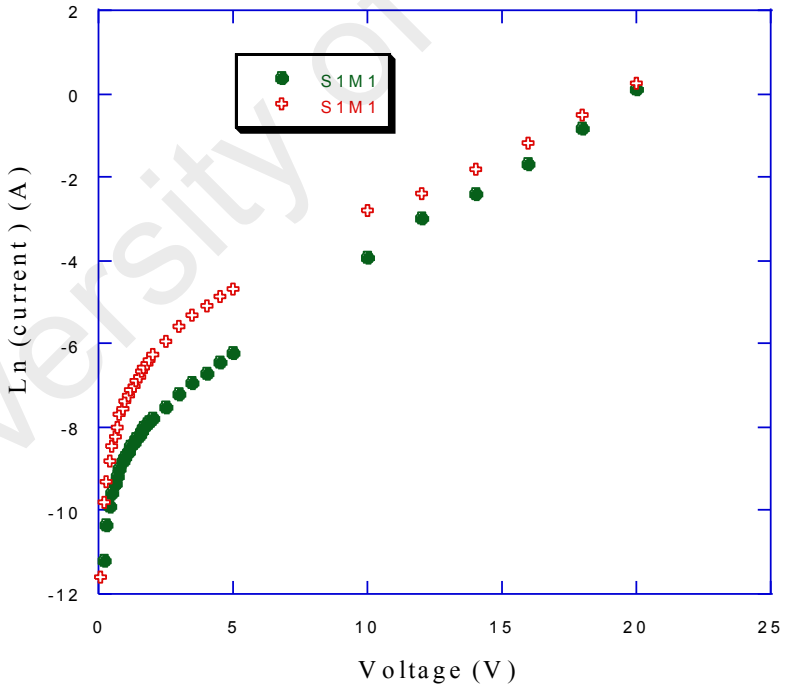

(b)

Figure 5.27: a) Dark I-V curves for modules S1M1 and S1M11 (b) Dark I-V curve in semi-logarithmic plane

Shunt resistance (R_{sh}) of modules S1M1 and S1M11 are found 1220 and 4891 Ω respectively. As a result of PID, shunt resistance of negative end (S1M1) module is found to drop by 75% more than that of positive end (S1M11) module.

5.3.4 Wet Leakage Current under HVS

Leakage current due to high voltage stress (HVS) functionally influence potential induced degradation. Field aged PV modules (both positive end S1M11 and negative end S1M1) demonstrate drastic rise in leakage current generation compared to the new module (Figure 5.28). Kang et al. (2015) recommended the following relationship between the leakage current and PID:

$$PID_{V1} = PID_{V2} \times \frac{I_2}{I_2} \tag{5.4}$$

where at voltage stress of V_1 and V_2 the PID values are PID_{V1} and PID_{V2} and leakage current values are I_1 and I_2 respectively. In the present investigation, the on-site PID value for negative end module has been obtained 42.40%, whereas the performance drop of positive end module due to normal aging (as a consequence of LID) is 17.04%. Thus the only PID involvement (without LID contribution) to the PV module degradation for the 120 V stress and 9 years is near about 25.36%. The possible PIDs at onsite under different higher system voltage stresses have been projected according to equation (5.4) as shown in Figure 5.29. The overall PV module degradation is reached up to near about 64.75% at a system string voltage of 600 V.

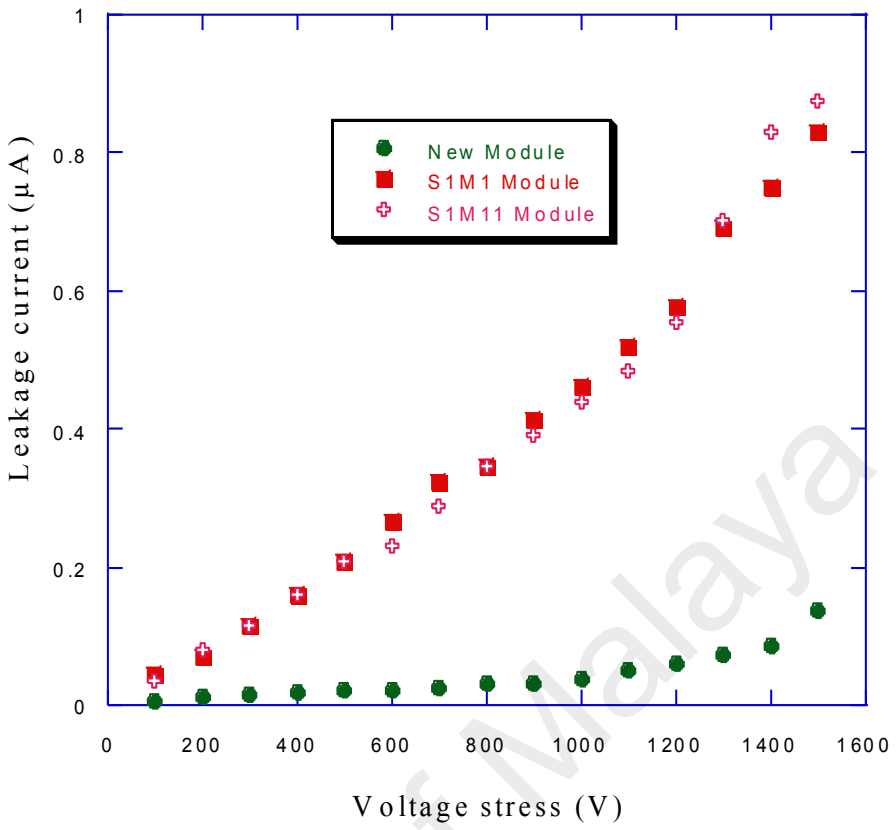

Figure 5.28: Effect of different HVS on the wet leakage current of new and on-site aged module S1M1 and S1M11

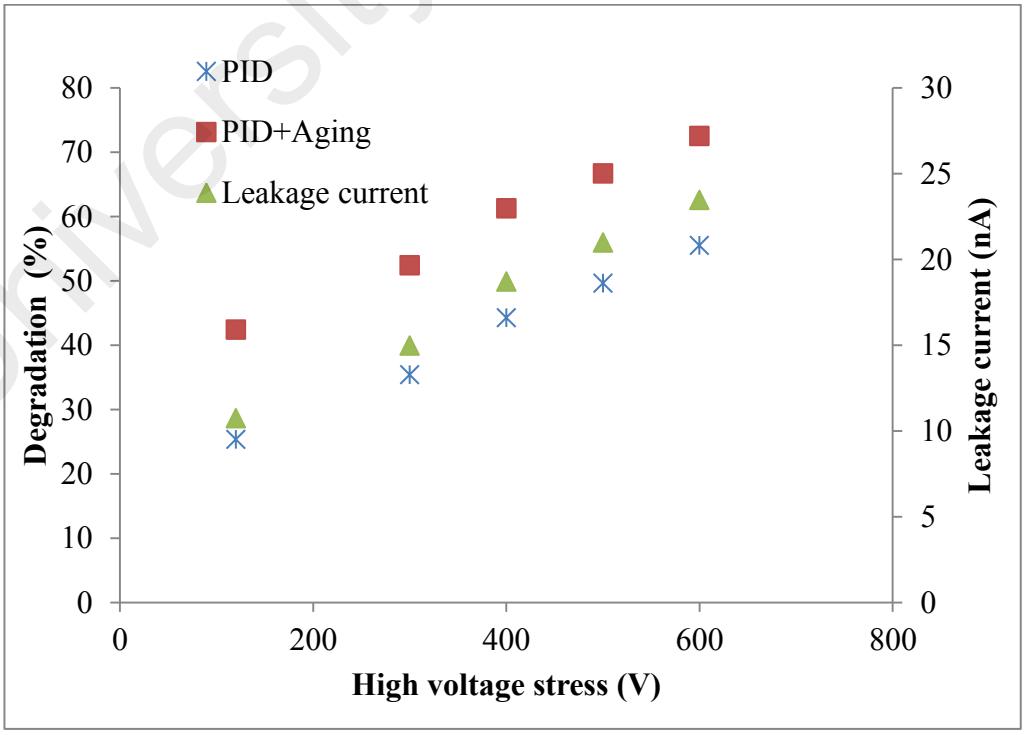

Figure 5.29: Assessed on-site PID of PV module at several high voltage stresses

5.3.5 Annual Degradation of PV Module

The extent of degradation of both positive end and negative end PV modules at different 3 years has been investigated by using electroluminescence imaging technique. For the negative PV module (S1M1), EL images are taken time intervals of 9, 9.5, 10, 10.5 and 11 years as shown in Figure 5.30. The intensity of EL image of PV module gradually decreases as a consequence of higher aging time. The dark amount of shunted areas and cracks also rises and become clearly visible as aging time increase. The rate of surface recombination of PV cell has been enhanced as a consequence of shunted dark regions and cracks. A newly formed cracking cell has been found in 9.5^{th} year that was not present at 9^{th} year aging period. That can be due to the cyclic high voltage and thermal stress on the negative end PV module. The amount of degradation at respective time of aging period has been presented in Table 5.7. The degradation versus aging time curve appears an exponential characteristic as shown in Figure 5.31 (a). The degradation curve has been drawn by extrapolating toward the initial zero degradation level according to a previously reported literature as shown in Figure 5.31 (b) (Hattendorf et al., 2012). For the positive end PV module (S1M11), EL images are taken at different aging time intervals such as 9, 10, and 11 years as shown in Figure 5.32. A small extent of reduction in of EL images; brightness has been detected as a result of on-site field aging under positive voltage stress. Localized shunting defect is not observed for the positive voltage stress on the PV module S1M11 that proves the absence of PID. Although, in positive end PV module, the cell cracks are observed, however, initiation of new crack within the monitoring period was not observed.

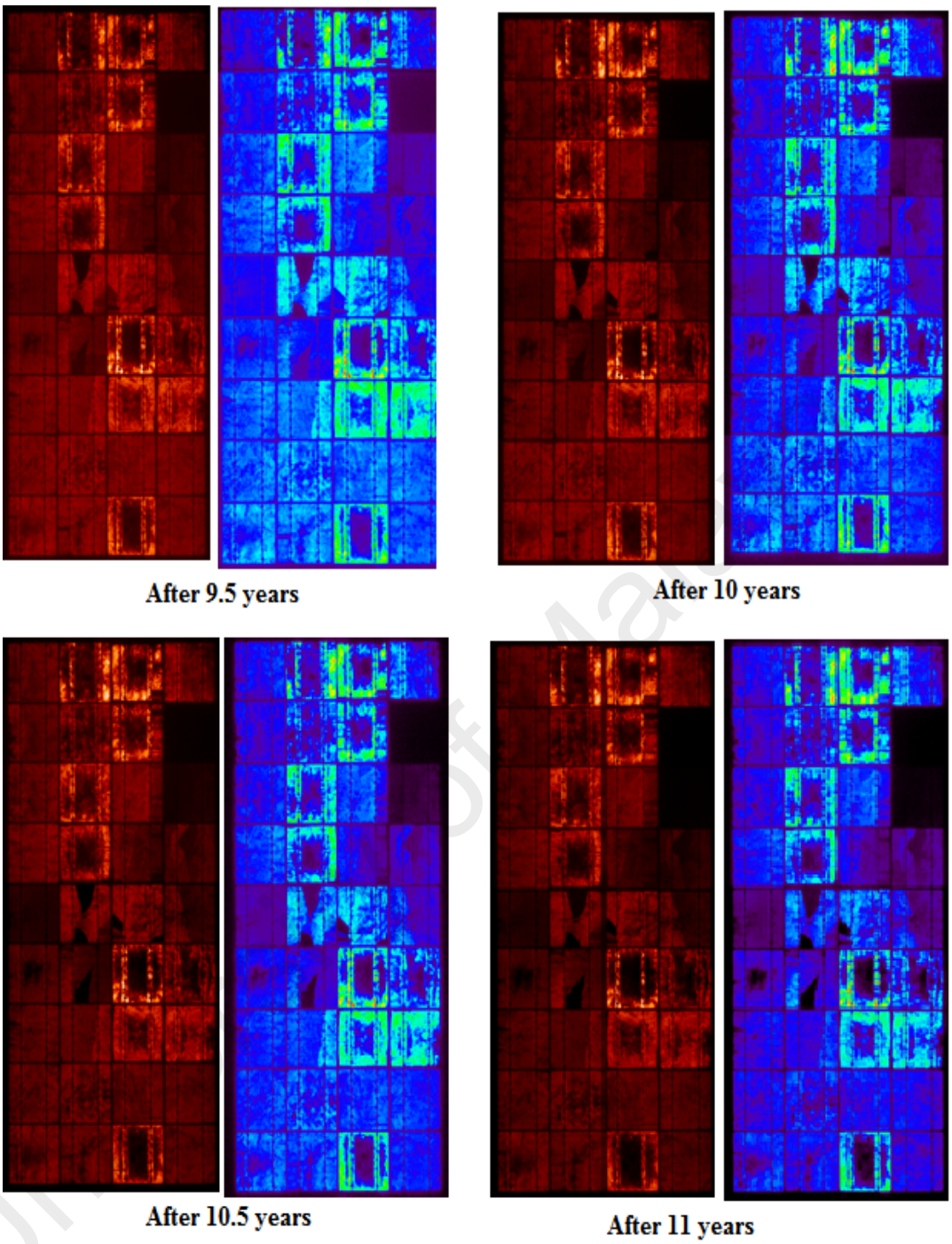

Figure 5.30: Electroluminescence images at several of aging periods of PV module (S1M1) situated at the negative end

Table 5.7: Measuring the extent of degradation through EL image of S1M1 negative end module

Aging Period (year)	**Number of pixels**	**EL Intensity Mean Value for S1M1**	$P_{max(STC)}/A_{cell}$	**EL Intensity Mean Value for a Brand New 125-W Module** [Eq. (4.2)]	**Degradation (%)** [Eq. (4.1)]
9	10395× 23389	81.35	142.68	141.25	42.25
9.5		78.97	142.68	141.25	44.09
10		77.08	142.68	141.25	45.48
10.5		75.60	142.68	141.25	46.15
11		75.26	142.68	141.25	46.71

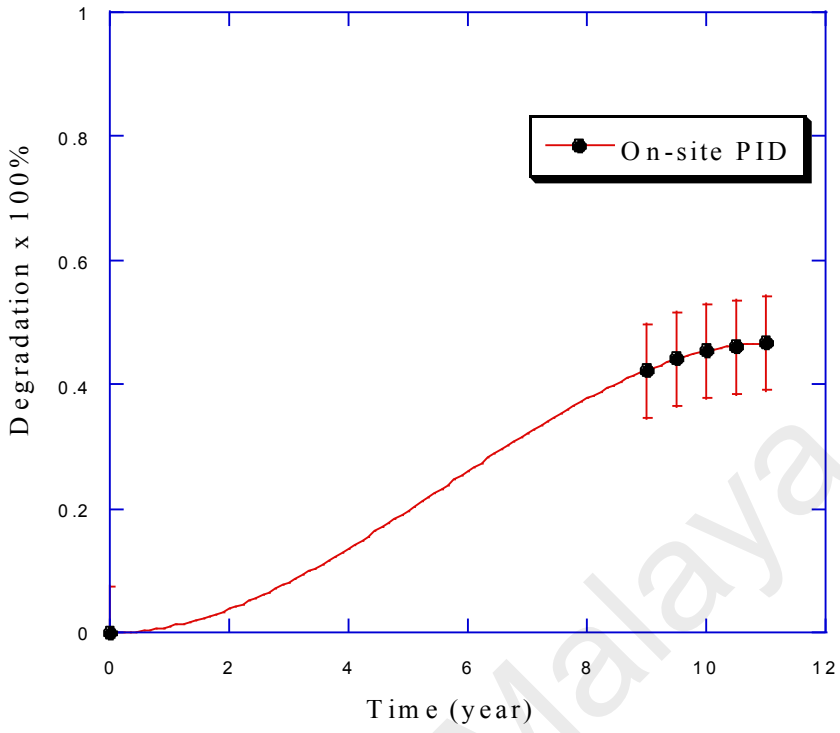

(a)

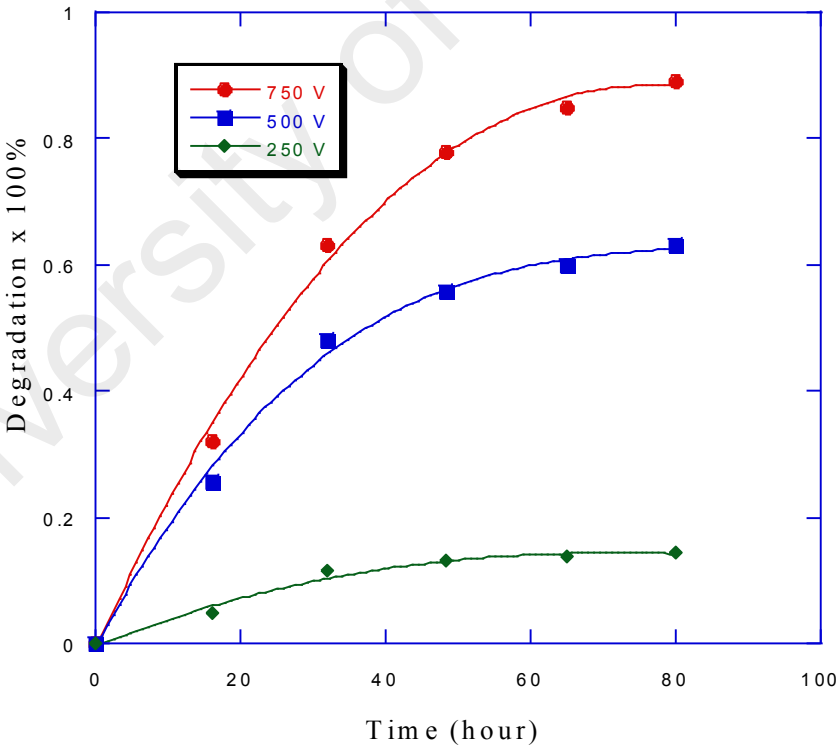

(b)

Figure 5.31: Effect of aging time on the degradation of (a) on-site PID (240V string size) in present study (b) laboratory tested module at different voltage stresses reported by Hattendorf et al. (2012)

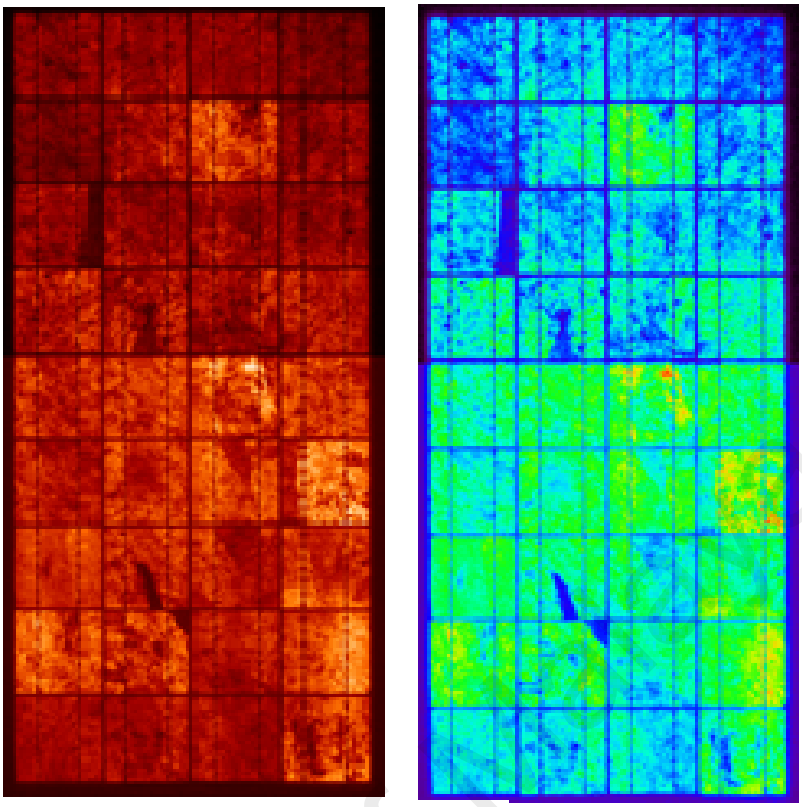

(a) 9 year

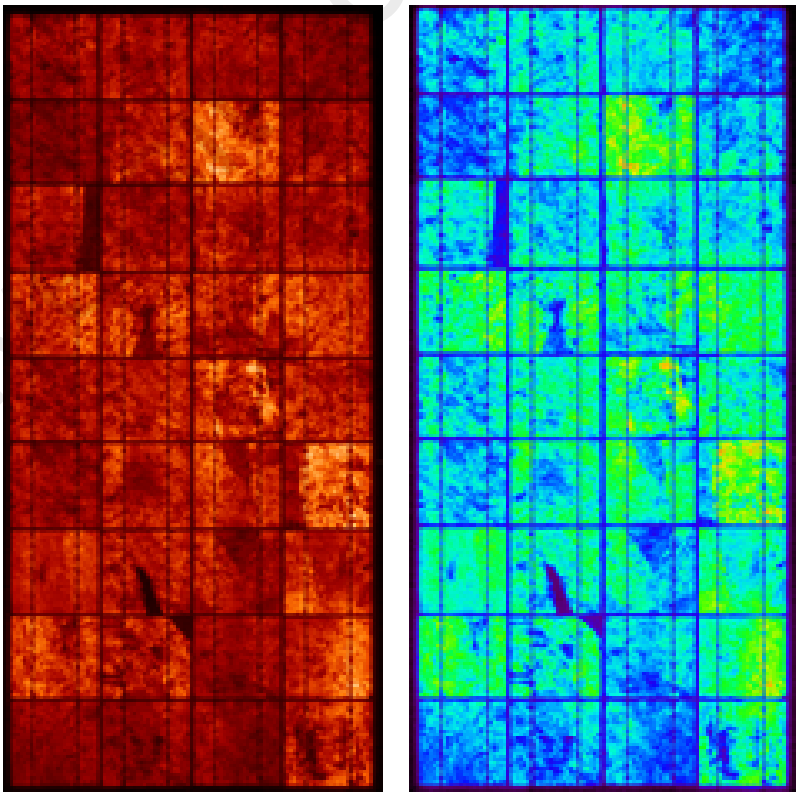

(b) 10 year

Figure 5.32: Electroluminescence images of positive end PV module (S1M11) at different aging periods of (a) 9 years, (b) 10 years and (c) 11 years

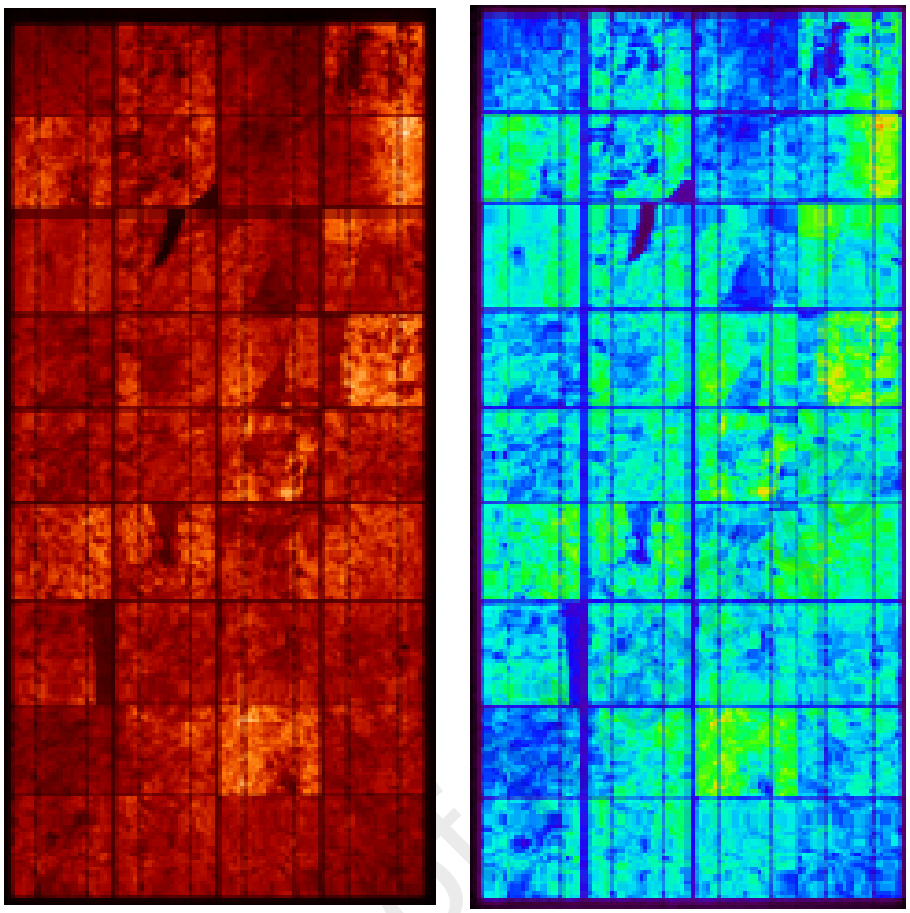

(c) 11 year

Figure 5.29, continue

5.4 On-site PID and Laboratory Test Standard: Comparison

In order to make a comparative appraisal between the laboratory standard test and on-site PID behaviour, the same brand new PV module has been used as a sample for laboratory PID test which is degraded due to on-site PID. The laboratory PID test is done according to IEC 62804 method: B (aluminium foil) method. The PV module upper surface along with frame was covered with aluminium foil and a flexible polymer mat was used to provide weighting on the foil to follow the surface morphology of the module glass to achieve a uniform electrical electrode. Negative 1000 V has been applied to the PV cells respect to module fame by the PID insulation tester. The shunt resistance (R_{sh}) progression of both on-site and laboratory tested PV modules was monitored within a certain period interval through the DIV characterization.

5.4.1 Dark I-V Characteristics

The dark I-V (DIV) characteristics of on-site degraded PV modules have been monitored at the different aging period. The positive end PV module DIV and semi logarithm DIV are shown in Figure 5.33. There is a minor amount of change has been observed in DIV characteristics due to 2 years of field aging from 2015 to 2017 might be due to LID. A similar behaviour has been observed for laboratory PID testing as shown in Figure 5.34. There is no increase in biasing current in DIV characteristics for the laboratory tested PV module under the positive voltage stress. This indicates that PID impact does not occur on positive end PV module or under positive voltage stress for the p-type c-Si PV module.

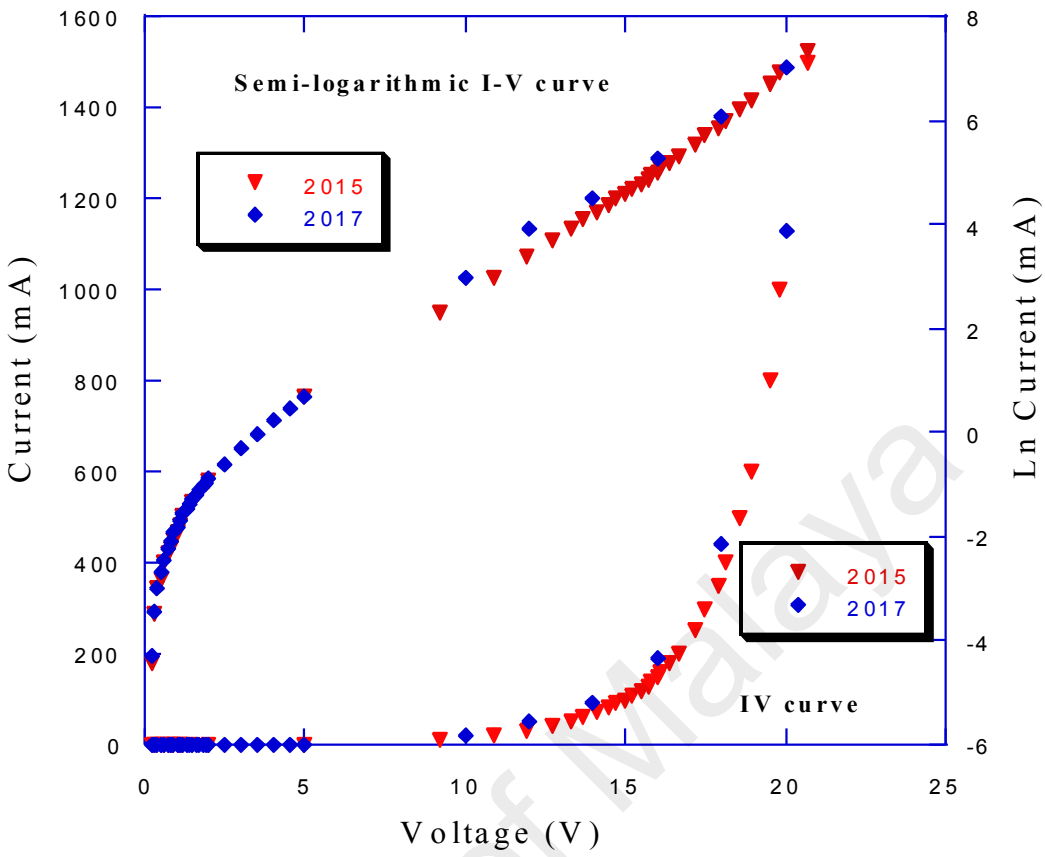

Figure 5.33: Effect of aging period on the dark I-V characteristics of S1M11 module.

Figure 5.35 shows the DIV and semi logarithm DIV characteristics of negative end S1M1 PV module. Dark IV and semi-logarithmic DIV curves at different aging periods of 9, 9.5, 10, 10.5 and 11 years are plated to evaluate the degradation of p-n junction properties. The semi-logarithmic curve gives the clear picture of current increment. The DIV characteristic of laboratory tested PV module under negative voltage stress condition is shown in Figure 5.36.

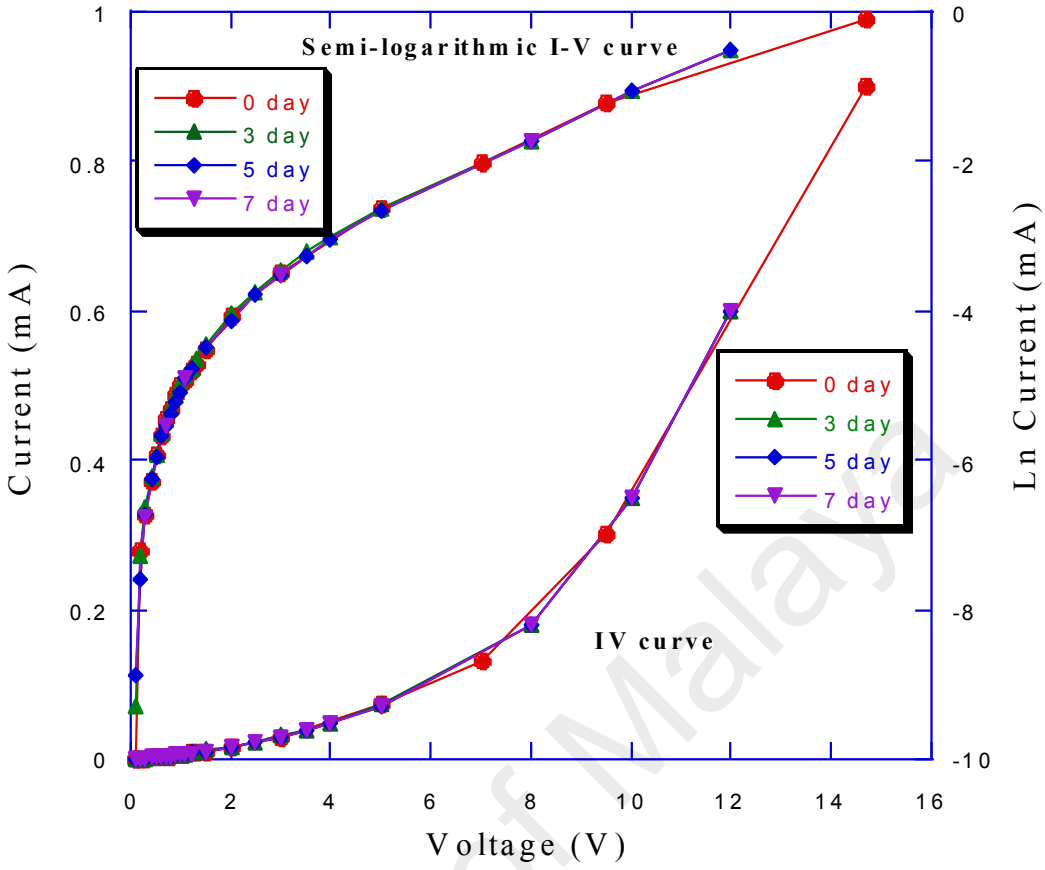

Figure 5.34: Effect of aging period on the dark I-V characteristics of PV module under positive stress condition (laboratory PID test)

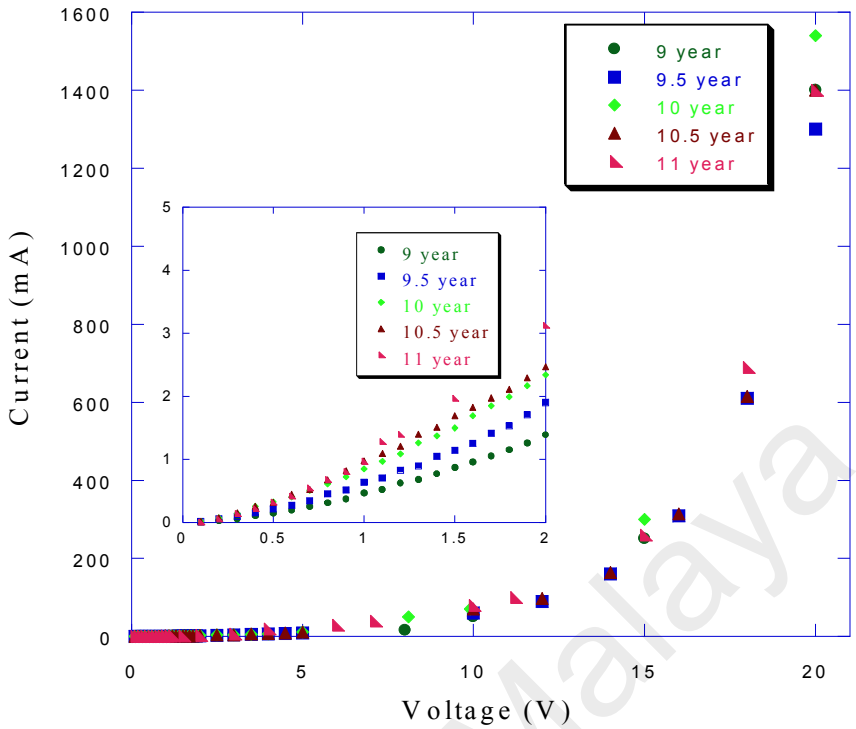

(a)

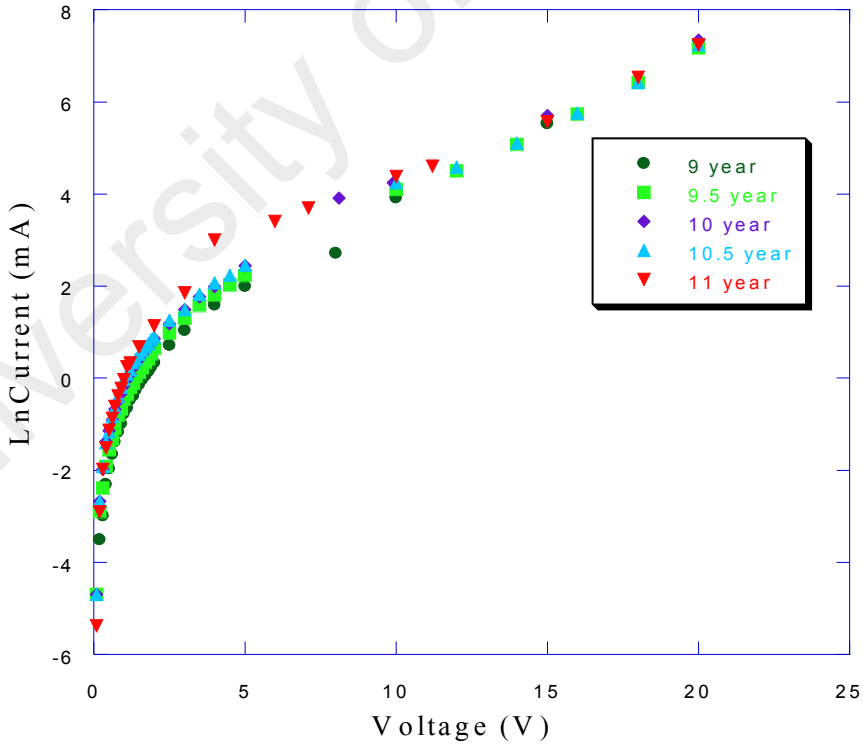

(b)

Figure 5.35: Effect of aging period on the dark I-V characteristics of S1M1 module

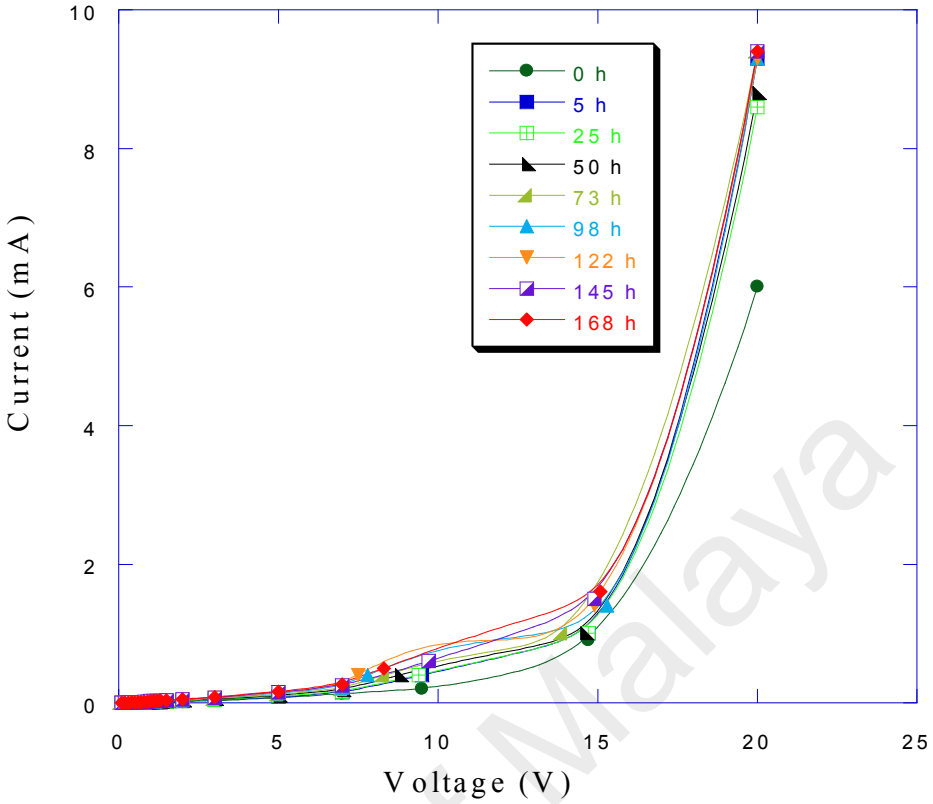

(a)

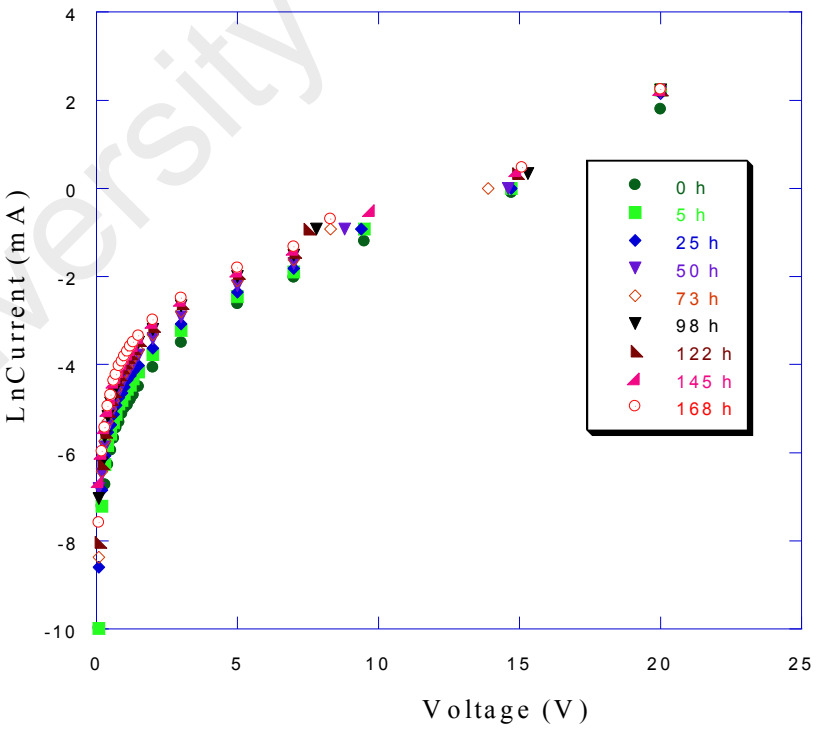

(b)

Figure 5.36: Effect of aging period on the dark I-V characteristics of PV module under negative stress condition (laboratory PID test)

5.4.2 Shunt Resistance

Shunt resistance has been determined from the dark I-V characteristic by taking reverse slope at the I-V characteristic near to the zero voltage, where I-V characteristic is a perfect straight line. The shunt resistance versus aging period curve of on-site PID affected module is shown in Figure 5.37. The curve follows basic exponential equation as shown in the fitted line. The exponential equation is as below:

$$R_{sh}(t) = Ae^{-Bt} \tag{5.5}$$

where R_{sh} is shunt resistance, t is aging period, A and B are the constant depended on the PV module and environmental condition. The similar shunt resistance degradation model was reported by (Taubitz et al., 2014) as Eq.(5.6). The constant B is depended on module temperature T_m.

$$R_{sh}(t) = Ae^{\frac{-t}{B[T_m]}} \tag{5.6}$$

The shunt resistance versus aging period curve of laboratory PID tested module is shown in Figure 5.38. Initially, the shunt resistance decreases rapidly after then the curve follows the exponential characteristic in a similar manner to that of the on-site PID affected module. The shunt resistance value of the PV module after laboratory PID testing (at negative 1000 V and for 7 days) is about 40.25 kΩ. On the other hand, the shunt resistance value of PV module degraded at on-site PID testing under negative voltage stress from the string size of 240 V and after 11 years fielded conditions, is about 0.91 kΩ. Compared to the laboratory PID testing, the shunt resistance of on-site degraded PV module reduces about 44 times. Higher degradation of shunt resistance at on-site PID testing is happened as a consequence of long period of field stressing.

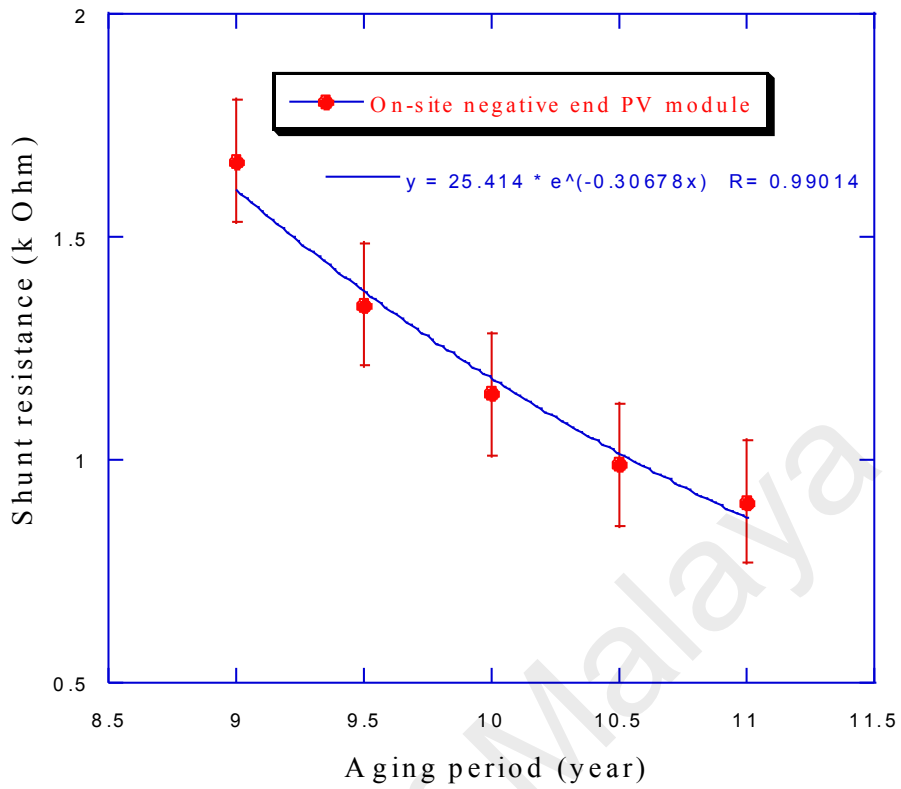

Figure 5.37: Effect of aging period on shunt resistance of degraded module placed at on-site and negative end of string

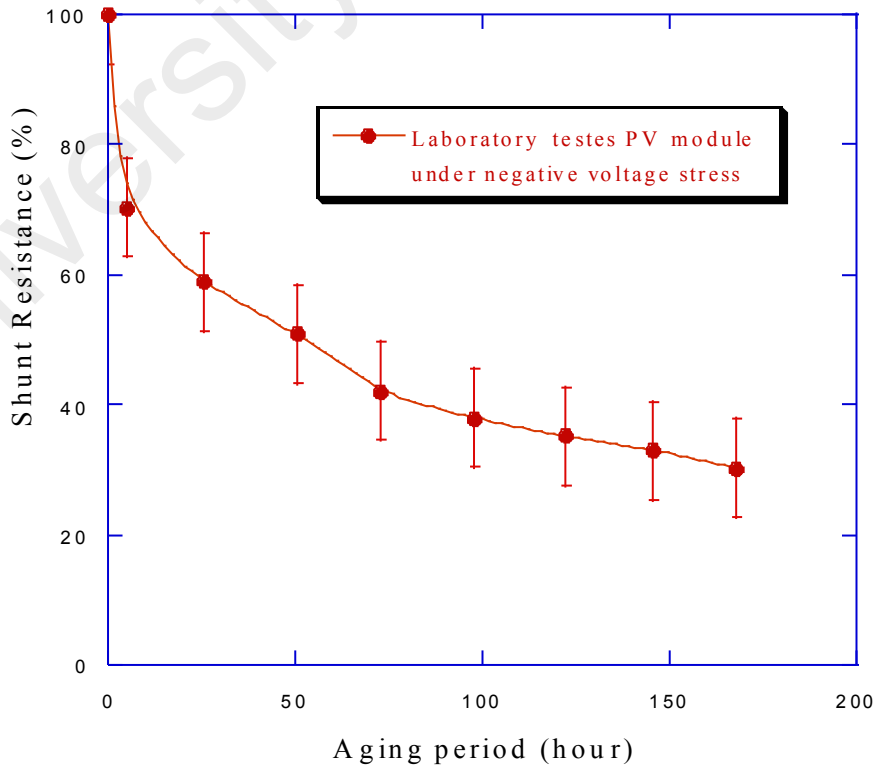

Figure 5.38: Shunt resistance decreasing profile of PID affected module in laboratory tested under negative voltage stress

5.4.3 Light I-V Performance

The light I-V (LIV) performance of PV module degraded by PID has been measured at 1000W/m^2 and 25°C condition under solar simulator made of halogen bulbs. The degradation of different I-V parameter of the negative end module (S1M1) in the PV module string at on-site and the PV module stressed under −1000 V at the laboratory conditions has been illustrated in Figure 5.39, wherein the comparative degradation features of onsite and laboratory PID testing processes are highlighted. The laboratory PID test (IEC 62804 Method B) results for I-V parameters such as P_{max}, V_{oc}, $I_{sc,}$ and FF are degraded by 6.83, 1.9, 1.5, and 3.5% respectively. A similar degradation sequence of different I-V parameters of p-type crystalline Si PV module has been also reported in the literature (Pingel et al., 2010; Schwark et al., 2013). Localized shunts in PID affected PV cell causes to decrease the FF and V_{oc} and ultimately PV power drops (Naumann et al., 2014). In addition, the quantum efficiency of PV module is reduced as a consequence of localized shunting created by PID (Oh et al., 2015). Surface recombination of minority carriers occurs due to PID defect that causes the reduction of quantum efficiency of the solar cell (Yamaguchi et al., 2016). The decrease of quantum efficiency in sthe hort wavelength region (λ < 500 nm) indicates a high rate of surface recombination in front emitter side and consequently I_{sc} of the solar cell drops (Sharma et al., 2007). On the other hand, the on-site PID test result (after about 11 years of aging in a 240-volt PV string) shows that I-V parameters such as P_{max}, V_{oc}, $I_{sc,}$ and FF are degraded by 46.5, 7.15, 30.4, and 17.35% respectively. PV module I-V parameters decrease by higher extent at on-site PID compared to the laboratory PID testing. Although in lthe aboratory an accelerated PID stress condition (covered by Al foil and 1000 V stress) has been used, still the time of field exposing in on-site PID testing is very much higher, almost 570 times compared to that of laboratory PID test. In addition, at on-site, the module temperature reaches near 60°C during sunny days (Rahman et al.,

2017) which also accelerates the PID progression. To evaluate the comparison between on-site PID test and laboratory PID test, the ratio of degradation values different I-V parameters have been taken.

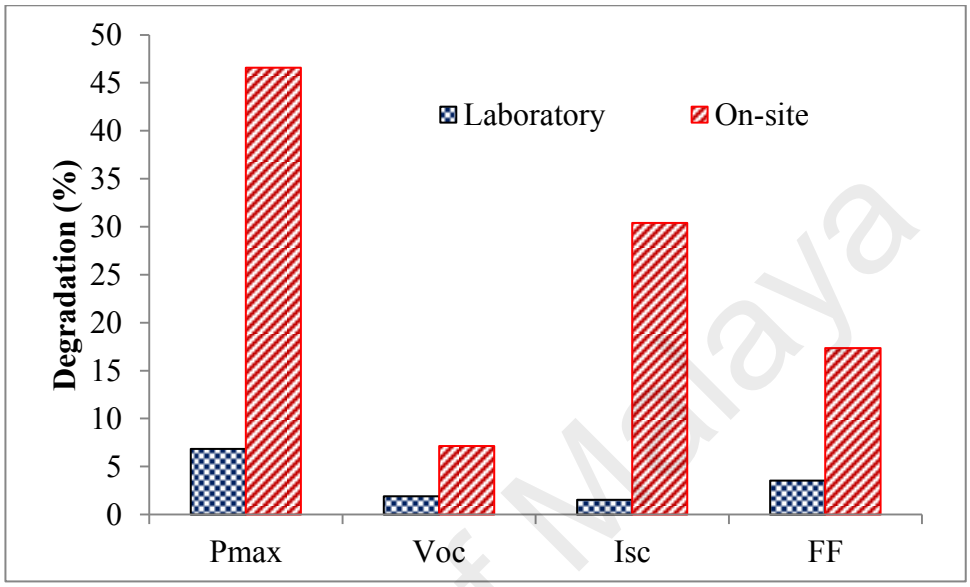

Figure 5.39: Comparative degradation values of light I-V parameters (P_{max}, V_{oc}, I_{sc}, and FF at 1000 W/m^2 and 25 °C) of PV module due to on-site PID and laboratory test standard

The degradation intensities of on-site PID (in terms of the ratio of on-site PID and laboratory PID) of different I-V parameters of PV module are shown in Figure 5.40. The ratio of on-site PID and laboratory PID for different I-V parameters such as P_{max}, V_{oc}, $I_{sc,}$ and FF are 6.81, 3.76, 19.54, and 4.92% respectively. The highest degradation intensity of on-site PID testing over laboratory PID testing has been observed for I_{sc} then followed by P_{max}, FF and V_{oc}. Oh et al. (2017) also reported a significant amount of I_{sc} degradation of p-type crystalline Si PV module after 3 years at on-site. At on-site, PV modules are stressed by a longtime field aging in outdoor condition. During the field aging, different phenomena can happen on the PV modules such as cell cracking, EVA discoloration, delamination, corrosion of bus bar or contact finger gridlines and light-

induced degradation (LID) due to longtime sun-light exposing etc. (Chandel et al., 2015; Kumar & Kumar, 2017). All these phenomena have a great impact to reduce I_{sc} of PV module those do not happen in laboratory PID testing especially in Al foil method. Moreover glass transitivity of PV module can be reduced due to soiling effect at onsite that reduces the I_{sc} of PV module (Yilbas et al., 2015). In this laboratory PID testing, the PV module degrades more than 5% that does not satisfy the pass criteria of the IEC-62804 standard testing process. Failure of a PV module to pass the PID laboratory test according to IEC standard results in a serious power drop of PV module at on-site in the early stage of its lifetime.

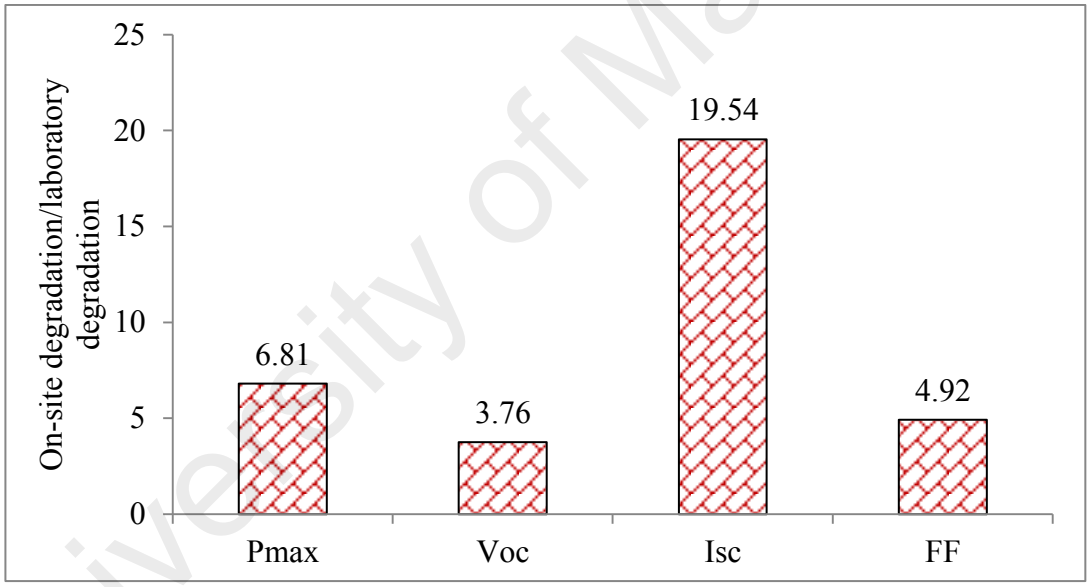

Figure 5.40: Immensity of degradation of different PV module's I-V parameters due to on-site PID over laboratory test standard

5.5 LID Behaviour of PV Module due to Real Field Aging

5.5.1 Degradation Detection by EL Imaging

Figure 5.41 shows the EL image of a type B EPV-250 brand new PV module. The mean EL intensity of individual cell is presented on the right side. Different values of mean EL intensities are obtained for different cells ranging from 140 to 200. This is due

to the dissimilar doping concentration of different cells. Average mean EL intensity of all the cells is 170.36 as previously presented in Table 5.5. The nominal value of "P_{max}/*total cell area*" of the PV module is 171.21, from which the calibration factor *C* in the equation 4.3 has been calculated as 0.99. With this *C* value and "$P_{max}(STC)/A_{cell}$" value, the mean EL intensity of a brand new non-degraded different PV modules has been calculated by using equation 4.2. The mean EL intensity ($EL_{mean(STC)}$) of type B nondegraded brand new module as by using equation 4.2 is 169.50. Figure 5.42 shows the EL image (left) and individual cell performance deviation (%) from the $EL_{mean(STC)}$ value (right) of an 8-month field aged PV module type A. It has been observed no crack in the PV module. Inhomogeneous individual cell performance has been obtained from the EL image. The negative and positive sign of cell performance indicates the less and more performance compared to the $EL_{mean(STC)}$. Overall degradation of the PV module has been calculated from the average performance of all cells within the module. The degradation value is 1.78% due to 8-month aging. Figure 5.43 shows the EL image (left) and individual cell performance deviation (%) from the $EL_{mean(STC)}$ value (right) of a 16-month aged PV module of type B, wherein both dark and bright cells are seen. A very small amount of contact finger interruptions are observed throughout the PV module (Mansouri et al., 2012). This is the interruption of electrical conductance of the front side metalized fingers, that alters the ideal current flow path through the front metal grid, which results in both an increased effective series resistance and a decreased power output (Zafirovska et al., 2017).

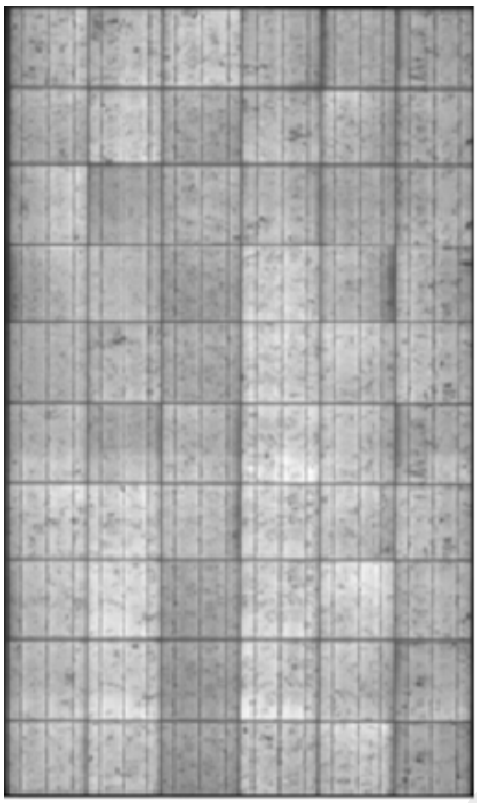

150	172	180	151	152	145
158	182	156	167	168	156
171	159	168	170	160	160
165	175	154	192	164	160
162	169	162	191	184	171
170	167	171	199	184	157
183	197	175	190	180	171
174	200	154	192	200	163
173	194	157	194	179	153
166	173	142	171	178	140

Figure 5.41: EL image and individual cell mean EL intensity of the new unused and "B" type PV module

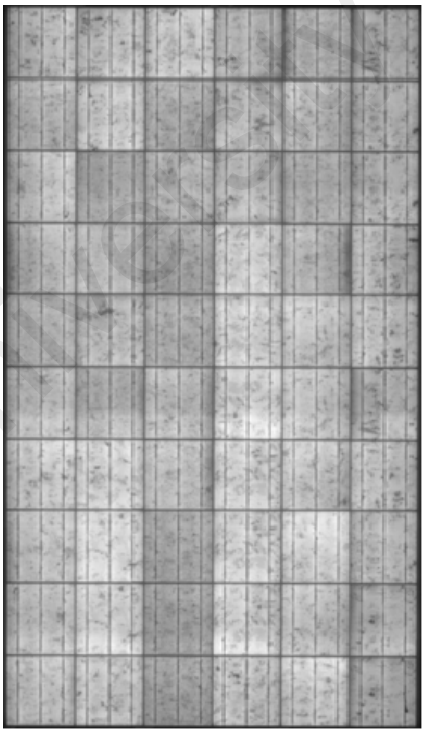

-18.57	0.57	-1.53	2.86	-2.05	-8.21
-11.21	18.50	7.92	10.28	-3.85	-10.24
-10.50	7.99	10.16	0.64	-13.05	-10.94
-23.09	3.31	4.64	0.58	0.26	-10.28
-2.36	12.78	-2.14	19.10	6.58	-12.67
-11.20	14.15	1.10	0.54	7.81	-12.72
-22.86	6.21	-2.64	7.09	8.88	-10.38
-16.01	0.40	-1.37	6.17	2.34	-6.21
-2.57	5.77	-1.07	4.52	-2.29	-12.37
-15.50	-7.14	4.06	-6.38	7.72	-18.48

*Note: (+) and (-) value of individual cell performance indicate higher and lower performance than standard cell performance respectively

Figure 5.42: EL image and individual cell performance (%) of the 8-month aged type B module

The highest negative and positive deviations of cell performance from the $EL_{mean(STC)}$ value are −30.33% and + 20.86% respectively. Overall degradation of the PV module has been calculated from the average performance of all cells within the module. The average mean EL intensity of total module has been found 157.53 counts as presented in Table 5.8. The degradation value is 7.06% due to 16-month aging. Figure 5.44 shows the EL image (left) and individual cell performance deviation (%) from the $EL_{mean(STC)}$ value (right) of a 4-years aged PV type A module. The existence of contact grid problems, namely broken fingers have been revealed more clearly compared to 16-month aged PV module. Dark lines indicate the presence of cracks. Also, a dark region is visible in some solar cells, which is indicative of the existence of a high recombination region (either due to bulk or surface defects) (Frazão et al., 2017). Highest negative and positive deviations of cell performance from the $EL_{mean(STC)}$ value are −32.23% and + 16.39% respectively. Overall degradation of PV module has been calculated from the average performance of all the cells within the module. The average mean EL intensity of total module has been found 136.35 counts as presented in Table 5.8. The degradation value is 13.92% due to 4 years of aging.

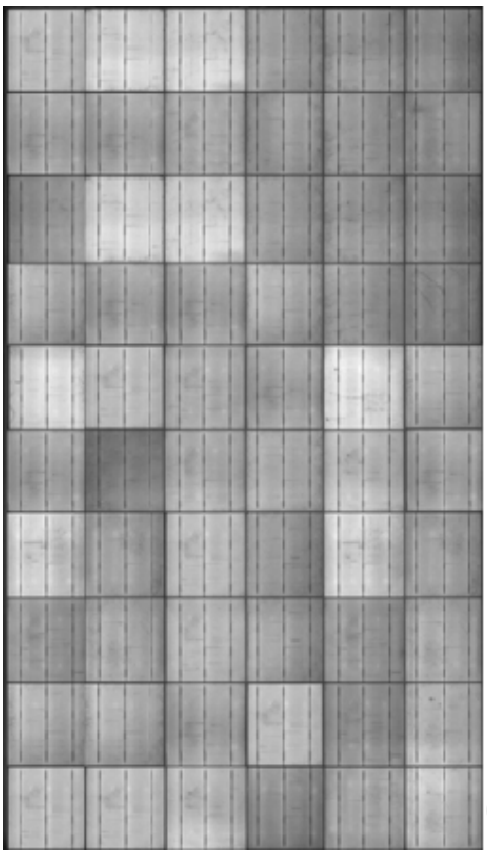

2.93	15.79	14.68	-14.58	-19.04	-27.83
-10.31	-9.53	-5.57	-16.76	-16.93	-22.82
-18.61	15.53	14.90	-13.24	-16.67	-27.32
-6.89	-9.47	-9.32	-6.40	-16.88	-28.90
15.69	5.22	-4.09	-10.19	20.86	-7.31
-10.70	-30.33	-2.90	-6.35	3.62	-10.54
11.19	-15.01	4.07	-16.88	9.36	-14.33
-15.93	-9.14	1.58	-13.90	-16.08	-9.73
-7.19	-6.82	-9.81	4.49	-20.34	-3.76
2.01	3.51	2.81	-24.66	-9.39	0.68

*Note: (+) and (-) value of individual cell performance indicate higher and lower performance than standard cell performance respectively

Figure 5.43: EL image and individual cell performance of the 16 months aged type B module

Figure 5.45 (a) shows the EL image (left) and individual cell performance deviation (%) from the $EL_{mean(STC)}$ value (right) of 9 years aged PV module C type. The highest negative and positive deviations of cell performance from the $EL_{mean(STC)}$ values are found −46.87% and + 12.88% respectively. The average mean EL intensity of total module has been found 117.18 as presented in Table 5.8. The degradation value is 17.04% due to 9 years of aging and the degradation rate is 1.89% per year which is very close to the reported rate of 1.87% per year in Italy after 10 years of aging (Parretta et al., 2005). Figure 5.45 (b) shows the EL image (left) and individual cell performance deviation (%) from the $EL_{mean(STC)}$ value (right) of 11-year aged type D module. Maximum negative and positive deviations of cell performance from the $EL_{mean(STC)}$

value are − 48.18% and + 14.99% respectively. The average mean EL intensity of total module has been found as 123.53 counts and 17.42% degradation is occurred due to 11 of years aging.

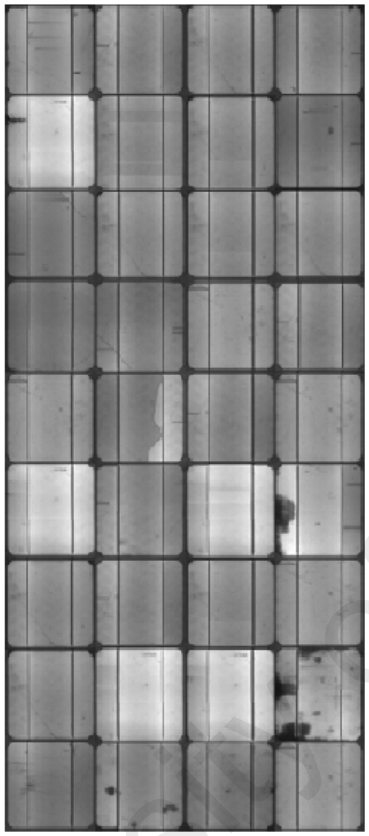

-15.47	-19.36	-15.53	-23.33
14.71	-17.41	-17.05	-32.23
-28.22	-18.43	-17.55	-18.03
-31.45	-26.60	-11.94	-19.39
-12.76	-16.93	-19.77	-13.65
15.01	-17.36	15.05	-1.59
-18.41	-19.49	-16.05	-11.09
-17.10	16.39	15.61	-14.65
-28.86	-19.95	-27.79	-11.98

*Note: (+) and (-) value of individual cell performance indicate higher and lower performance than standard cell performance respectively

Figure 5.44: EL image and individual cell performance of the 4 years aged type A module

The EL images of polycrystalline PV module contain some dark and bright spots, while the EL images of monocrystalline PV module show homogeneous brightness all over the module. This is due to the presence of grain boundary related dislocation defect in polycrystalline PV modules (Frazão et al., 2017).

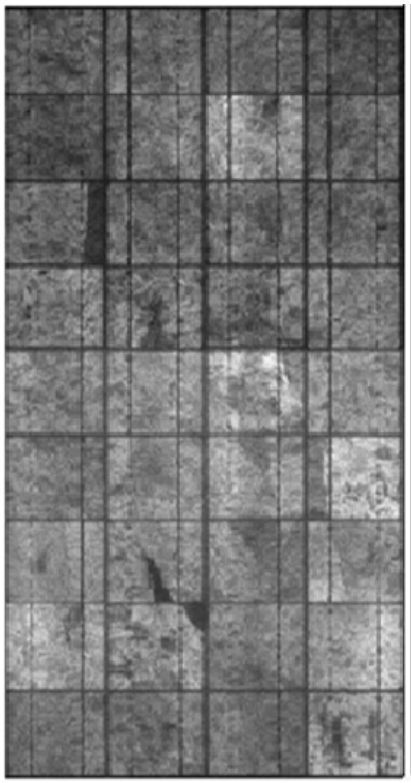

-40.07	-31.50	-34.22	-46.87
-46.74	-24.74	-1.28	-33.91
-38.23	-30.68	-27.77	-32.68
-18.56	-25.64	-27.29	-17.71
-11.43	-2.27	5.27	-0.88
-16.23	-5.23	3.06	12.88
-3.78	-12.48	-16.14	-2.09
5.76	-7.61	-16.84	11.37
-24.09	-23.38	-24.93	-6.65

(a)

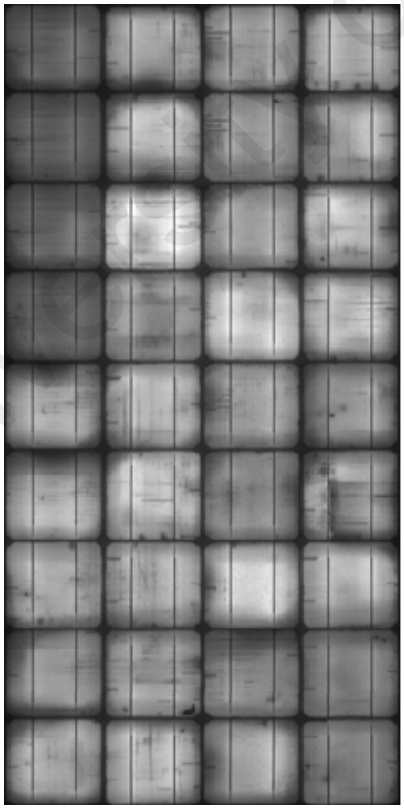

-46.65	-19.52	-16.68	-11.34
-48.18	-11.57	-18.69	-18.46
-44.79	14.99	-13.98	-7.15
-44.81	-16.78	8.12	-8.19
-20.07	-3.62	-16.72	-27.29
-14.85	2.21	-23.61	-26.28
-10.53	-9.25	3.29	-7.23
-25.47	-16.06	-29.75	-29.83
-13.07	-6.21	-18.14	-30.82

(b)

*Note: (+) and (-) value of individual cell performance indicate higher and lower performance than standard cell performance respectively

Figure 5.45: EL image and individual cell performance of the (a) 9 years aged type C module and (b) 11 years aged type D module

Degradation parameters and their respective values for different aged PV modules are shown in Table 5.8. The mean EL image intensity has been calculated from the EL image histogram. $P_{max(STC)}/A_{cell}$ obtained from the manufacturer data sheet. Mean EL image intensity of new PV module has been calculated by using equation 4.2. Finally, the degradation of respective PV module has been calculated by equation 4.1.

Table 5.8: Measuring the degradation of PV module by means of EL imaging

Module Type	Aging Period	Mean EL Intensity of Degraded Module	$P_{max(STC)}/A_{cell}$	Mean EL Intensity of Brand New PV Module	Degradation (%)
B	8 month	166.47	171.21	169.50	1.78
B	16 month	157.53	171.21	169.50	7.06
A	4 year	136.35	160	158.4	13.92
C	9 year	117.18	142.68	141.25	17.04
D	11 year	123.53	151.11	149.60	17.42

Figure 5.46 shows the PV module degradation behaviour as a result of varying aging period. The extents of degradation are 1.78, 7.06, 13.92, 17.04 and 7.42% for 8 months, 16 months, 4 years, 9 years and 11 years of field aging respectively. At the initial stage of aging, the degradation rate is very high and the rate decreases gradually at the higher aging period. Similar behaviour is also reported in the literature (Jordan et al., 2017). From the experimental data, a curve has been fitted to estimate the possible degradation at a high aging period in Malaysian climatic condition. The estimated degradation after 21 years is 18.61%, which satisfy the manufacturer warranty (< 20%), the degradation rate being 0.86% per year. The rate is comparable with other reports such as 0.96% per year at Patras, Greece after 22 years (Kaplani, 2012) and 0.81% per year in Trinidad, California after 20 years of natural aging (Chamberlin et al., 2011). Table 5.9 summaries the degradation rates of PV modules in a different location, which were published previously, together with the results of this work.

Table 5.9: Degradation rates of PV modules in different locations

Location	Type PV Module	Aging Period	Degradation Rate (%/year)	Reference
Dakar, Senegal	Monocrystalline	1.3 years	0.22	Ndiaye et al. (2014)
	Polycrystalline	3.4 years	1.62	
	Monocrystalline	4 years	2.99	
	Polycrystalline	4 years	2.96	
Algeria	Monocrystalline	28 years	1.22	Bandou et al. (2015)
Thailand	Multicrystalline	4 years	1.2	Limmanee et al. (2017)
	HIT	4 years	1.3	
	Micromorph	4 years	1.8-6.1	
	CIGS	4 years	1.7	
Algeria	Monocrystalline	5 years	3.63	Charrouf et al. (2017)
	Monocrystalline	10 years	1.74	
Singapore	Multicrystaline	3 years	near 1.2	(Ye et al., 2014)
	CIGS	3 years	6.0	
Kuala Lumpur, Malaysia	Monocrystalline (module A)	4 years	3.48	Present study (2017)
	Polycrystalline (module B)	16 months	5.30	
	Polycrystalline (module C)	9 years	1.89	
	Monocrystalline (module D)	11 years	1.58	

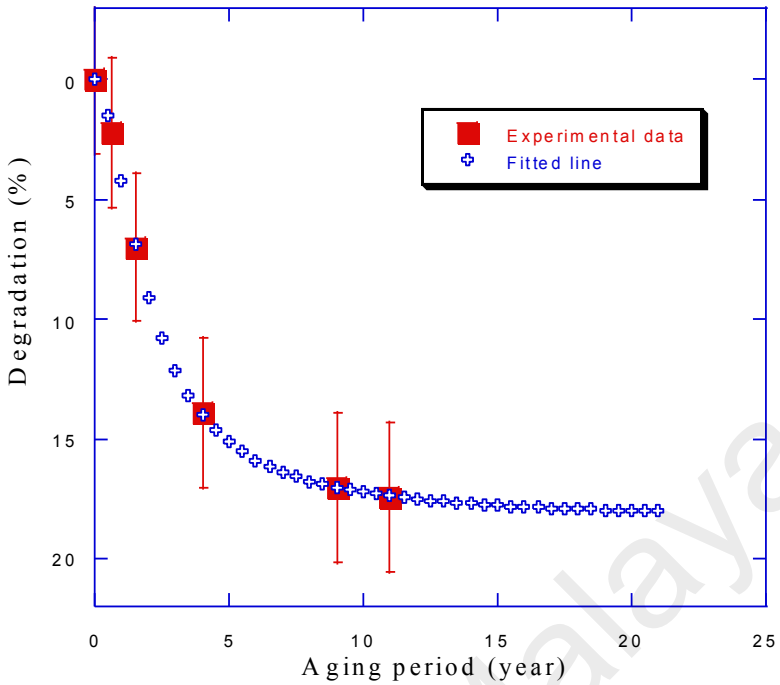

Figure 5.46 Effect of aging period on the degradation of PV module

5.5.2 Dark I-V Characteristics

The shunt resistance of different aged PV module has been calculated by measuring I-V at the dark condition. Semi logarithm current density (J) versus voltage (V) curves of different aged PV module is revealed in Figure 5.47. The obtained shunt resistance values of different PV modules are 125, 86.95, 60.39, 10.15, 4.04 and 3.36 $k\Omega.m^2$ for brand new, 8 months, 16 months, 4 years, 9 years and 11 years aging respectively. Shunt resistance gradually decreases with the increase of aging periods due to increase of different types of defects as revealed by respective EL images. The decrease of shunt resistance due to aging is also reported for crystalline PV module (Rabii et al., 2003). The possible cause of severe power loss due to aging is the low value of shunt resistance.

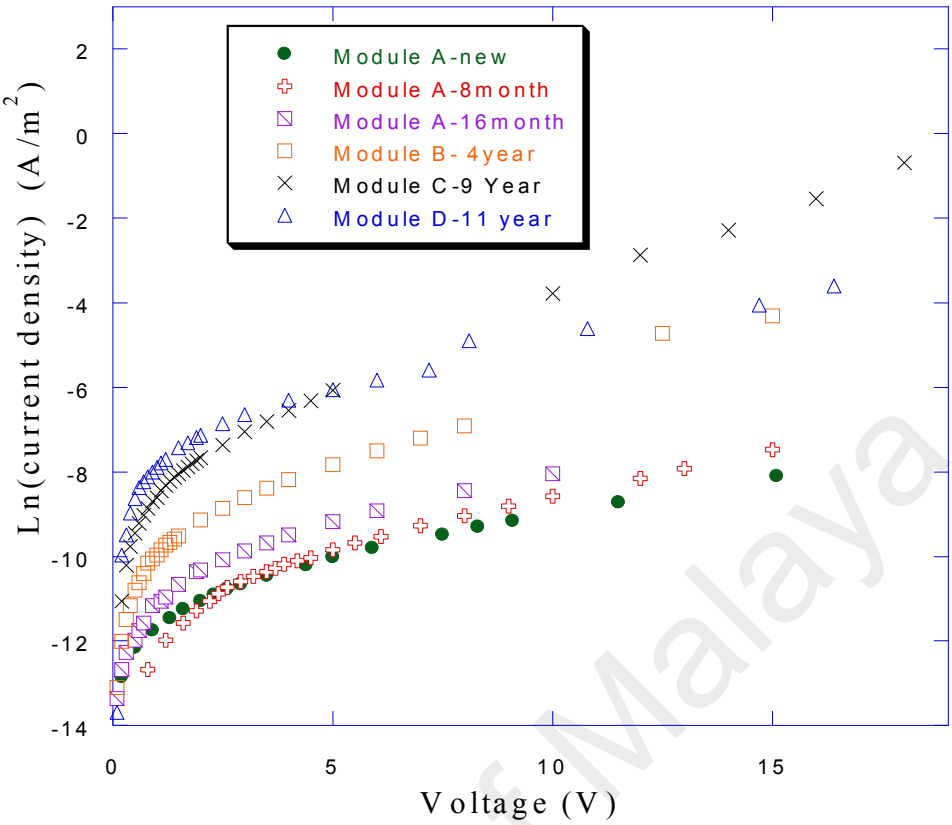

Figure 5.47: Effect of different aging period on the semi-logarithmic dark J-V characteristics of PV modules

5.5.3 Temperature Coefficient of Maximum Power

The cell temperature dependent P_{max} behaviour of different PV modules aged at different periods (such as 16 months, 4 years, 9 years and 11 years) are shown in Figure 5.48. From the linear curve fitting and using Eq.4.5, the temperature coefficient of P_{max} (γ) has been determined. The obtained γ values are 0.898, 1.164, 1.37 and 1.468% for the PV module of 16 months, 4 years, 9 years and 11 years aged respectively. PV module performance decreases at high temperature because of bandgap reduction at high temperatures (Singh & Ravindra, 2012). The γ value depends on the band gap reduction rate with temperature which depends on the semiconductor materials properties. Due to aging, the temperature dependent band gap shrinkage resistant property might be degraded and consequently γ value increases. Initially, the increasing

rate of γ per year is high and then at the higher aging period, the rate decreases gradually. The obtained degradation rate of γ values of PV module under aging at 16 months, 4 years, 9 years and 11 years are 75%, 28% 22.56% and 25% per year respectively.

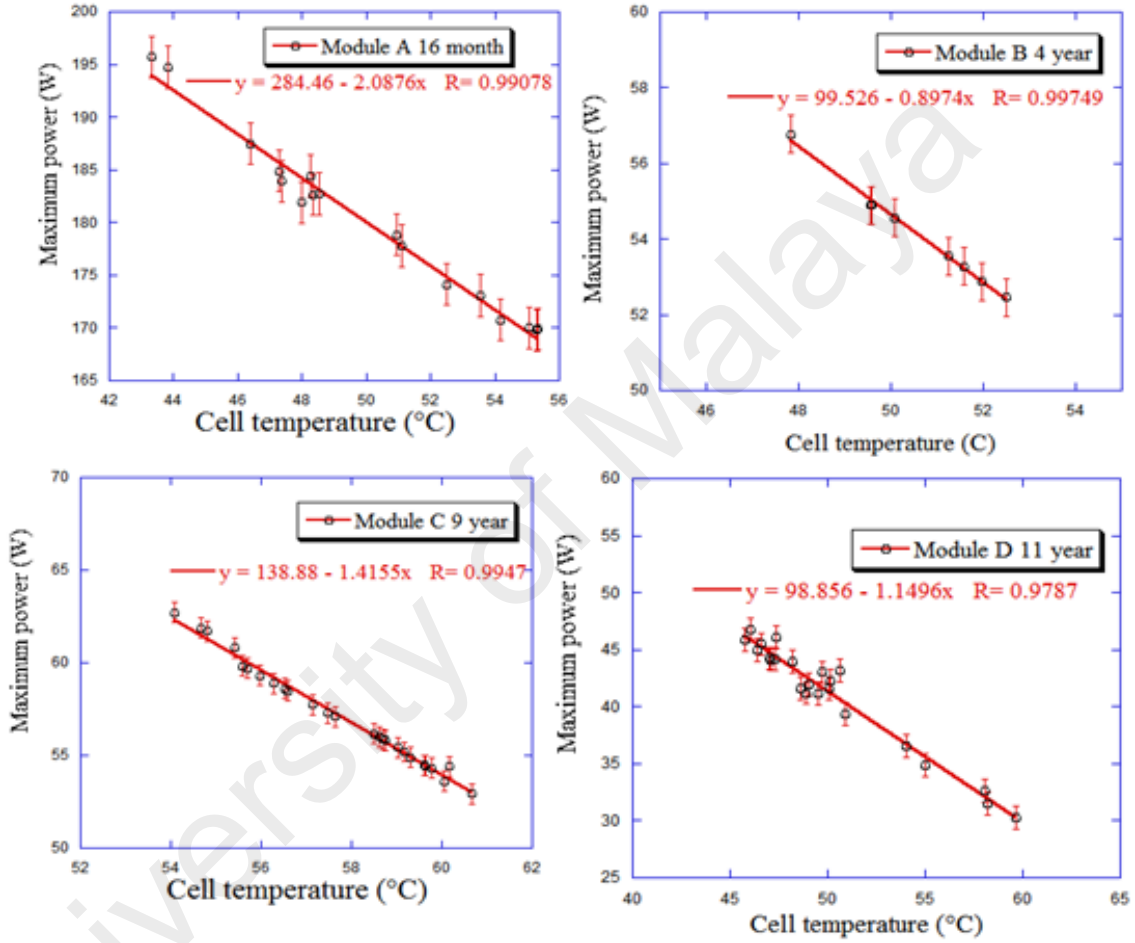

Figure 5.48: Cell temperature-dependent maximum output (at 1000W/m^2 irradiance) of PV modules aged at different periods

CHAPTER 6: CONCLUSIONS AND RECOMMENDATIONS

6.1 Introduction

Degradation of PV module under HVS leads to catastrophic failure of PV power plant which has become a principal concern for the PV industry. Investigation of the HVS degradation related issues of PV module has drawn notable interest of the PV researchers. In the present research, some critical issues such as the impact of various parameters on HVS leakage current, PID test both on-site and laboratory and LID of the solar photovoltaic module have been investigated. The PID characteristic of polycrystalline PV modules at on-site has been investigated under the Malaysian climatic condition. To assess and explain the PID occurrences, the PV modules are characterized in different methods. In addition, PV module leakage current has been investigated by applying high DC voltage stresses at different environmental conditions. Moreover, LID behaviour of different crystalline Si PV modules aged over different periods in Malaysian climate has been investigated through EL imaging, dark I-V, and cell temperature-dependent maximum power measurement processes.

The major inferences drawn from the present investigation have been enumerated in following sections.

6.1.1 Effect of Various Parameters on HVS Leakage Current

- A nonlinear increase of leakage current has been observed due to increase of voltage stress at room temperature.
- A remarkable consequence of PV module surface temperature, water film, salt and dust particle accumulation on the leakage current of PV module has been obtained.

- An almost linear increase of leakage current with the increase of temperature of PV module has been found.
- The module temperature impact on the leakage current of PV module becomes massive in wet surface condition. The amounts of leakage current (45°C and wet surface condition) at voltage stress of 600, 1000 and 1500 V are 11.45, 20.00, and 29.85 μA respectively.
- A linear increase in leakage current due to the presence of salt on the module surface has been noticed.
- Dust accumulation on PV module surface causes to increase the HVS leakage current of the PV module.
- Resistance to leakage current generation of PV module deteriorates substantially due to long-time real field aging.

6.1.2 On-site PID Behaviour and its comparison with laboratory test standard

- A novel quantitative degradation detection method of photovoltaic modules through the EL imaging process has been presented for the first time in the present research.
- The PV module degrades by 42% at on-site as a consequence of negative voltage stress from the 240 V string size at 9 years and PID is not observed in positive voltage stressed PV module. However, 17% degradation occurs due to LID under 9 years of field aging. Then again, the values of shunt resistance are 4891 and 1220 Ω for the positive and negative end PV modules respectively.
- At on-site, the cell cracking of poly c-Si photovoltaic module is hastened as a result of cyclic thermal and voltage stress.
- Negative voltage stress condition causes to occur PID of PV module in both on-site test and laboratory test.

6.1.3 Real field Aging LID Behaviour

- The EL images of both poly c-Si and mono c-Si PV modules showed that various sorts of defects in PV cells are conceivable, for example, contact finger grid problem cracks and dislocation related defect, etc.
- The contact grid problems and cracks increase as a result of longtime field aging.
- The degradation values due to 8 months, 16 months, 4 years, 9 years and 11 years of aging of PV modules have been found to be 1.78, 7.06, 13.92, 17.04 and 17.42% respectively. One of the reasons behind this degradation is detected to be the reduction in shunt resistance which declines gradually as a result of aging.
- Degradation versus aging period curve shows exponential characteristic. The estimated degradation of a PV module after 21 years of aging is obtained 18.61%.
- The temperature coefficient of P_{max} degrades as a result of field aging. Initially, the temperature coefficient of P_{max} degrades at a higher rate, and then it becomes fairly constant.

6.2 Contribution of the Present Research

An all-inclusive investigation has been carried out to observe and develop an on-site PID detection technique and LID behaviour for PV modules along with the response of HVS leakage current. The key contributions of this research are summarized as follows:

(1) Novel method for quantitative measurement of PV module degradation: In the present research, a new quantitative method to gauge PV module degradation has been presented by making use of EL image pixel mean intensity.

(2) New mode of PV module degradation detected: A very new mode of module degradation has been detected in course of this research work. It has been observed that the crack propagation of poly c-Si PV module is accelerated by on-site cyclic HVS.

(3) Novel concept about the impact of different PV module's operating parameters on HVS leakage current introduced: It has been confirmed through this research that PV module's HVS leakage current is stimulated at the wet surface condition. And the HVS leakage current increases furthermore salt and dust deposition and resistance to the leakage current of the modules is degraded by field aging.

(4) Established a relationship between on-site PID testing and laboratory standards: It has been confirmed through the present study that on-site PID and laboratory tested PID follow the similar degradation trend as a function of time lapse.

6.3 Recommendation

Experimental investigations on the consequence of various operating parameters on HVS leakage current characteristics of PV module, real field PID characteristics of silicon crystalline PV module and effect of long-time real field aging on the PV module's performance have been done. Although some significant novel achievements like development of a novel method for quantitative measurement of module degradation, establishing a functional relationship between on-site and laboratory PID test procedure, etc. have been accomplished in the present research, the followings may be taken into consideration for future endeavours:

- Potential induced degradation at on-site and different higher string voltages of the order of 600 to 1000 V and different periods of aging may be studied.
- Real field PID of different thin-film PV modules (a-Si, CdTe, CIGS) is also necessary to make a comparative assessment.
- Different microstructural characterization such as EDX, TEM, SIMS and SEM etc. of on-site PID affected modules to evaluate the root cause of PID of different types of PV module should be investigated.

- The root cause of PID can be investigated during the p-type c-Si PV module is stressed with a high positive potential relative to the frame.
- Investigating the effect of different hydrophobic self-cleaning coating on the leakage current as well as PID process of PV modules and also the effect of different parameters such humidity, temperature, dust, and salt deposition etc. on the coated module to evaluate the sustainability of the coatings.
- The lifetime of PV modules can be prolonged by using several techniques as follows:
    i) Applying hydrophobic coating into the top surface of PV module.
    ii) Using high PID resistance encapsulant materials
    iii) Applying proper dust cleaning system.
    iv) Avoiding the areas of PV plant installation where salt can easily deposit on the module surface.

REFERENCES

Adinoyi, M. J., & Said, S. A. M. (2013). Effect of dust accumulation on the power outputs of solar photovoltaic modules. *Renewable Energy, 60*, 633-636.

Ali-Oettinger, S. (2015, 08/2015). The 1500 Volt modus operandi. *PV Magazine*.

Almasoud, A. H., & Gandayh, H. M. (2015). Future of solar energy in Saudi Arabia. *Journal of King Saud University - Engineering Sciences, 27*(2), 153-157.

Andrew. (2011, 29 December). Activ Solar Commissions 100-Plus MW Perovo Solar PV Station in Ukraine's Crimea. Retrieved 17 March 2016, from http://cleantechnica.com/

Aubry, E., Lambert, J., Demange, V., & Billard, A. (2012). Effect of Na diffusion from glass substrate on the microstructural and photocatalytic properties of post-annealed TiO2 films synthesised by reactive sputtering. *Surface and Coatings Technology, 206*(23), 4999-5005.

Bandou, F., Hadj Arab, A., Belkaid, M. S., Logerais, P.-O., Riou, O., & Charki, A. (2015). Evaluation performance of photovoltaic modules after a long time operation in Saharan environment. *International Journal of Hydrogen Energy, 40*(39), 13839-13848.

Bauer, J., Frühauf, F., & Breitenstein, O. (2017). Quantitative local current-voltage analysis and calculation of performance parameters of single solar cells in modules. *Solar Energy Materials and Solar Cells, 159*, 8-19.

Bauer, J., Naumann, V., Großer, S., Hagendorf, C., Schütze, M., & Breitenstein, O. (2012). On the mechanism of potential-induced degradation in crystalline silicon solar cells. *physica status solidi (RRL) – Rapid Research Letters, 6*(8), 331-333.

Bedrich, K. G., Luo, W., Pravettoni, M., Chen, D., Chen, Y., Wang, Z., . . . Khoo, Y. S. (2018). Quantitative Electroluminescence Imaging Analysis for Performance Estimation of PID-Influenced PV Modules. *IEEE Journal of Photovoltaics*, 1-8.

Berghold, J., Frank, O., Hoehne, H., Pingel, S., Richardson, B., & Winkler, M. (2010),*Potential Induced Degradation of solar cells and panels.* Paper presented at the 25th EUPVSEC, Valencia, Spain,.

Berghold, J., Koch, S., Böttcher, A., Ukar, A., Leers, M., & Grunow, P. (2013). Potential-induced degradation (PID) and its correlation with experience in the field. *Photovoltaics International. 19th edition*, 85-92.

Bouraiou, A., Hamouda, M., Chaker, A., Neçaibia, A., Mostefaoui, M., Boutasseta, N., . . . Lachtar, S. (2018). Experimental investigation of observed defects in crystalline silicon PV modules under outdoor hot dry climatic conditions in Algeria. *Solar Energy, 159*, 475-487.

Bouzidi, K., Chegaar, M., & Aillerie, M. (2012). Solar Cells Parameters Evaluation from Dark I-V Characteristics. *Energy Procedia, 18*, 1601-1610.

Braisaz, B., & Radouane, K. (2014),*PID results at low irradiances on c-Si modules.* Paper presented at the Photovoltaic Specialist Conference (PVSC), 2014 IEEE 40th.

Breitenstein, O. (2012). Local efficiency analysis of solar cells based on lock-in thermography. *Solar Energy Materials and Solar Cells, 107*(0), 381-389.

Breitenstein, O., Bauer, J., Bothe, K., Hinken, D., Muller, J., Kwapil, W., . . . Warta, W. (2011). Can Luminescence Imaging Replace Lock-in Thermography on Solar Cells? *IEEE Journal of Photovoltaics, 1*(2), 159-167.

Breitenstein, O., Bauer, J., Trupke, T., & Bardos, R. A. (2008). On the detection of shunts in silicon solar cells by photo- and electroluminescence imaging. *Progress in Photovoltaics: Research and Applications, 16*(4), 325-330.

Breitenstein, O., Fertig, F., & Bauer, J. (2015). An empirical method for imaging the short circuit current density in silicon solar cells based on dark lock-in thermography. *Solar Energy Materials and Solar Cells, 143*, 406-410.

Buerhop, C., Schlegel, D., Niess, M., Vodermayer, C., Weißmann, R., & Brabec, C. J. (2012). Reliability of IR-imaging of PV-plants under operating conditions. *Solar Energy Materials and Solar Cells, 107*(0), 154-164.

Cabanillas, R. E., & Munguía, H. (2011). Dust accumulation effect on efficiency of Si photovoltaic modules. *Journal of Renewable and Sustainable Energy, 3*(4), 043114.

Carrillo, J. M., Martinez-Moreno, F., Lorenzo, C., & Lorenzo, E. (2017). Uncertainties on the outdoor characterization of PV modules and the calibration of reference modules. *Solar Energy, 155*, 880-892.

Chamberlin, C. E., Rocheleau, M. A., Marshall, M. W., Reis, A. M., Coleman, N. T., & Lehman, P. A. (2011),*Comparison of PV module performance before and after 11 and 20 years of field exposure.* Paper presented at the 37th IEEE Photovoltaic Specialists Conference, Washington, USA.

Chandel, S. S., Nagaraju Naik, M., Sharma, V., & Chandel, R. (2015). Degradation analysis of 28 year field exposed mono-c-Si photovoltaic modules of a direct coupled solar water pumping system in western Himalayan region of India. *Renewable Energy, 78*, 193-202.

Charrouf, O., Betka, A., hadef, H., Djebabra, M., & Tiar, M. (2017),*Degradation evaluation of PV modules operating under Northern Saharan environment in Algeria.* Paper presented at the AIP Conference Proceedings.

Chen, Y.-C., Wang, C.-C., Yang, S.-H., Wang, Y.-H., Tsai, C.-T., Lin, K.-C., . . . Huang, W. K. W. (2014a),*Improvements on PID for c-Si based solar cells* Paper presented at the NREL Photovoltaic Module Reliability Workshop.

Chen, Y. (2014). Polyolefin packaging film used for photovoltaic module, comprises preset amount of ethylene-octylene copolymer, polyethylene having preset density, ethylene-methyl methacrylate copolymer, melamine, crosslinking agent and antioxidant. Patent No. CN103694910-A.

Chen, Y., Lu, T., & Chen, H. (2014b). Potential induced degradation-resistant ethylene-vinyl acetate packaging film comprises specified amount of ethylene-vinyl acetate copolymer, crosslinking curing agent, antioxidant, hydroxybenzophenone and silica. Patent No. CN104152066-A.

de Oliveira, M. C. C., Diniz, A., Viana, M. M., & Lins, V. D. C. (2018). The causes and effects of degradation of encapsulant ethylene vinyl acetate copolymer (EVA) in crystalline silicon photovoltaic modules: A review. *Renewable & Sustainable Energy Reviews, 81*, 2299-2317.

del Cueto, J. A., & McMahon, T. J. (2002). Analysis of leakage currents in photovoltaic modules under high-voltage bias in the field. *Progress in Photovoltaics: Research and Applications, 10*(1), 15-28.

del Cueto, J. A., & Rummel, S. R. (2010),*Degradation of photovoltaic modules under high voltage stress in the field.* Paper presented at the SPIE, Reliability of Photovoltaic Cells, Modules, Components, and Systems III, .

Dhere, N., Pethe, S., & Kaul, A. (2011). High voltage bias testing of specially designed c-Si PV modules. *Proc. of the 2011 PVMRW*.

Dhere, N. G., Pethe, S. A., & Kaul, A. (2009),*Outdoor monitoring and high voltage bias testing of PV modules as necessary test for assuring long term reliability.* Paper presented at the Reliability of Photovoltaic Cells, Modules, Components, and Systems II.

Dhere, N. G., Shiradkar, N. S., & Schneller, E. (2014a),*Device for comprehensive analysis of leakage current paths in photovoltaic module packaging materials.* Paper presented at the Photovoltaic Specialist Conference (PVSC), 2014 IEEE 40th.

Dhere, N. G., Shiradkar, N. S., & Schneller, E. (2014b). Device for detailed analysis of leakage current paths in photovoltaic modules under high voltage bias. *Applied Physics Letters, 104*(11), 112103.

Dhere, N. G., Shiradkar, N. S., & Schneller, E. (2014c). Evolution of Leakage Current Paths in MC-Si PV Modules From Leading Manufacturers Undergoing High-Voltage Bias Testing. *IEEE Journal of Photovoltaics, 4*(2), 654-658.

Ding, M., Xu, Z., Wang, W., Wang, X., Song, Y., & Chen, D. (2016). A review on China's large-scale PV integration: Progress, challenges and recommendations. *Renewable and Sustainable Energy Reviews, 53*, 639-652.

Du, C. H., Chen, C. H., Lung, C. H., Chen, S. Y., Li, L. Y., Lin, Y. H., & Yeh, J. A. (2015). A Well-Controlled PSG Layer on Silicon Solar Cells against Potential Induced Degradation. *Ecs Journal of Solid State Science and Technology, 4*(3), P97-P100.

Dubey, S., & Tay, A. A. O. (2013). Testing of two different types of photovoltaic–thermal (PVT) modules with heat flow pattern under tropical climatic conditions. *Energy for Sustainable Development, 17*(1), 1-12.

FCSP. (2012). Fraunhofer CSP presents results of potential induced degradation (PID) [Press release]. Retrieved from http://www.en.csp.fraunhofer.de/news/details/id/857/

Fjaellstroem, V., Szaniawski, P., Vermang, B., Salome, P. M. P., Rostvall, F., Zimmermann, U., & Edoff, M. (2015). Recovery After Potential-Induced Degradation of CuIn1-xGaxSe2 Solar Cells With CdS and Zn(O,S) Buffer Layers. *IEEE Journal of Photovoltaics, 5*(2), 664-669.

Fjallstrom, V., Salome, P. M. P., Hultqvist, A., Edoff, M., Jarmar, T., Aitken, B. G., . . . Williams, C. K. (2013). Potential-Induced Degradation of CuIn1−xGaxSe2 Thin Film Solar Cells. *IEEE Journal of Photovoltaics, 3*(3), 1090-1094.

Fraunhofer, I. (2016). Photovoltaics Report by Fraunhofer Institute for Solar Energy Systems

Frazão, M., Silva, J. A., Lobato, K., & Serra, J. M. (2017). Electroluminescence of silicon solar cells using a consumer grade digital camera. *Measurement, 99*, 7-12.

Fujioka, Y. (2014). Crystalline-silicon solar cell module has ionomer resin layer, transparent resin layer, and ethylene-vinyl acetate copolymer resin layer which are laminated in order between light-receiving surface side cover glass and photovoltaic cell. Patent No. JP2014157874-A.

Goranti, S. (2011). *Potential Induced Degradation (PID) Study of Fresh and Accelerated Stress Tested Photovoltaic Modules.* (Master of Science in Technology), Arizona State University.

Goranti, S., & TamizhMani, G. (2012),*Potential induced degradation (PID) study on accelerated stress tested PV modules.* Paper presented at the Photovoltaic Specialists Conference (PVSC), 2012 38th IEEE.

Hacke, P., Burton, P., Hendrickson, A., Spataru, S., Glick, S., & Terwilliger, K. (2015a),*Effects of photovoltaic module soiling on glass surface resistance and potential-induced degradation.* Paper presented at the Photovoltaic Specialist Conference (PVSC), 2015 IEEE 42nd.

Hacke, P., Glick, S., Johnston, S., Reedy, R., Pankow, J., Terwilliger, K., & Kurtz, S. (2012). *Influence of Impurities in Module Packaging on Potential-Induced Degradation*. Paper presented at the 22nd Workshop on Crystalline Silicon Solar Cells & Modules: Materials and Processes, Vail, Colorado.

Hacke, P., Kempe, M., Terwilliger, K., Glick, S., Call, N., Johnston, S., . . . Kloos, M. (2010),*Characterization of Multicrystalline Silicon Modules with System Bias Voltage Applied in Damp Heat.* Paper presented at the European Photovoltaic Solar Energy Conference, Valencia, Spain.

Hacke, P., Smith, R., Terwilliger, K., Glick, S., Jordan, D., Johnston, S., . . . Kurtz, S. (2013). Testing and Analysis for Lifetime Prediction of Crystalline Silicon PV Modules Undergoing Degradation by System Voltage Stress. *Photovoltaics, IEEE Journal of, 3*(1), 246-253.

Hacke, P., Terwilliger, K., Glick, S., Tamizhmani, G., Tatapudi, S., Stark, C., . . . Mathiak, G. (2015b). Interlaboratory Study to Determine Repeatability of the Damp-Heat Test Method for Potential-Induced Degradation and Polarization in Crystalline Silicon Photovoltaic Modules. *IEEE Journal of Photovoltaics, 5*(1), 94-101.

Hacke, P., Terwilliger, K., Smith, R., Glick, S., Pankow, J., Kempe, M., . . . Kloos, M. (2011), *System voltage potential-induced degradation mechanisms in PV*

modules and methods for test. Paper presented at the Photovoltaic Specialists Conference (PVSC), 2011 37th IEEE.

Hara, K., Jonai, S., & Masuda, A. (2015a). Crystalline Si photovoltaic modules functionalized by a thin polyethylene film against potential and damp-heat-induced degradation. *RSC Advances, 5*(20), 15017-15023.

Hara, K., Jonai, S., & Masuda, A. (2015b). Potential-induced degradation in photovoltaic modules based on n-type single crystalline Si solar cells. *Solar Energy Materials and Solar Cells, 140*(0), 361-365.

Hattendorf, J., Löw, R., Gnehr, W.-M., Wulff, L., Koekten, M. C., Koshnicharov, D., . . . Esquivel, J. A. (2012). *Potential Induced Degradation in Mono-Crystalline Silicon Based Modules: An Acceleration Model*. Paper presented at the 27th European Photovoltaic Solar Energy Conference and Exhibition.

Hoffman, A., & Ross, R. (1978). *Environmental qualification testing of terrestrial solar cell modules*. Paper presented at the 13th IEEE PV Spec. Conference., Washington.

Hoffmann, S., & Koehl, M. (2012). Effect of humidity and temperature on the potential-induced degradation. *Progress in Photovoltaics: Research and Applications, 22*(2), 173-179.

Hoffmann, S., & Koehl, M. (2013). *Investigation on the impact of macro- and micro-climate on the potential induced degradation*. Paper presented at the IEEE 39th Photovoltaic Specialists Conference (PVSC), Florida, USA.

Hong, S., Han, I., Kim, B., & Lee, Y. (2014). Solar cell module for converting sunlight into electrical energy, has edge tape that is located between solar cell panel and frame, and having cushion that contains at least one of silicone and polyolefin. Patent No. EP2802015-A2; JP2014221000-A; KR2014132885-A; US2014332058-A1; CN104143951-A; EP2802015-A3.

Hosenuzzaman, M., Rahim, N. A., Selvaraj, J., Hasanuzzaman, M., Malek, A. B. M. A., & Nahar, A. (2015). Global prospects, progress, policies, and environmental impact of solar photovoltaic power generation. *Renewable and Sustainable Energy Reviews, 41*(0), 284-297.

Hossain, F. M., Hasanuzzaman, M., Rahim, N. A., & Ping, H. W. (2015). Impact of renewable energy on rural electrification in Malaysia: a review. *Clean Technologies and Environmental Policy, 17*(4), 859-871.

Hwang, J. (2014). Solar cell module for use e.g. outdoor for producing electricity has hydrophobic coating that covers at least portion of frame and at least portion of glass sheet. Patent No. US2014150850-A1.

Hylsky, J., Strachala, D., Vyroubal, P., Cudek, P., Vanek, J., & Vanysek, P. (2018). Effect of negative potential on the extent of PID degradation in photovoltaic power plant in a real operation mode. *Microelectronics Reliability, 85*, 12-18.

IEC 62804. (2015). System voltage durability test for crystalline silicon modules – design qualification and type approval *IEC TC 82 /PV), WG 2 (module)*. Geneva: Int. Electrotech. Comm.

Ikenaga, S., & Ito, T. (2015). Sheet used for sealing solar cell modules, consists of sealing sheets consisting of ethylene-alpha-olefin copolymer, and ethylene-polar monomer copolymer, epoxy group-containing silane coupling agent, and acid acceptor. Patent No. JP2015005646-A.

Ikenaga, S., Takeuchi, F., Ito, T., & Ikenaga, N. (2015). Sealing material for solar-cell elements, comprises ethylene-alpha-olefin copolymer, organic peroxide, and crosslinking adjuvant e.g. divinyl aromatic compound and cyanurate, and (meth)acrylate type monomer in preset weight ratio. Patent No. WO2013118504-A1; TW201339227-A; JP5405699-B1; KR2014117489-A; CN104105773-A; US2015013755-A1.

Jaeckel, B., Cosic, M., & Arp, J. (2014),*Investigation of c-Si modules degradation and recovery effect under high potentials: CV-PID.* Paper presented at the Photovoltaic Specialist Conference (PVSC), 2014 IEEE 40th.

Jaeckel, B., Krömke, F., & Arp, J. (2013). No confidence in manufacturer tests. *PV Magazine*.

Jaewon, O., Bowden, S., & Tamizhmani, G. (2014),*Application of reverse bias recovery technique to address PID issue: Incompleteness of shunt resistance and quantum efficiency recovery.* Paper presented at the Photovoltaic Specialist Conference (PVSC), 2014 IEEE 40th.

Jäger-Waldau, A. (2013). Overview of the Global PV Industry☆ *Reference Module in Earth Systems and Environmental Sciences*: Elsevier.

Jakhrani, A. Q., Othman, A.-K., Rigit, A. R. H., Samo, S. R., & Kamboh, S. A. (2013). Sensitivity Analysis of a Standalone Photovoltaic System Model Parameters. *Journal of Applied Sciences, 13*(2), 220-231.

Jambon, A., & Carron, J. P. (1976). Diffusion of Na, K, Rb and Cs in glasses of albite and orthoclase composition. *Geochimica et Cosmochimica Acta, 40*(8), 897-903.

Janghyosig, Kang, G., Gimhanbyeol, & Jeongtaehui. (2013). The Effect of PID Generation by Components of the PV Module. *Journal of the Korean Institute of Electrical and Electronic Material Engineers, 26*(10), 760-765.

Joh, J., Alamo, J. A. D., Langworthy, K., Xie, S., & Zheleva, T. (2011). Role of stress voltage on structural degradation of GaN high-electron-mobility transistors. *Microelectronics Reliability, 51*(2), 201-206.

Jordan, D. C., Silverman, T. J., Sekulic, B., & Kurtz, S. R. (2017). PV degradation curves: non-linearities and failure modes. *Progress in Photovoltaics: Research and Applications, 25*(7), 583-591.

Kaden, T., Lammers, K., & Möller, H. J. (2015). Power loss prognosis from thermographic images of PID affected silicon solar modules. *Solar Energy Materials and Solar Cells, 124*, 24-28.

Kaewkhao, J., Limsuwan, P., P.Yupapin, P. P. Y., JanJai, S. J., Kamkird, P., Ketjoy, N., . . . Sukchai, S. (2012). Investigation on Temperature Coefficients of Three Types Photovoltaic Module Technologies under Thailand Operating Condition. *Procedia Engineering, 32*, 376-383.

Kajari-Schröder, S., Kunze, I., Eitner, U., & Köntges, M. (2011). Spatial and orientational distribution of cracks in crystalline photovoltaic modules generated by mechanical load tests. *Solar Energy Materials and Solar Cells, 95*(11), 3054-3059.

Kajisa, T., Miyauchi, H., Mizuhara, K., Hayashi, K., Tokimitsu, T., Inoue, M., . . . Masuda, A. (2014). Novel lighter weight crystalline silicon photovoltaic module using acrylic-film as a cover sheet. *Japanese Journal of Applied Physics, 53*(9), 092302.

Kambe, M., Hara, K., Mitarai, K., Takeda, S., Fukawa, M., Ishimaru, N., & Kondo, M. (2013),*Chemically strengthened cover glass for preventing potential induced degradation of crystalline silicon solar cells.* Paper presented at the Photovoltaic Specialists Conference (PVSC), 2013 IEEE 39th.

Kang, G. H., Kim, H. B., Jung, T. H., Ju, Y. C., Ko, S. W., & Song, H. E. (2015). Prediction of the Potential Induced Degradation of Photovoltaic Modules Based on the Leakage Current Flowing Through Glass Laminated With Ethylene-Vinly Acetate. *Journal of Solar Energy Engineering-Transactions of the Asme, 137*(4), 041001-041006.

Kaplani, E. (2012). Detection of Degradation Effects in Field-Aged c-Si Solar Cells through IR Thermography and Digital Image Processing. *International Journal of Photoenergy, 2012*, 11.

Kapur, J., Bennett, A., Norwood, J., Hamzavytehrany, B., & Kueppenbender, I. (2013),*Tailoring ionomer encapsulants as a low cost solution to potential induced degradation.* Paper presented at the 28th European Photovoltaic Solar Energy Conference, Paris, France.

Kapur, J., Stika, K. M., Westphal, C. S., Norwood, J. L., & Hamzavytehrany, B. (2015). Prevention of Potential-Induced Degradation With Thin Ionomer Film. *Photovoltaics, IEEE Journal of, 5*(1), 219-223.

Kerekes, T., Teodorescu, R., Rodriguez, P., Vazquez, G., & Aldabas, E. (2011). A New High-Efficiency Single-Phase Transformerless PV Inverter Topology. *IEEE Transactions on Industrial Electronics, 58*(1), 184-191.

Kim, S. H., Maccracken, C., & Edmonds, J. (2000). Solar energy technologies and stabilizing atmospheric CO2 concentrations. *Progress in Photovoltaics: Research and Applications, 8*(1), 3-15.

Kindyni, N., & Georghiou, G. E. (2013),*Application of an analytical model based on transistor concepts for the characterization of potential-induced degradation in crystalline silicon photovoltaics.* Paper presented at the Photovoltaic Specialists Conference (PVSC), 2013 IEEE 39th.

Koch, S., Berghold, J., Okoroafor, O., Krauter, S., & Grunow, P. (2012a). *Encapsulation influence on the potential induced degradation of crystalline silicon cells with selective emitter structures*. Paper presented at the 27th European Photovoltaic Solar Energy Conference and Exhibition (EU-PVSEC-27), Germany.

Koch, S., Nieschalk, D., Berghold, J., Wendlandt, S., Krauter, S., & Grunow, P. (2012b),*Potential induced degradation effects on crystalline silicon cells with various antireflective coatings*. Paper presented at the 27th European Photovoltaic Solar Energy Conference and Exhibition (EU-PVSEC-27), Frankfurt a. M., Germany.

Koch, S., Seidel, C., Krauter, S., Grunow, P., & Schoppa, M. (2011). *Polarization effects and tests for crystalline silicon cells*. Paper presented at the 26th EUPVSEC, Hamburg, Germany.

Koehl, M., & Hoffmann, S. (2016). Impact of rain and soiling on potential induced degradation. *Progress in Photovoltaics: Research and Applications*, n/a-n/a.

Koentopp, M. B., Krober, M., & Taubitz, C. (2016). Toward a PID Test Standard: Understanding and Modeling of Laboratory Tests and Field Progression. *IEEE Journal of Photovoltaics, 6*(1), 252 - 257.

Komatsu, Y., Yamaguchi, S., Masuda, A., & Ohdaira, K. (2018). Multistage performance deterioration in n-type crystalline silicon photovoltaic modules undergoing potential-induced degradation. *Microelectronics Reliability, 84*, 127-133.

Kuan, T.-M., Huang, C.-C., Wu, L.-G., Chan, Y.-C., Yu, C.-Y., & Ieee. (2013). *Process Optimization for Potential Induced Degradation Improvement on Cell Level*. Paper presented at the 39th Photovoltaic Specialists Conference.

Kumar, G. M., & Park, J. (2014). Structural and optical property studies on indium doped ZnO nanostructures for solution based organic–inorganic hybrid p–n junctions. *Journal of Colloid and Interface Science, 430*(0), 229-233.

Kumar, M., & Kumar, A. (2017). Performance assessment and degradation analysis of solar photovoltaic technologies: A review. *Renewable and Sustainable Energy Reviews, 78*, 554-587.

Lausch, D., Naumann, V., Breitenstein, O., Bauer, J., Graff, A., Bagdahn, J., & Hagendorf, C. (2014a). Potential-Induced Degradation (PID): Introduction of a Novel Test Approach and Explanation of Increased Depletion Region Recombination. *IEEE Journal of Photovoltaics, 4*(3), 834-840.

Lausch, D., Naumann, V., Graff, A., Hähnel, A., Breitenstein, O., Hagendorf, C., & Bagdahn, J. (2014b). Sodium Outdiffusion from Stacking Faults as Root Cause for the Recovery Process of Potential-induced Degradation (PID). *Energy Procedia, 55*(0), 486-493.

Limmanee, A., Songtrai, S., Udomdachanut, N., Kaewniyompanit, S., Sato, Y., Nakaishi, M., . . . Sakamoto, Y. (2017). Degradation analysis of photovoltaic modules under tropical climatic conditions and its impacts on LCOE. *Renewable Energy, 102, Part A*, 199-204.

Lin, J., Yang, C., Hou, H., Lin, W., & Zhou, G. (2013). Integrated photovoltaic assembly back plate material having anti-potential induced degradation effect comprises olefin copolymer layer, polyester layer, and heat-UV light double crosslinking and curing polyester coating layer. Patent No. CN103252953-A.

Liu, H.-C., Huang, C.-T., & Lee, W.-K. (2012),*Study of potential induced degradation mechanism in commercial PV module.* Paper presented at the Photovoltaic Specialists Conference (PVSC), 2012 38th IEEE.

Liu, H. C., Huang, C. T., Lee, W. K., & Lin, M. H. (2013). High Voltage Stress Impact on P Type Crystalline Silicon PV Module. *Energy and Power Engineering, 5*(7), 455-458

Luo, W., Khoo, Y. S., Hacke, P., Naumann, V., Lausch, D., Harvey, S. P., . . . Ramakrishna, S. (2017). Potential-induced degradation in photovoltaic modules: a critical review. *Energy & Environmental Science, 10*(1), 43-68.

Mansouri, A., Zettl, M., Mayer, O., Lynass, M., Bucher, M., & Stern, O. (2012),*Defect detection in photovoltaic modules using electroluminescence imaging.* Paper presented at the 27th European Photovoltaic Solar Energy Conference and Exhibition, Frankfurt, Germany.

Martínez-Moreno, F., Figueiredo, G., & Lorenzo, E. (2018). In-the-field PID related experiences. *Solar Energy Materials and Solar Cells, 174*(Supplement C), 485-493.

Masuda, A., Hara, Y., & Jonai, S. (2016). Consideration on Na diffusion and recovery phenomena in potential-induced degradation for crystalline Si photovoltaic modules. *Japanese Journal of Applied Physics, 55*(2S), 02BF10.

Meydbray, J., & Dross, F. (2016). PV Module Reliability Scorecard Report: DNV GL.

Min'ko, N. I., & Binaliev, I. M. (2013). Role of sodium sulfate in glass technology. *Glass and Ceramics, 69*(11-12), 361-365.

Mints, P. (2012). The history and future of incentives and the photovoltaic industry and how demand is driven. *Progress in Photovoltaics: Research and Applications, 20*(6), 711-716.

Mochizuki, T., Kim, C., Yoshita, M., Mitchell, J., Lin, Z., Chen, S., . . . Akiyama, H. (2016). Solar-cell radiance standard for absolute electroluminescence measurements and open-circuit voltage mapping of silicon solar modules. *Journal of Applied Physics, 119*(3), 034501.

Moreno, F. M., Lorenzo, E., Munoz, J., Parra, R., & Espino, T. (2013), *On Site Tests for the Detection of Potential Induced Degradation in Modules.* Paper presented at the European Photovoltaic Solar Energy Conference (PVSEC), Paris.

Moriyama, N., & Yamazaki, T. (2014). Sealing material sheet used for photovoltaic cell of solar cell module, is multilayered constitution made from polyethylene-type resin, and has layers containing white pigments in specified mass ratio. Patent No. JP2014103369-A.

Moskowitz, S. (2015, 14 May, 2015). The Next Opportunity for Utility PV Cost Reductions: 1,500 Volts DC. *Greentech Media*.

Munoz, M. A., Alonso-García, M. C., Vela, N., & Chenlo, F. (2011). Early degradation of silicon PV modules and guaranty conditions. *Solar Energy, 85*(9), 2264-2274.

Nagel, H., Metz, A., & Wangemann, K. (2011),*Crystalline Si solar cells and modules featuring excellent stability against potential induced degradation.* Paper presented at the 26th EUPVSEC, Hamburg, Germany.

Nagel, H., Pfeiffer, R., Roykov, A., & Wangemann, K. (2012). *Lifetime Warranty Testing of Crystalline Silicone Modules for Potential-Induced Degradation*. Paper presented at the 27th European PV Solar Energy Conference.

Nagel, H., Saint-Cast, P., Glatthaar, M., & Glunz, S. W. (2014). *Inline processes for the stabilization of p-type crystalline si solar cells against potential-induced degradation* Paper presented at the 29th European Photovoltaic Solar Energy Conference and Exhibition, Amsterdam, Netherlands.

NASA. (2017). NASA Surface meteorology and Solar Energy - Location. Retrieved 25-03-2017 https://eosweb.larc.nasa.gov/cgi-bin/sse/grid.cgi?email=skip@larc.nasa.gov

Nasrin, R., Rahim, N. A., Fayaz, H., & Hasanuzzaman, M. (2018). Water/MWCNT nanofluid based cooling system of PVT: Experimental and numerical research. *Renewable Energy*.

Naumann, V., Hagendorf, C., Grosser, S., Werner, M., & Bagdahn, J. (2012). Micro Structural Root Cause Analysis of Potential Induced Degradation in c-Si Solar Cells. *Energy Procedia, 27*(0), 1-6.

Naumann, V., Ilse, K., & Hagendorf, C. (2013). *On the discrepancy between leakage currents and potential induced degradation of crystalline silicon modules*. Paper presented at the Proceedings of the 28th European Photovoltaic Solar Energy Conference, Paris, France.

Naumann, V., Lausch, D., Haehnel, A., Bauer, J., Breitenstein, O., Graff, A., . . . Hagendorf, C. (2014). Explanation of potential-induced degradation of the shunting type by Na decoration of stacking faults in Si solar cells. *Solar Energy Materials and Solar Cells, 120*, 383-389.

Ndiaye, A., Kébé, C. M. F., Charki, A., Ndiaye, P. A., Sambou, V., & Kobi, A. (2014). Degradation evaluation of crystalline-silicon photovoltaic modules after a few operation years in a tropical environment. *Solar Energy, 103*, 70-77.

Nehme, B., M'Sirdi, N. K., Akiki, T., & Naamane, A. (2014). Contribution to the Modeling of Ageing Effects in PV Cells and Modules. *Energy Procedia, 62*, 565-575.

Ogita, Y.-I., & Tachihara, M. (2015). Reduction of surface recombination velocity by rapid thermal annealing of p-Si passivated by catalytic-chemical vapor deposited alumina films. *Thin Solid Films, 575*(0), 56-59.

Oh, J., Bowden, S., & TamizhMani, G. (2015). Potential-Induced Degradation (PID): Incomplete Recovery of Shunt Resistance and Quantum Efficiency Losses. *IEEE Journal of Photovoltaics, 5*(6), 1540-1548.

Oh, J., TamizhMani, G., Bowden, S., & Garner, S. (2016). Surface Disruption Method With Flexible Glass to Prevent Potential-Induced Degradation of the Shunting Type in PV Modules. *IEEE Journal of Photovoltaics*.

Oh, W., Bae, S., Chan, S.-I., Lee, H.-S., Kim, D., & Park, N. (2017). Field degradation prediction of potential induced degradation of the crystalline silicon photovoltaic modules based on accelerated test and climatic data. *Microelectronics Reliability, 76-77*, 596-600.

Oka, Y., Kokubo, Y., & Miyashita, M. (2015). Sealing material used for solar cell modules, has layer containing modified polyolefin-type resin obtained by copolymerizing polyolefin resin with cyclopentene dione derivative. Patent No. JP2015032804-A.

Osterwald, C. R., McMahon, T. J., & del Cueto, J. A. (2003). Electrochemical corrosion of SnO2:F transparent conducting layers in thin-film photovoltaic modules. *Solar Energy Materials and Solar Cells, 79*(1), 21-33.

Parretta, A., Bombace, M., Graditi, G., & Schioppo, R. (2005). Optical degradation of long-term, field-aged c-Si photovoltaic modules. *Solar Energy Materials and Solar Cells, 86*(3), 349-364.

Pingel, S., Frank, O., Winkler, M., Daryan, S., Geipel, T., Hoehne, H., & Berghold, J. (2010). *Potential Induced Degradation of solar cells and panels*. Paper presented at the 35th IEEE Photovoltaic Specialists Conference (PVSC), Honolulu, HI, USA.

Pingel, S., Janke, S., & Frank, O. (2012). *Recovery Methods for Modules Affected by Potential Induced Degradation (PID)*. Paper presented at the 27th European Photovoltaic Solar Energy Conference and Exhibition.

Pingel, S., Janke, S., Seydewitz, J., Alam, R., Koch, S., Kupke, J., & Berghold, J. (2014). *The Local Potential Distribution as Driver of PID & "Live PID Monitoring" Method*. Paper presented at the 29th European Photovoltaic Solar Energy Conference and Exhibition.

Pop, S. C., Schulze, R., Wang, X., Yuan, B., Kapur, J., Stika, K. M., . . . Meisel, A. (2014). *Ionomer-Based PiD-Resistant Encapsulant for PV Modules*. Paper presented at the 29th European Photovoltaic Solar Energy Conference and Exhibition.

Pozza, A., & Sample, T. (2016). Crystalline silicon PV module degradation after 20 years of field exposure studied by electrical tests, electroluminescence, and LBIC. *Progress in Photovoltaics: Research and Applications, 24*(3), 368-378.

PVresources. (2016, 29 February, 2016). Large-Scale PV Power Plants - Top50. Retrieved 17 March 2016, from http://www.pvresources.com/en/top50pv.php

Quintana, M. A., King, D. L., McMahon, T. J., & Osterwald, C. R. (2002),*Commonly observed degradation in field-aged photovoltaic modules.* Paper presented at the 29th IEEE Photovoltaic Specialists Conference, New Orleans, Louisiana.

Rabii, A. B., Jraidi, M., & Bouazzi, A. S. (2003),*Investigation of the degradation in field-aged photovoltaic modules.* Paper presented at the 3rd World Conference onPhotovoltaic Energy Conversion, Osaka, Japan.

Rahman, M. M., Hasanuzzaman, M., & Rahim, N. A. (2015). Effects of various parameters on PV-module power and efficiency. *Energy Conversion and Management, 103*, 348-358.

Rahman, M. M., Hasanuzzaman, M., & Rahim, N. A. (2017). Effects of Operational Conditions on the Energy Efficiency of Photovoltaic Modules Operating in Malaysia. *Journal of Cleaner Production, 143*, 912-924.

Rajput, A. S., Ho, J. W., Zhang, Y., Nalluri, S., & Aberle, A. G. (2018). Quantitative estimation of electrical performance parameters of individual solar cells in silicon photovoltaic modules using electroluminescence imaging. *Solar Energy, 173*, 201-208.

Raykov, A., Stegemann, K.-H., Hahn, H., Bitnar, B., Kutzer, M., Neuhaus, D.-H., & Bergholz, W. (2014). *Root Cause Analysis of Potential-Induced Degradation in Crystalline Silicon Photovoltaic Cells and Modules*. Paper presented at the European Photovoltaic Solar Energy Conference and Exhibition.

Reid, C. G., Ferrigan, S. A., Martínez, J. I. F., & Woods, J. T. (2013),*Contribution of pv encapsulant composition to reduction of potential induced degradation (pid) of crystalline silicon pv cells* Paper presented at the 28th European Photovoltaic Solar Energy Conference, Paris, France.

REN21. (2016). Renewables 2016 : global status report. REN21. Renewable Energy Policy Network for the 21st Century.

Ross, J. R. G., Mon, G. R., Wen, L. C., & Sugimura, R. S. (1989). Measurement and characterization of voltage- and current-induced degradation of thin-film photovoltaic modules. *Solar Cells, 27*(1–4), 289-298.

Rutschmann, I. (2012, November). Power losses below the surface Laboratory testing is neededto diagnose the reasons for negative impact of PID on solar modules. *Photon International,* 130-137.

Saha, J. M., & Rowley, C. (2015). The role of human resources in sustaining the growth of industries *The Changing Role of the Human Resource Profession in the Asia Pacific Region* (pp. 123-133): Chandos Publishing.

Schladitz, A., MÜLler, T., Nowak, A., Kandler, K., Lieke, K., Massling, A., & Wiedensohler, A. (2011). In situ aerosol characterization at Cape Verde. *Tellus B, 63*(4), 531-548.

Schneller, E., Shiradkar, N. S., & Dhere, N. G. (2014),*Performance variation of commercially available modules after six months of outdoor system voltage stress testing.* Paper presented at the Photovoltaic Specialist Conference (PVSC), 2014 IEEE 40th.

Schubert, U. (1997). Book Review: Introduction to glass science and technology. By J. E. Shelby. *Angewandte Chemie International Edition in English, 36*(20), 2248-2249.

Schutze, M., Junghanel, M., Friedrichs, O., Wichtendahl, R., Scherff, M., Müller, J., & Wawer, P. (2011a). *Investigations of Potential Induced Degradation of Silicon Photovoltaic Modules*. Paper presented at the 26th European Photovoltaic Solar Energy Conference and Exhibition.

Schutze, M., Junghanel, M., Koentopp, M. B., Cwikla, S., Friedrich, S., Muller, J. W., & Wawer, P. (2011b). *Laboratory study of potential induced degradation of silicon photovoltaic modules*. Paper presented at the Photovoltaic Specialists Conference (PVSC), 2011 37th IEEE.

Schwark, M., Berger, K., Ebner, R., Ujvari, G., Hirschl, C., Neumaier, L., & Muhleisen, W. (2013),*Investigation of potential induced degradation (PID) of solar modules from different manufacturers.* Paper presented at the Industrial Electronics Society, IECON 2013 - 39th Annual Conference of the IEEE.

Schwark, M., Hirschl, C., Ebner, R., Újvári, G., Mühleisen, W., Neumaier, L., . . . Ledinger, S. (2014). *Time Depending Shunt Resistor Changes during PID Stress of PV Modules with Different Encapsulants Varying in Epsilon R and Bulk Resistance*. Paper presented at the 29th European Photovoltaic Solar Energy Conference and Exhibition, Amsterdam, Netherlands

Scopus. (2018). Document search. Retrieved 10 January 2018 https://www.scopus.com/search/form.uri?display=basic

Serrano-Luján, L., García-Valverde, R., Espinosa, N., García-Cascales, M. S., Sánchez-Lozano, J. M., & Urbina, A. (2015). Environmental benefits of parking-integrated photovoltaics: a 222 kWp experience. *Progress in Photovoltaics: Research and Applications, 23*(2), 253-264.

Sharma, A. K., Agarwal, S. K., & Singh, S. N. (2007). Determination of front surface recombination velocity of silicon solar cells using the short-wavelength spectral response. *Solar Energy Materials and Solar Cells, 91*(15), 1515-1520.

Sharma, V., & Chandel, S. S. (2013). Performance and degradation analysis for long term reliability of solar photovoltaic systems: A review. *Renewable and Sustainable Energy Reviews, 27*(0), 753-767.

Shiradkar, N., Schneller, E., & Dhere, N. G. (2013). Finite Element Analysis based model to study the electric field distribution and leakage current in PV modules under high voltage bias. *Reliability of Photovoltaic Cells, Modules, Components, and Systems Vi, 8825*, 8825G-8821.

Shirazi, A. D., Book, F., Haverkamp, H., Raabe, B., & Hahn, G. (2009). *Investigations of High Refractive Silicon Nitride Layers for Etched Back Emitters: Enhanced Surface Passivation for Selective Emitter Concept (SECT)*. Paper presented at the European Photovoltaic Solar Energy Conference, Hamburg, Germany.

Simon, M., & Meyer, E. L. (2010). Detection and analysis of hot-spot formation in solar cells. *Solar Energy Materials and Solar Cells, 94*(2), 106-113.

Singh, P., & Ravindra, N. M. (2012). Temperature dependence of solar cell performance—an analysis. *Solar Energy Materials and Solar Cells, 101*, 36-45.

Singh, R. (2015). Maximising power production of large PV systems: PID detection and mitigation. Retrieved from http://www.pv-tech.org/mobile/blogs/maximising_power_production_of_large_pv_systems_pid_detection_and_mitigatio

Sinha, A., Sastry, O. S., & Gupta, R. (2016). Nondestructive characterization of encapsulant discoloration effects in crystalline-silicon PV modules. *Solar Energy Materials and Solar Cells, 155*, 234-242.

Sinton, C. W., & LaCourse, W. C. (2001). Experimental survey of the chemical durability of commercial soda-lime-silicate glasses. *Materials Research Bulletin, 36*(13–14), 2471-2479.

Solangi, K. H., Saidur, R., Luhur, M. R., Aman, M. M., Badarudin, A., Kazi, S. N., . . . Islam, M. R. (2015). Social acceptance of solar energy in Malaysia: users' perspective. *Clean Technologies and Environmental Policy, 17*(7), 1975-1986.

Spataru, S., Hacke, P., Sera, D., Packard, C., Kerekes, T., & Teodorescu, R. (2015). Temperature-dependency analysis and correction methods of in situ power-loss estimation for crystalline silicon modules undergoing potential-induced degradation stress testing. *Progress in Photovoltaics: Research and Applications, 23*(11), 1536-1549.

Stika, K. M., Westphal, C. S., Kapur, J., Raty, R. G., Jing, L., Kopchick, J. G., . . . Foltz, B. W. (2014),*Mapping chemical and mechanical property degradation in photovoltaic modules*. Paper presented at the Photovoltaic Specialist Conference (PVSC), 2014 IEEE 40th.

Suzuki, S., Nishiyama, N., Yoshino, S., Ujiro, T., Watanabe, S., Doi, T., . . . Tanahashi, T. (2015). Acceleration of potential-induced degradation by salt-mist preconditioning in crystalline silicon photovoltaic modules. *Japanese Journal of Applied Physics, 54*(8S1), 08KG08-01-08.

Swanson, R., Cudzinovic, M., DeCeuster, D., Desai, V., Jürgens, J., Kaminar, N., & Mulligan, W. (2005),*The Surface Polarization Effect in High-Efficiency Silicon Solar Cells*. Paper presented at the International Photovoltaic Science & Engineering Conference (PVSEC-15).

Swanson, R. M., De Ceuster, D., Desai, V., Rose, D. H., Smith, D. D., & Kaminar, N. (2009). Preventing harmful polarization of solar cells. Patent No. US 7,554,031 B2.

Takashi, F., Hayato, K., Tsutomu, Y., Yu, T., & Yukiharu, U. (2005). Photographic surveying of minority carrier diffusion length in polycrystalline silicon solar cells by electroluminescence. *Applied Physics Letters, 86*(26), 262108.

Tatapudi, S., Ebneali, F., Kuitche, J., & Tamizhmani, G. (2013),*Potential induced degradation of pre-stressed photovoltaic modules: Effect of glass surface conductivity disruption.* Paper presented at the Photovoltaic Specialists Conference (PVSC), 2013 IEEE 39th.

Taubitz, C., Schütze, M., Kröber, M., & Köntopp, M. B. (2014). *Potential Induced Degradation: Model Calculations and Correlation between Laboratory Tests and Outdoor Occurrence*. Paper presented at the 29th European Photovoltaic Solar Energy Conference, Amsterdam, Netherlands.

Thevenard, D., & Pelland, S. (2013). Estimating the uncertainty in long-term photovoltaic yield predictions. *Solar Energy, 91*, 432-445.

Tsanakas, J. A., Ha, L., & Buerhop, C. (2016). Faults and infrared thermographic diagnosis in operating c-Si photovoltaic modules: A review of research and future challenges. *Renewable and Sustainable Energy Reviews, 62*, 695-709.

Vigdu. (2017). What is PID Retrieved 28/06/2017, 2017, from http://www.vigdu.com/single-post/What-is-PID

Wesoff, E. (2015, June 26). Solar Star, Largest PV Power Plant in the World, Now Operational. *Greentech Media*.

Wu, X., Lu, Y., Zhou, S., Chen, L., & Xu, B. (2016). Impact of climate change on human infectious diseases: Empirical evidence and human adaptation. *Environment International, 86*, 14-23.

Würfel, P., Trupke, T., Puzzer, T., Schäffer, E., Warta, W., & Glunz, S. W. (2007). Diffusion lengths of silicon solar cells from luminescence images. *Journal of Applied Physics, 101*(12), 123110.

Yamaguch, S., Masuda, A., & Ohdaira, K. (2016). Behavior of the potential-induced degradation of photovoltaic modules fabricated using flat mono-crystalline silicon cells with different surface orientations. *Japanese Journal of Applied Physics, 55*(4S), 04ES14.

Yamaguchi, S., Masuda, A., & Ohdaira, K. (2016). Changes in the current density–voltage and external quantum efficiency characteristics of n-type single-crystalline silicon photovoltaic modules with a rear-side emitter undergoing potential-induced degradation. *Solar Energy Materials and Solar Cells, 151*, 113-119.

Yang, H., Wang, F., Wang, H., Chang, J., Song, D., & Su, C. (2017). Performance deterioration of p-type single crystalline silicon solar modules affected by

potential induced degradation in photovoltaic power plant. *Microelectronics Reliability, 72*, 18-23.

Ye, J. Y., Reindl, T., Aberle, A. G., & Walsh, T. M. (2014). Performance Degradation of Various PV Module Technologies in Tropical Singapore. *IEEE Journal of Photovoltaics, 4*(5), 1288-1294.

Yilbas, B. S., Ali, H., Khaled, M. M., Al-Aqeeli, N., Abu-Dheir, N., & Varanasi, K. K. (2015). Influence of dust and mud on the optical, chemical, and mechanical properties of a pv protective glass. *Scientific Reports, 5*, 15833.

Yu, H. J. J., Popiolek, N., & Geoffron, P. (2016). Solar photovoltaic energy policy and globalization: a multiperspective approach with case studies of Germany, Japan, and China. *Progress in Photovoltaics: Research and Applications, 24*(4), 458–476.

Zafirovska, I., Juhl, M. K., Weber, J. W., Wong, J., & Trupke, T. (2017). Detection of Finger Interruptions in Silicon Solar Cells Using Line Scan Photoluminescence Imaging. *IEEE Journal of Photovoltaics, 7*(6), 1496-1502.

Zhou, C., Zhu, J., Foss, S. E., Haug, H., Nordseth, Ø., Marstein, E. S., & Wang, W. (2015). SiOyNx/SiNx Stack Anti-reflection Coating with PID-resistance for Crystalline Silicon Solar Cells. *Energy Procedia, 77*, 434-439.

Ziebarth, B., Mrovec, M., Elsässer, C., & Gumbsch, P. (2014). Potential-induced degradation in solar cells: Electronic structure and diffusion mechanism of sodium in stacking faults of silicon. *Journal of Applied Physics, 116*(9), 093510.

Zita, J., Maixner, J., & Krýsa, J. (2010). Multilayer TiO2/SiO2 thin sol–gel films: Effect of calcination temperature and Na+ diffusion. *Journal of Photochemistry and Photobiology A: Chemistry, 216*(2–3), 194-200.

LIST OF PUBLICATIONS AND PAPERS PRESENTED

Journal Articles

1. **M.A. Islam**, M. Hasanuzzaman and Nasrudin Abd Rahim, 2018, "Investigation of the potential induced degradation behaviour of on-site aged polycrystalline PV modules in Malaysian climate", ***Measurement*** 119, 283-294 *(ISI Indexed Publication).*
2. **M.A. Islam**, M. Hasanuzzaman and Nasrudin Abd Rahim, "Degradation analysis of crystalline silicon PV modules due to on-site aging under Malaysian climate" ***Ind. J Pure & Applied Physics*** 56, 226-237 *(ISI Indexed Publication).*
3. **M.A. Islam**, M. Hasanuzzaman and Nasrudin Abd Rahim, "Investigation on the effect of different factors on leakage current of PV module at high string voltage stress" ***IEEE journal of photovoltaic*** (2018) **8**(5) 1259 - 1265 *(ISI Indexed Publication).*
4. **M.A. Islam**, M. Hasanuzzaman, Nasrudin Abd Rahim, "Comparative investigation of on-site and laboratory test standard of potential induced degradation PID of crystalline Si PV module" ***Renewable Energy*** (2018) 127, 102-113 *(ISI Indexed Publication).*
5. **M.A. Islam**, M. Hasanuzzaman, Nasrudin Abd Rahim, "Potential Induced Degradation of PV Modules: An Overview on the Impact of Different Module Constituting Materials" ***Journal of Renewable and Sustainable Energy Review*** (Under Review) *(ISI Indexed Publication).*

Conference Papers

1. **M.A. Islam,** M. Hasanuzzaman and Nasrudin Abd Rahim, Design and analysis of PV power plant at different location in Malaysia, ***International Conference on Global Sustainability and Chemical Engineering,*** 15-16 February 2017, Putrajaya Marriot Hotel, Malaysia.
2. **M.A. Islam,** M. Hasanuzzaman and Nasrudin Abd Rahim, Investigation the impact of high string voltage stress on polycrystalline silicon PV module performance, ***UMPEDAC Postgraduate Research on Energy (PRoE) Symposium***, 6 & 7th September 2017.